ADVANCED FUEL CYCLE SCENARIOS

WITH AP1000 PWRS AND VHTRS

AND FISSION SPECTRUM UNCERTAINTIES

A Thesis

by

MARIE-HERMINE MATHILDE SOLANGE CUVELIER

Submitted to the Office of Graduate Studies of
Texas A&M University
in partial fulfillment of the requirements for the degree of

MASTER OF SCIENCE

May 2012

Major Subject: Nuclear Engineering

Advanced Fuel Cycle Scenarios with AP1000 PWRs and VHTRs

and Fission Spectrum Uncertainties

ADVANCED FUEL CYCLE SCENARIOS

WITH AP1000 PWRS AND VHTRS

AND FISSION SPECTRUM UNCERTAINTIES

A Thesis

by

MARIE-HERMINE MATHILDE SOLANGE CUVELIER

Submitted to the Office of Graduate Studies of
Texas A&M University
in partial fulfillment of the requirements for the degree of

MASTER OF SCIENCE

Approved by:

Chair of Committee,	Pavel V. Tsvetkov
Committee Members,	Sean M. McDeavitt
	Christine Ehlig-Economides
Head of Department,	Yassin A. Hassan

May 2012

Major Subject: Nuclear Engineering

ABSTRACT

Advanced Fuel Cycle Scenarios with AP1000 PWRs and VHTRs

and Fission Spectrum Uncertainties.

(May 2012)

Marie-Hermine Mathilde Solange Cuvelier, B.S., EPF-Ecole d'Ingénieurs

Chair of Advisory Committee: Dr. Pavel V. Tsvetkov

Minimization of HLW inventories and U consumption are key elements guaranteeing nuclear energy expansion. The integration of complex nuclear systems into a viable cycle yet constitutes a challenging multi-parametric optimization problem. The reactors and fuel cycle performance parameters may be strongly dependent on minor variations in the system's input data. Proven discrepancies in nuclear data evaluations could affect the validity of the system optimization metrics.

This study first analyzes various advanced AP1000-VHTR fuel cycle scenarios by assessing their TRU destruction and their U consumption minimization capabilities, and by computing reactor performance parameters such as the time evolution of the effective multiplication factor k_{eff}, the reactors' energy spectrum or the isotopic composition/activity at EOL. The performance metrics dependence to prompt neutron fission spectrum discrepancies is then quantified to assess the viability of one strategy. Fission spectrum evaluations are indeed intensively used in reactors' calculations. Discrepancies higher than 10% have been computed among nuclear data libraries for energies above 8MeV for ^{235}U.

TRU arising from a 3wt% ^{235}U-enriched UO_2-fueled AP1000 were incinerated in a VHTR. Fuels consisting of 20%, 40% and 100% of TRU completed by UO_2 were examined. MCNPX results indicate that up to 88.9% of the TRU initially present in a VHTR fueled with 20% of TRU and 80% of ThO_2 were transmuted. Additionally, the use of WgPu instead of RgPu should reduce the daily consumption of ^{235}U by 1.3 and augment core lifetime.

To estimate the system metrics dependence to fission spectrum discrepancies and validate optimization studies outputs, the VTHR ^{235}U fission spectrum distribution was altered successively in three manners. k_{eff} is at worst lowered by 1.7% of the reference value and the energy spectrum by 5% between 50meV and 2MeV when a significantly distorted fission spectrum tail is used. ^{233}U, ^{236}Pu and ^{237}Pu inventories and activities are multiplied by 263, 523 and 34 but are still negligible compared to ^{239}Pu mass or the total activity.

The AP1000-VHTR system is in conclusion not dependent on the selected fission spectrum variations. TRU elimination optimization studies in AP1000-VHTR systems will be facilitated by freeing performance metrics dependency from 1 input parameter.

.

ACKNOWLEDGEMENTS

I would like to genuinely thank my advisor, Dr. Pavel V. Tsvetkov for his guidance and support during the course of this thesis. I am deeply grateful to his dedication, patience and kind encouragements which allowed me to complete this Master.

In addition, I would like to extend my gratitude to my committee members, Dr. Christine Ehlig-Economides from the Petroleum Engineering Department and Dr. Sean McDeavitt from the Nuclear Engineering Department.

A special thanks to my officemates for their help and accompaniment in this academic journey, in particular Sathish K. Lakshmipathy for his constant happiness, Jesse M. Johns for his patience, exemplary hardworking skills and thoughtful advice, Matt P. Johnson and Christopher W. Chapman.

I would also like to particularly recognize the work of two members of the Nuclear Engineering Department: Jennifer A. House, the Administrative Assistant for Graduate Admissions and William D. Hawkins, TEES Research Engineer Associate II. Thanks Jennifer for constantly finding solutions to the various administrative complications encountered from my application into the Master's Program to my graduation. Thanks Daryl for skillfully assisting us while using the computational servers of the Department.

I am also infinitely grateful to Dr. Shannon Bragg-Sitton for having accepted to recruit me from abroad as an intern and having given me my first opportunity to be part of the Department of Nuclear Engineering at Texas A&M University.

I'm also indebted to:

- Texas A&M University for having welcomed me and whose core values of Excellence, Integrity, Leadership, Loyalty, Respect and Selfless Services will always be source of inspiration. Thank you to its staff for its excellent support during my stay.
- The State of Texas for giving me access to high-education and for providing me with an exceptional quality of life.
- My Texan friends Zachry Gibson and Julian Habib for being so inspirational to me.
- My friend Ayodeji B. Alajo for saving my life multiple times.
- My friends, Henry Tanaruno, Adam Parkison and Pavan Dharwadkar simply for being wonderful people.
- Nessie, Lucy and Ranger for being such priceless companions.

And of course, the acknowledgement could not be completed without honoring my parents and my grand-parents. I will never enough appreciate all the sacrifices you made to allow me to meet success. Finally, thank you to my brother for being that big brother I am forever tied to.

This thesis is based upon work partially supported by the U.S. Department of Energy Nuclear Energy University Program Awards 09-414 and 09-475.

NOMENCLATURE

AFCI	Advanced Fuel Cycle Initiative
AVR	Arbeitsgemeinschaft Versuchsreaktor
BOL	Beginning Of Life
DB-MHR	Deep-Burn Modular Helium Reactor
ENDF	Evaluated Nuclear Data File
EOL	End Of Life
GIF	Generation-IV Energy Forum
GNEP	Global Nuclear Energy Partnership
GWt/EFPD	GigaWatt ton per Effective Full Power Day
HTGR	High Temperature Gas-cooled Reactor
HTR	High Temperature Reactor
HTTR	High Temperature Test Reactor
IEA	International Energy Agency
JAERI	Japan Atomic Energy Research Institute
k_{eff}	Effective Multiplication Factor
LWR	Light Water Reactor
LEU	Low Enriched Uranium
MCNP	Monte-Carlo N-Particle
MCNPX	Monte-Carlo N-Particle eXtended
MSR	Molten Salt Reactor

MW(e)	MegaWatt electric
MW(th)	MegaWatt thermic
NEA	Nuclear Energy Agency
OECD	Organization for Economic Co-operation and Development
OTTO	Once Through Then Out
PWR	Pressurized Water Reactor
RgPu	Reactor-grade Plutonium
SFR	Sodium Fast Reactor
Th	Thorium
TRISO	TRistructural ISOtropic
TRU	Transuranic isotopes
U.S. NRC	United States National Regulatory Commission
U	Uranium
VHTR	Very High Temperature Reactor
WgPu	Weapon-grade Plutonium
wt%	weight-percent
ZAiD	Z number followed by A number for isotope identification

TABLE OF CONTENTS

Page

LIST OF FIGURES

Page

LIST OF TABLES

Page

CHAPTER I

INTRODUCTION

1.1 WORLD ENERGY OUTLOOK

A world population estimated to increase by 25% from 2010 to 2040 and a global energy demand projected to be 30% higher in 2040 than in 2010 raise remarkable challenges for our world [1]. Improving energy systems efficiency and diversifying the energy mix will be keys in sustaining countries needs and growth while reducing greenhouse gases emissions. Maintaining price stability, guaranteeing energy supply and reducing the energy dependence are likely to be substantial parameters of the world stability.

Non-OECD countries are expected to be the main actors of this energy demand change. Indeed, their global energy demand will be 60% higher in the next 30 years while OECD countries will see their global energy demand stationary [1, 2]. The total number of passenger cars will double to almost 1.7 billion in 2035. Sales in non-OECD markets will exceed those in the OECD by 2020, with the center of gravity of car manufacturing shifting to non-OECD countries before 2015 [3]. The demand in oil, the primary source of energy used for transportation, will keep growing as can be seen in Figure 1 and will stay the most widely-used source of energy [1, 3].

This thesis follows the style of *Energy Conversion and Management*.

Coal demand is expected to peak and then weaken as natural gas gradually starts to replace coal and finally overtakes it. Natural gas is projected to be 60% higher in 2040 than in 2010 [1, 2].

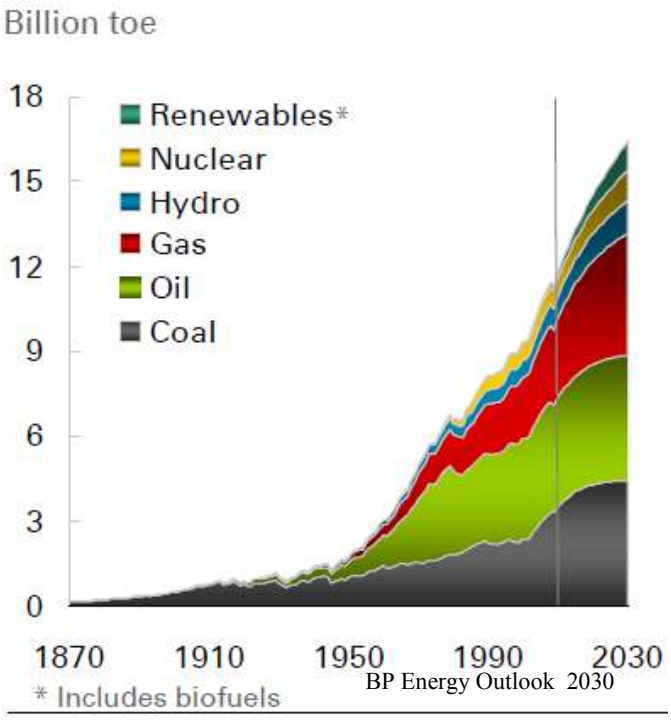

Figure 1. World Energy Use

However, replacing coal by natural gas, implementing new energy policy or improving energy technologies efficiencies will not be enough to curb the production of greenhouse gases [2] and the 2°C climate change goal is very unlikely to be met [3]. A strong reliance on oil will neither reduce energy dependence nor prices volatility.

The development of nuclear energy as the principal electricity generation source could reduce supply risks while strongly reducing greenhouse gases emissions. Indeed

32% of CO_2 emissions are due to electricity and heat production in the power sector [4]. In 2040, electricity generation should account for 40% of the global energy consumption [1].

1.2 ADVANTAGES OF NUCLEAR ENERGY

Nuclear power is currently the only source of energy that can provide electricity at an industrial scale – like oil, coal or gas – but with very limited GHG emissions. However, the renaissance of nuclear power is mostly driven by several other factors, mainly politic and economical. Indeed, energy independence can be gained by developing nuclear power. Although a majority of nuclear-powered countries import uranium ore, the latter is well-distributed around the globe and thus, no region detains a monopoly of the ore. Furthermore, the biggest producer of uranium are politically stable countries like Canada and Australia [5]. Additionally, Uranium fuel can be stored more easily than liquid oil and gas and the high energy density of nuclear fuel enables storage of more energy supplies than conventional fuels – providing supplies for longer periods of time. Also, high energy density allows smaller quantities of fuel to be bought, strengthening again the energy security of a country. Secondly, even though capital costs are high, the cost of the fuel is a minor component of the overall cost of nuclear power. Therefore the price of nuclear-produced electricity stays very stable. Moreover, contrarily to domestic renewable sources of energy – such as wind or solar plants that produce energy intermittently and that strongly depend on meteorological conditions nuclear power plants run reliably at full power most of the time, having a very high

capacity factor. A second advantage of nuclear power versus renewable energies is that nuclear energy is a proven technology with reactors producing power since 1956 and the first commercial power station Calder Hall (UK).

Finally, nuclear could replace natural gas in energy-intensive industries. The tremendous amount of heat produced by nuclear reactors has been thought to be used as process heat for petrochemical industries, for water desalinization or for hydrogen production. Should hydrogen be used as a transportation fuel, nuclear energy could gradually increase its share against oil in the transportation sector.

1.3 THE CHALLENGES OF THE NUCLEAR INDUSTRY

As stated by Yury Sokolov, IAEA Deputy Director General on the 9th June 2008, "*For the global nuclear power to be sustainable and to contribute to the world´s energy supply mix in the long term, it must respond to the challenges of further development. Among these challenges are the availability of uranium resources, management of waste, safety, public acceptance, aging of the facilities and workforce, complex infrastructure, and non-proliferation*." The availability of uranium can be improved by developing and implementing new fuel reprocessing facilities, using of recycled fuel mixes or Thorium as nuclear fuels to reduce the consumption of uranium resources. The challenge posed by nuclear wastes lies mainly in providing long-term solutions to reduce or eliminate high level nuclear waste (HLW) and transuranics (TRU).

Transuranium elements or transuranics are elements whose atomic number is above 92 (Uranium). Neptunium, with an atomic number of 93 is thus the first transuranium

element. Plutonium, Americium and Curium are other examples of transuranics. Transuranics are artificially generated isotopes created during the operation of current nuclear reactors. In commercial reactors, UO_2 is made up with LEU (Low Enriched Uranium) that is natural uranium with a ^{235}U-enrichment below 20wt%, the rest being ^{238}U. Under neutron irradiation in the reactor, ^{235}U can either fission, resulting in two or three isotopes called fission products, or can capture a neutron becoming ^{236}U. ^{236}U can also absorb a neutron, becoming ^{237}U that can decay into ^{237}Np. ^{238}U does not fission; when this isotope captures a neutron it becomes ^{239}U that decays into ^{239}Np and ^{239}Pu. Consequently, at discharge for a burnup of 50MWd/kg, used nuclear fuel contains 94% of uranium, 5% of fission products and only 1% of transuranics [6]. Even if present in a very small amount, the radiotoxicity combined with very long half-lives characterizing transuranics pose heavy burden when it comes to their final disposal.

Additionally, growing concerns regarding national and international security are rising with the accumulation of Plutonium: approximately 1,300T of Pu have been accumulated since the first nuclear reactor was set operational and about 70T are added annually in the world by nuclear power plants. This is without counting the Plutonium accumulated in nuclear weapons.

1.4 OVERCOMING THESE CHALLENGES

1.4.1 RECYCLING TRU

Therefore, providing long-term nuclear wastes solutions for the reduction or elimination of high level nuclear waste and transuranics and minimizing uranium

utilization are some of the main factors contributing in the optimization of the nuclear fuel cycle – optimization necessary to ensure a deployment of nuclear energy at a competitive price [7]. Long-term manageable solutions to nuclear wastes include the recycling of TRU arising from conventional Light Water Reactors (LWR) into advanced reactors. Advanced reactors can be of two types: fast reactors or thermal reactors.

Thermal reactors take advantage of the higher fission cross section of the fissile materials at thermal temperatures. As a consequence, these reactors can sustain fission chain reactions with a smaller fraction of fissile material than in fast reactors. However, neutron captures are also predominant at thermal temperatures, favoring the buildup of high actinides or TRU. In fast reactors, neutrons are not moderated and consequently have higher energies than in thermal reactors. The ratio of neutrons inducing fission-to-neutrons captured increasing with energy for minor actinides (MA) and Plutonium (Pu), the amount of parasitic captures is diminished in fast reactors, reducing the amount of TRU produced. In addition odd-actinides like ^{241}Pu split more easily with fast neutrons, reducing again the buildup of TRU in fast reactors. As a consequence reactors operated with fast neutrons appear superior to thermal reactors regarding the transmutation of TRU. Nevertheless, comparatively to thermal reactors, fast reactors suffer from lack of commercial scale experiences. Only 10 experimental fast reactors and 6 demonstration fast reactors reached first criticality since the 1950's [8]. Comparatively, there were 437 thermal reactors operating in the world in 2010 [9]. Therefore, in an intermediate-term future, the reduction of high-level wastes must be accomplished using proven

technologies, i.e. by building new advanced thermal reactors such as the Very High Temperature Reactor (VHTR).

The VHTR offers several advantages that should support its near-term deployment. The reactor has been designed to accept a variety of fuels in form of TRISO particles [10]. This particularity makes the VHTR a very interesting reactor in a period of transition towards the deployment of other Generation-IV reactors. Thanks to its high coolant outlet temperatures, the VHTR can also provide process heat for a wide variety of industrial applications including desalination, district heating, petrochemical applications [11] and the production of hydrogen [12]. In the current energy market landscape, this feature makes the VHTR economically more competitive than fast reactors. The characteristics of the VHTR will be discussed in more details in Chapter 2.

Finally, the use of TRU as a new fuel in advanced reactors spares uranium and thorium resources for the generations to come. Transuranics in used fuel are indeed able to produce 20% of the energy originally produced by uranium [13].

To conclude, burning TRU in advanced reactors such as the VHTR provides new sources of energy, reduces long-term storage, the environmental risks and the size capacity concerns associated with it, reduces heat loads to repositories and enhances the fuel cycle resistance against diversion of plutonium for non-civilian purposes.

1.4.2 USING THORIUM AS A FUEL

Long-term manageable solutions to nuclear wastes and energy security also include the use of Thorium as a fuel. Thorium is an isotope three times more abundant in nature than uranium [14]. Unlike the latter which contained 0.7% of fissile material in form of

^{235}U, Thorium is only made up of the fertile isotope ^{232}Th. To produce useful nuclear fuel ^{232}Th must consequently be mixed with fissile material such as ^{235}U or ^{239}Pu. The immense potential of ^{232}Th lies in its capacity to produce ^{233}U after a neutron capture and a beta-decay. Figure 2 describes the production chain of ^{233}U and shows a striking parallel between natural uranium and thorium.

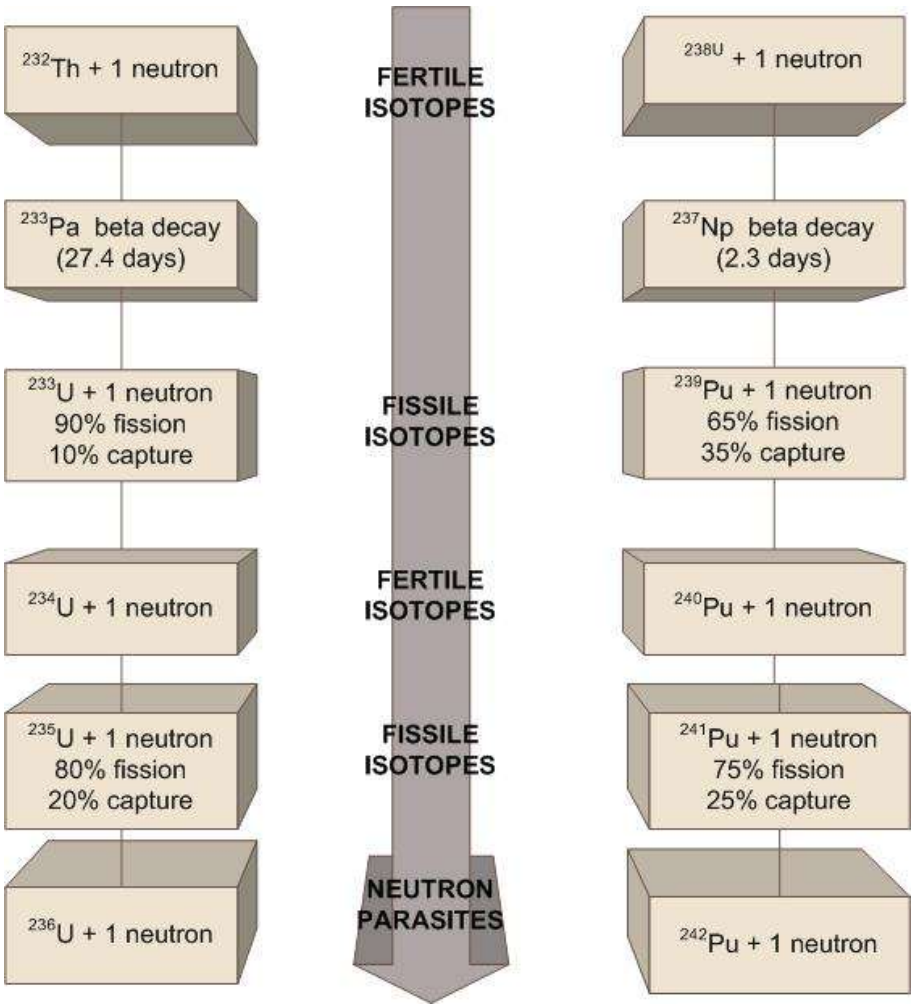

Figure 2. Parallel between ^{232}Th and ^{238}U systems

^{233}U is the best fissile isotope for thermal spectra. Indeed ^{233}U has a neutron reproduction factor η of 2.29 in average, ^{235}U of 2.05 and ^{239}Pu of 1.80. Furthermore ^{233}U shows less parasitic captures than ^{235}U and ^{239}Pu. Parasitic captures occur when a thermal neutron is capture by a fissile isotope without producing fission. Reducing the amount of parasitic captures improves neutron economy and reduces the creation of higher actinides such as ^{236}U or ^{240}Pu, respectively created by ^{235}U and ^{239}Pu. The capture cross section of ^{232}Th being higher than that of ^{238}U, ^{232}Th produces more ^{233}U than ^{238}U produces ^{239}Pu. Breeding - the ability of a reactor to produce more fissile fuel than it consumes - has been demonstrated in the Shippingport light-water reactor in the early 1970s in the United States. High Temperature Gas-cooled Reactors (HTGR) operated successfully with Thorium-based fuel in the U.S.: the Peach Bottom I reactor operated from 1966 to 1974 and the Fort St. Vrain reactor from 1977 to 1989. In Germany, an experimental AVR (Arbeitsgemeinschaft Versuchsreaktor) of 15MW(e) was operated between 1967 and 1989 showing remarkable performances: 80,000 pebbles were loaded in the reactor for a period of 2 to 6 years and a burnup of 100,000 MWd/t was reached. The pebbles underwent a maximum temperature of 1,350°C without any damage. The THTR, for Thorium High Temperature Reactor, was also operational in Germany from 1986 to 1989. In the U.K. the Dragon reactor was in operation from 1966-1975. All were fueled with a U-Th fuel [15, 16].

The first interesting feature of Th-based fuels is that they produce less MA, reducing the toxicity and facilitating the reprocessing of spent fuels. An IAEA study has found that a ^{233}U + ^{232}Th fuel produces 3g/tHM (ton of Heavy Metal) of ^{237}Np against

900g/tHM produced by a ^{235}U+ ^{238}U fuel, 1.8e-3g/tHM of Am against 470g/tHM and 6.37e-4g/tHM against 220g/tHM after discharge of a 60MWd (Mega Watt-day) burnup fuel [17].

Also, being among the highest known refractory isotopes (ThO_2 melting around 3300°C), quadrivalent Thorium and its compounds provide stability at high temperatures and high burnups, making Thorium a fuel of choice for HTR [17]. High burnups enable HTR to display amazing capabilities in Pu destruction with minimizing the production of secondary Pu. Secondary Pu isotopes are currently produced in reactors using MOX (Mixed OXides) fuels from neutron captures in ^{238}U. If ^{238}U is replaced by the fertile ^{232}Th, ^{233}U will be created instead of Pu isotopes. Consequently instead of creating very radiotoxic isotopes of Pu that will have to be disposed, Thorium-based HTR produce new fresh nuclear fuel that can be burnt inside the reactor, reducing the amount of fuel to be used. A pebble-bed HTR fueled with ^{233}U, ^{232}Th and weapons-grade Pu (^{239}Pu, ^{240}Pu, ^{241}Pu and ^{242}Pu) displayed ^{239}Pu utilization of 95.3% [18]. Thorium-based fuels have shown capacity to destroy 88.2% of civilian ^{239}Pu and 95.3% of weapons-grade ^{239}Pu initially loaded [17]. Therefore Th-based fueled reactors produce two orders of magnitude less radioactive wastes than current LWR [19] reducing the size of repositories for final disposal of HLW.

Regarding proliferation, both U-based and Th-based fuels produce fissile material that can be diverted to create a nuclear explosive device. ^{232}Th produces ^{233}U and ^{238}U produces ^{239}Pu. In both cases only 8kg of the fissile material would be necessary to develop one small device. However, the production of ^{233}U from ^{232}Th leads to a buildup

of ^{232}U in the fuel whose daughters produce very highly penetrating gamma-ray enhancing the detection of ^{233}U diversion or production [20]. These gamma-rays also make the handling of ^{233}U very challenging. Stockpiles of ^{233}U-based weapons could not be accumulated. However it still seems possible to use ^{233}U to assemble both gun and implosion type nuclear weapons even though it is much easier to do so with ^{235}U for the gun type and with ^{239}Pu for the implosion type [21, 22]. Additionally, the lack of engineering knowledge comparatively with Pu-based weapons and the difficulty to test successfully a ^{233}U-based weapon under the current moratorium make the development of such a device a challenge [23]. Finally Th-based reactors produce less weapon-usable Pu [21, 24] reducing the possibility of creating a weapon from Pu. Nevertheless Thorium reactors are not inherently proliferation resistant. Th-reactors have to be started with a fissile material like ^{235}U or ^{239}Pu until they reach the point where they have produced enough ^{233}U to maintain criticality. As a consequence, LEU or Pu could be diverted in the same way as in U-based fuel cycles. To prevent the diversion of ^{233}U, Th-based reactors will have to be designed in such a way that the ^{233}U produced is entirely consumed at EOL.

Thus, HTR fueled with Thorium may show improved proliferation resistance and participate in the reduction of HLW and TRU. Integrating Thorium in the nuclear fuel cycle also reduces the utilization of uranium resources and enhances the energy independence of countries having reserves of Thorium. All these reasons justify the study of TRU transmutation in VHTR with Thorium-based fuel.

1.5 OPTIMIZING FUEL CYCLES MODELING: A MULTI-PARAMETRIC PROBLEM

Integrating different reactor technologies into a viable system or cycle is a complex task. It is indeed a multi-parametric optimization problem: HLW, fission products (FP) and uranium utilization have to be minimized while maximizing reactor performances like the core lifetime and the electrical power production. Safety and proliferation concerns add constraints along with the production of energy at a competitive price. The output parameters thus depend on a multitude of input data, among them nuclear data. The latter have been evaluated with more or less accuracy and therefore some of them contain significant uncertainties. These uncertainties are propagated in the calculations along the fuel cycle and participate in the outputs' uncertainties. Therefore the accuracy of fuel cycle parameters and reactor physics metrics cannot be assessed without performing sensitivity calculations to evaluate the effects of nuclear data variations on the former parameters. Evaluating the current accuracy of the output results determine whether the fuel cycle is viable or not. Additionally it enables back-to-front thinking, where the required data accuracy is only determined once fuel cycle performances objectives have been quantified and fixed. It thus stresses the particular nuclear data requiring reevaluation and the specific parts of the fuel cycle demanding higher modeling fidelity.

1.6 EXISTING UNCERTAINTIES IN NUCLEAR DATA

With increasing requirements regarding safety and competitiveness, higher accuracy in neutronics calculations is required. Advances in computational simulations have been made but full benefit from these improvements will only be obtained if parallel efforts to reduce nuclear data uncertainties are implemented [25]. Nuclear data, such as cross sections and fission spectrum, constitute input parameters at numerous points of the nuclear fuel cycle. Its performance and competitiveness are thus very likely to be sensitive to nuclear data. Fuel cycles designed for transuranics incineration will require more accurate data for higher actinides such as Pu, Am, or Cm. In the preliminary conclusions of the 2007 SG26 meeting, the inelastic cross-section uncertainties of ^{238}U, in the 0.498-6.07 MeV energy range, were evaluated at 10-20% while a target of 2-3% was established. A target accuracy of 4-7% in the 2.04-498 keV region was estimated by SG26 for the capture cross-section of ^{239}Pu while the current evaluation lied in the 7-15% range [26]. In the case of a VHTR, the SG26 requested in particular higher accuracy for the capture cross-sections of ^{239}Pu and ^{241}Pu below ~0.5 eV. The ^{241}Pu fission cross section had also to be improved below ~400eV [27]. In a previous study, the required cross-section uncertainties to meet design target accuracies were 1.9% of $\Delta k/k$ between 454eV and 22.6eV for the capture cross-section of ^{238}U and 1% between 0.10eV and 0.54eV for the fission cross-section of ^{239}Pu. The uncertainties in year 2006 were above the required values, being respectively 3% for ^{238}U and 2% for ^{239}Pu. The capture cross-section of ^{243}Am had a required uncertainty of 12.4% for a current uncertainty of 20% between 0.54eV and 4eV [28].

Neutron capture cross sections have been found discrepant mostly because of the difficulty of the measurements. In a particular study [29], the capture cross sections for ^{234}U have been found as much as 20% lower than the ENDF/B-VI evaluation in the keV region. The results for ^{236}U were consistent with the ENDF/B-VI evaluation. But discrepancies of 40–50% among the various evaluations for neutron capture on ^{238}Pu in the keV region were found. A dual parallel-plate avalanche counter fission-tagging detector was used for this study to overcome the presence of γ-rays arising from low energy neutron-induced fission.

Because reactor calculations codes rely heavily on these experimental data or on their best evaluations, it is necessary to measure the impact of nuclear data uncertainties/variations on the reactors parameters of paramount importance in fuel cycles design. The choice of the best fuel cycle option will depend on the accuracy level of the simulation.

1.7 OBJECTIVES

This thesis is focused on the evaluation and comparison of different TRU minimization strategies and the quantification of nuclear data variations effects on performance characteristics of an AP1000-VHTR fuel cycle. More explicitly, transuranics arising from a Gen-III+ Pressurized Water Reactor, the AP1000 reactor, will be considered as the fuel loading of a VHTR.

To attain this objective, the effort is divided into the following sub-objectives.

1. *Evaluation of nuclear data discrepancies* among nuclear data libraries. Radiative capture cross sections, fission cross sections and fission spectra of ^{235}U, ^{238}U and TRU are parameters of particular interest. Indeed the transmutation capabilities of a reactor rely strongly on these data. Discrepancies among these data could harm the accuracy of the reactors and fuel cycle parameters.

2. *Selection of parameters* describing reactors behavior and measuring fuel cycle capability of performing TRU destruction. The effective multiplication factor, the core lifetime, the fission spectrum and the transmutation efficiency of each reactor have been chosen to describe reactor parameters. The TRU destruction rate of each AP1000 – VHTR cycle determines the cycle ability to transmute TRU into higher actinides.

3. *Creation of reference cases* connecting the AP1000 and the VHTR into an interacting system of reactors aimed at producing electricity while preserving uranium resources and reducing the amount and the toxicity of nuclear wastes. Reference cases permits the establishment of reference values for each of the parameters studied. Reference values are mandatory when it comes to assessing variations in the results following changes in the input data of any calculation or experiment. They enable the comparison providing the amount of changes observed in the output data. Creating reference cases and references values was thus mandatory for the purpose of the present research.

4. *Variation of the fission spectrum and the corresponding sensitivity/uncertainty analysis at the system performance level*. The sensitivity of the reactor parameters and TRU destruction metric against these variations will be evaluated. One reactors

configuration is rerun with different altered fission spectrum and the values of the parameters are compared with their values in the reference cases.

These sub-objectives lead to a first analysis methodology developed in the next paragraph.

1.8 METHODOLOGY

An approach is sketched below to quantify the impact of nuclear data variations on the TRU transmutation performances parameters of the fuel cycle under study. This approach also tends to minimize uranium resources depletion through the use of Thorium based fuels.

1. In order to quantify nuclear data discrepancies between libraries, the NEA software JANIS is used [30].

2. The effective multiplication factor and the core lifetime being relevant parameters in fuel cycle design, they were decided to be computed for each reactor configuration. The effective multiplication factor defines the criticality condition in a finite system where neutron leakage is taken into account. It measures the ability of the reactor to self-sustain the neutron chain reaction. It is thus a parameter of paramount importance in any kind of reactor calculations. The core lifetime of a reactor – or its capacity to stay critical – is intrinsically related to the effective multiplication factor. It plays an important role in designing advance fuel cycles. But these two parameters do not measure the ability of a reactor or fuel cycle to transmute TRU. To do so, nuclide inventories at end of cycle and energy spectra will be evaluated to assess the transmutation efficiency. The latter

measures the fuel cycle ability to transmute TRU into less radiotoxic isotopes. It is defined as the percentage of initial fuel the TRU left at the end of life represent. Numerous studies have been conducted regarding the transmutation of TRU in thermal or fast reactors, encouraged by several programs such as the Advanced Fuel Cycle Initiative (AFCI), the Global Nuclear Energy Partnership (GNEP) or the Generation IV Energy Forum (GIF). Most studies include TRU destruction rates to justify the TRU transmutation efficiency of their fuel cycles. For instance, in a study focused on the destruction of ^{237}Np in a Supercritical CO_2-cooled Fast Reactor, the ^{237}Np consumption rate was found to be ~69kg/yr [31]. In the case of a fuel cycle consisting of a Deep-Burn Modular Helium Reactor (DB-MHR) followed by a Sodium Fast Reactor (SFR), the TRU consumption rate in the SFR was fixed at 250kg/GWt/EFPY (GigaWatt tons per Effective Full Power Years) [17]. In another study, where a DB-MHR is fueled with waste Pu and Np on one hand and TRU on the other hand, about 75% of the LWR TRU wastes and about 99% of the ^{239}Pu are destroyed [13].

3. To report the reactors behavior and compute their effective multiplication factor, core lifetime, nuclide inventories, or energy spectra, high-fidelity MCNPX models of the AP1000 fueled with 3% ^{235}U-enriched uranium and of the VHTR fueled with 15%-enriched uranium are used.

4. To analyze the performances of advanced nuclear fuel cycles and enable comparisons, a set of reactor configurations is created. In particular the VHTR fuel will be changed from UO_2 to TRU. The previous reactor parameters are computed again, analyzed and constitute the reference values that will be compared against.

5. TRU-fueled VHTR cases are re-run using a different set of prompt neutron fission spectrum evaluations. The parameters of interest are computed one more time and confronted to their reference values.

6. Similar efforts are conducted for a fuel cycle where the fuel UO_2 has been replaced by ThO_2, that is, where ^{238}U has been replaced by ^{232}Th.

CHAPTER II

AP1000 AND VHTR: THEIR ROLE IN THE FUEL CYCLE

2.1 THE FUEL CYCLE

2.1.1 AP1000

The AP1000 reactor designed by Westinghouse Electric Company LLC. has been selected for the study as it will be part of the nuclear landscape within several years. Six units are currently been built in the Zhejiang province in China and six others are under construction in the Shandong province. Operation is scheduled for 2013-14 and 2014-15 respectively. In the U. S. the AP1000 is the first Gen-III+ reactor to have received final design approval and standard design certification by the U. S. Nuclear Regulatory Commission (NRC). Combined License Applications for New Reactors have been issued by the U. S. NRC at seven different sites authorizing the licensee to construct and operate AP1000 reactors [32]. The AP1000 is a two-loop PWR capable of producing 1,154 MW(e). It is an evolutionary modification of the AP600 modular PWR. The design, in particular regarding the passive safety systems, is considerably simpler than conventional Gen-II and III PWRs: the AP1000 has 50% fewer valves, 35% fewer pumps, 80% less pipes, 45% less seismic building volume and 85% less cables than a conventional 1,000 MW(e) PWR. Simplification of the design guarantees lower operational and maintenance costs and shorter construction time. The AP1000 also has enhanced safety characteristics: neither AC power for safety systems to operate is required nor any action has to be taken during the 72 hours following an event [33].

These particularities make the AP1000 an attractive reactor and should warrant its worldwide deployment. However all these improvements will not prevent the AP1000 – a thermal reactor designed to be operated with UO_2 or mixed-oxides fuels – to produce high level nuclear wastes. In addition, should many more of thermal reactors to be built in a once-through then out (OTTO) cycle, the world's reserves of affordable uranium will be depleted within the next century [34]. The deployment of new and much more efficient nuclear fuel cycles recycling nuclear wastes into new nuclear fuel provides solutions to these challenges. From this perspective, the VHTR has been chosen to complete the fuel cycle and recycle TRU inventories arising from the AP1000 in a near-term future.

2.1.2 VHTR

The VHTR is a Gen-IV graphite-moderated helium-cooled high temperature reactor (HTR) with a thermal neutron spectrum. The reactor core can be of two types, in prismatic block configuration like the HTTR operating in Japan or a pebble bed core such as the Chinese HTR-10 (High Temperature Test Module). Although it is still a conceptual reactor, it is based on well-proven technologies implemented in High Temperature Gas Cooled Reactors (HTGR). HTGR have been built and operated in the U. S., in Germany and in England. The Peach Bottom reactor Unit 1 in the United States was the first HTGR to produce electricity successfully from 1966 to 1974 for demonstration. In addition, the VHTR has generated particular interest from the U. S. Department of Energy by its ability to supply heat for various energy-intensive industries such as seawater desalination, hydrogen production or process heat for the

petrochemical industry. A 600MW(th) VHTR dedicated to hydrogen production can indeed yield over 2 million cubic meters per day [35]. The VHTR also shows improved passive safety. The use of TRISO particles – for TRIstructural ISOtropic – ensures extra-safety by showing a great resistance to cracks at temperatures beyond 1,600°C and by providing containment for fission products within the coating during normal operation and during accidental temperature excursions. TRISO particles can be seen in Figure 12 later in this chapter.

Core outlet temperatures higher than 1,000°C provide higher thermal efficiency and reduce the size of gas turbines thus diminish the construction, operation and maintenance costs [35]. All these characteristics are particularly appealing and make the VHTR the most probable Gen-IV nuclear reactor to be built in a near future – where present needs have to be met without jeopardizing the ability of future generation to prosper. For the purpose of this work the VHTR is also appealing as it yield significant TRU wastes reductions while recovering more energy from the original fuel. TRU destruction rates approaching 40% in the VHTR and even up to 70% for the ^{239}Pu have been reported [36]. Another study reported TRU destruction rate of 63.7% in a DP-MHR [37]. Graphite used as moderator has the advantage to provide more neutrons in the intermediate energies range than light water moderated reactors. Neutrons lose less energy per collision with graphite atoms than with H_2O thus increasing the diversity in neutrons energies in the slowing-down energies range. The probability that the energy of a neutron will match that of a resonance and transmutes a transuranic isotope is thus increased [13]. For all these reasons the VHTR has been selected as the reactor

incinerating TRU in the present work. The different roles a VHTR could play in the energy market are discussed in the next paragraph and stress its versatility and adaptability.

2.2 ROLES OF THE AP1000 AND THE VHTR IN THE MODERN ENERGY LANDSCAPE

With an electrical power output of 1,154MW(e) and regular fuel pins the AP1000 was certainly designed to produce baseload electricity.

On the other side, with a thermal power more than 5 times lower than that of the AP1000, higher core outlet temperatures and with the use of TRISO particles, the modularity of the VHTR is increased. Indeed, lower electrical outputs can satisfy a wider range of electrical needs. The VHTR can be deployed in regions with small electrical grids or in remote locations. Moreover, the very high core outlet temperatures are an asset to supply district heating, support potable water production or energy for energy-intensive activities [38]. For example, in remote oil sands or gas shale, the VHTR could be used to power the settlement as well as produce the required heat to support the oil production [39].

In the present work, other assets of the VHTR are of interest. As explained in paragraph 2.1.2 TRISO particles permit the use of a variety of fuels such as TRU-based fuels. Higher core temperatures and the use of graphite as a moderator improve the transmutation of TRU into less radiotoxic actinides. Thus, in this study, the VHTR was chosen as part of a nuclear system optimizing nuclear wastes minimization. The role of

the VHTR in this system is therefore to transmute TRU wastes arising from the AP1000. The role of the latter is to produce baseload electricity as expected. With this configuration, should the VHTR be only fueled with TRU, it was found that the amount of TRU that could be loaded in one VHTR core was the equivalent of the amount of TRU produced by up to four AP1000 cores operated for two years.

However, the feasibility the TRU- based fuels used herein has not been studied. Further work is needed to assess the structural resistance of these fuels to high temperatures or to evaluate the practicability of producing TRU-based TRISO particles at an industrial scale. The use of TRU-based fuels is also very likely to raise regulatory issues which would have to be investigated.

This study focuses on the performance sensitivity of these nuclear reactor configurations to nuclear data variations. Nuclear data uncertainties have a potential to make a substantial impact on nuclear-related calculations. Evaluation and understanding of their impact on reactor parameters are of paramount interest. Computational models of the reactors used in these evaluations are presented in the next section.

2.3 MODELS USED FOR THE REACTORS

This section describes the computational models used for the AP1000 and the VHTR. Both reactors had been modeled with MCNP. Use of MCNP for reactor simulations has been extensively benchmarked in previous studies.

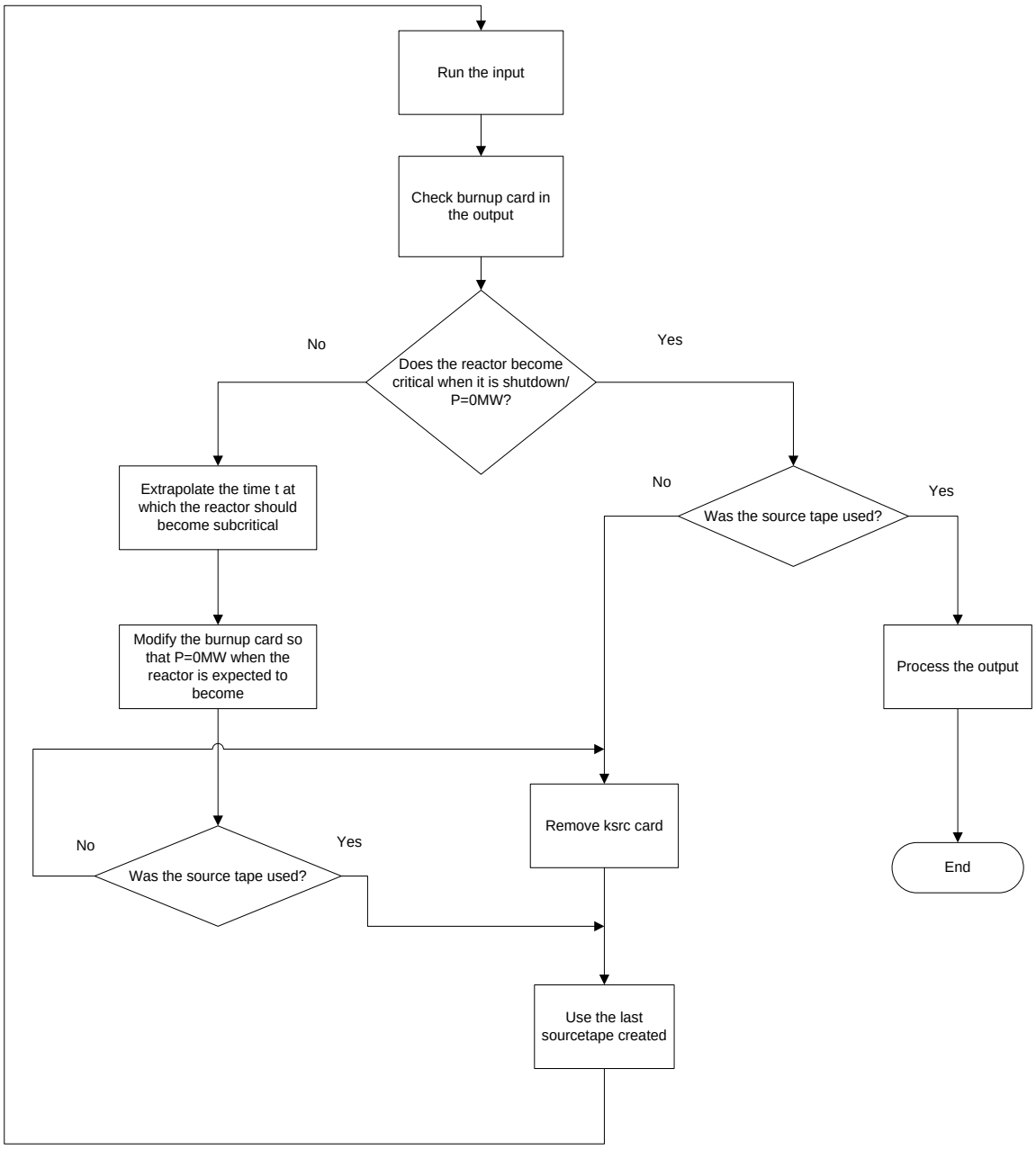

Figure 3. Computational Method used to Produce the Results

The computational method used to produce the results is described in Figure 3. First, the input was run. Once the output was produced, the burnup card was checked to see if the

reactor is shutdown when k_{eff} is approximately one. If not, the expected time at which k_{eff} =1 was extrapolated, the burnup steps modified and the input was run again using this time the source tape (SRCTP file) created during the first run. The source tape contains the initial distribution of the fission neutrons. Using the SRCTP file will make the problem converge to a stable k_{eff} in fewer generations. It is critical that k_{eff} has converged before the computation of the tallies to ensure the accuracy of the results. Thus even if k_{eff} becomes 1 when the power is set to 0 in the output, the file will have to be run again using the SRCTP file.

2.3.1 AP1000

The AP1000 model was based on the AP1000 Design Control Documentation [40] provided by the U.S. NRC.

The core modeled has a diameter of 304.4cm and an active core height of 426.72cm. There is a total of 86T of fuel disseminated among 41,448 fuel rods. The latter are grouped in assemblies containing 64 fuels rods, 24 guide tubes for control rod clusters and one centrally located guide tube for in-core instrumentation in a 17 x 17 square array. The 157 fuel assemblies are arranged in an approximately right cylinder pattern. Assemblies with three different enrichments were included to represent the AP1000 core following the design specification targeting a better radial power distribution. The fuel assembly loading pattern used for the AP1000 model is shown in Figure 4. Each plain square represents an assembly. MCNP Visual Editor was used to produce the cross sectional area of the reactor seen in Figure 4. The uranium enrichment in both radial and axial directions of any fuel rods within any assembly is the same conformably to an

initial core loading. Some of the fuel rods are also mixed with burnable absorbers. Burnable poisons and burnable absorbers have high neutron absorption cross sections and are converted in materials having a relatively low neutron absorption cross section after absorbing a neutron.

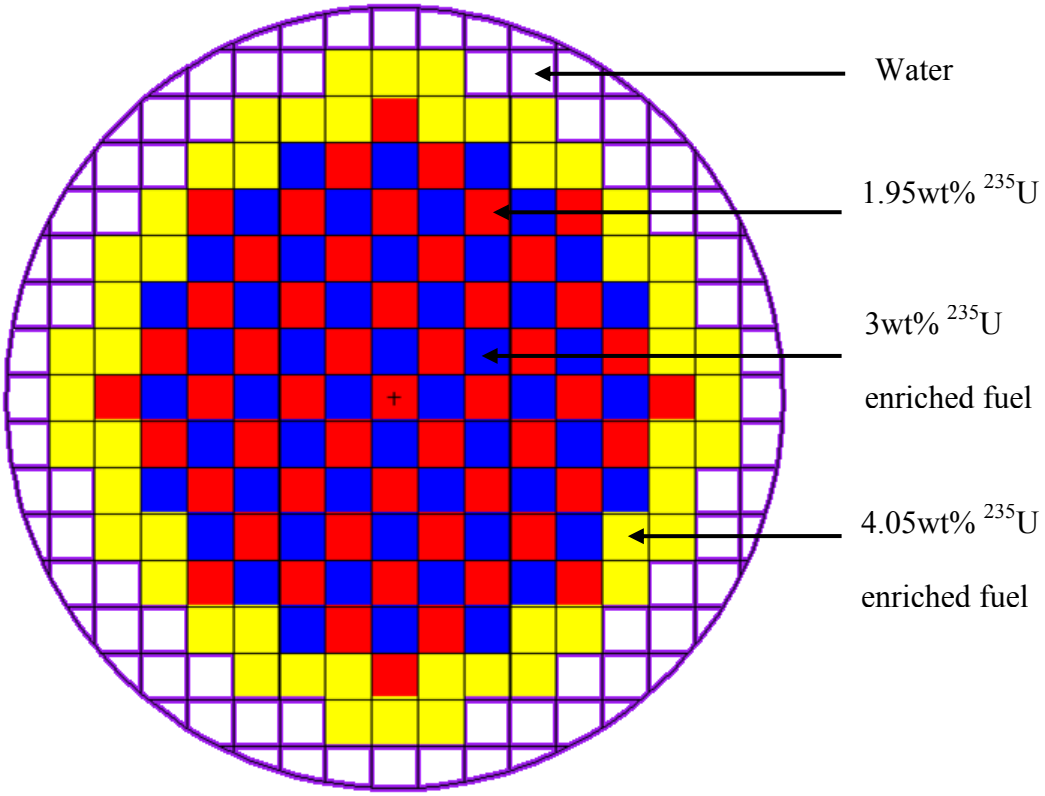

Figure 4. AP1000 Cross Sectional Reactor Map (obtained from MCNP Vised)

Their role is to remove the excess reactivity of the fuel, particularly at BOL. Fixed burnable poisons also reduce power peaking at locations in the core where the power is suspected to peak. They thus homogenize the radial power distribution in the core resulting in a better consumption of the fuel. 24 discrete burnable poison absorbers rods

can be seen on the assembly cross section obtained with MCNP Visual Editor and illustrated in Figure 5.

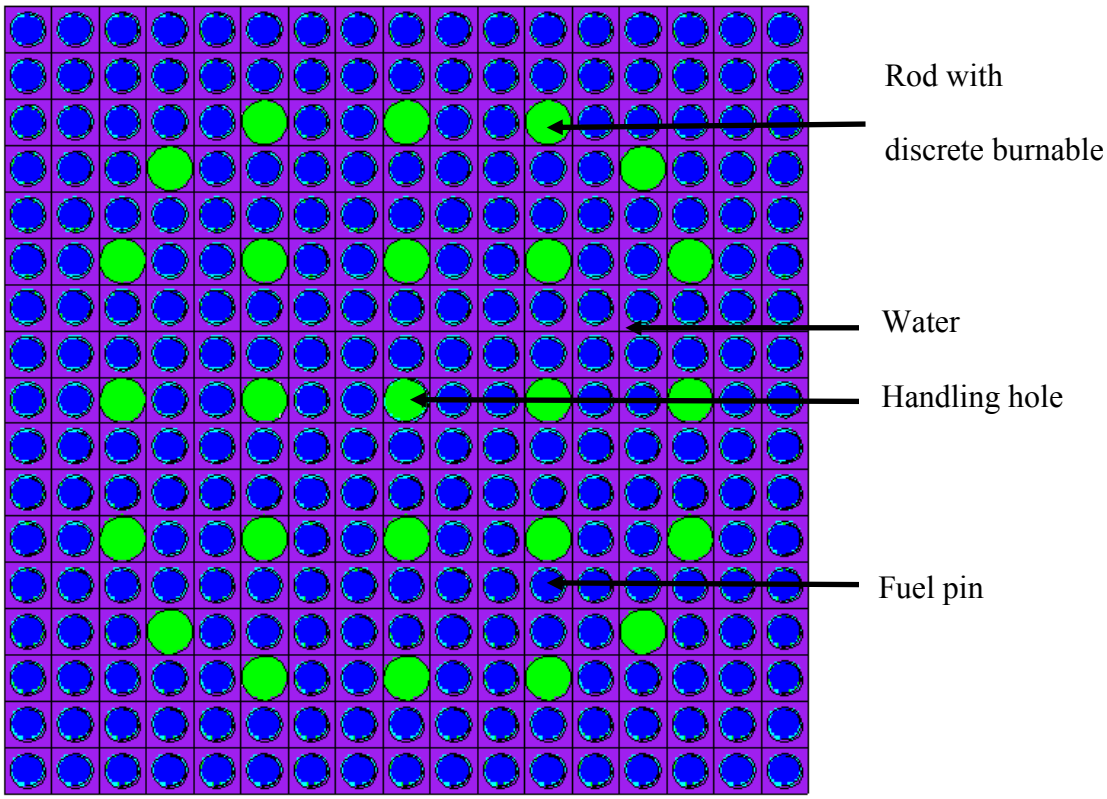

Figure 5. AP1000 Fuel Assembly Cross Section (obtained with MCNP Vised)

With such a configuration, a moderator-to-fuel ratio of 8.65 was calculated. It corresponds to the atomic ratio (H+O)/U. The moderator-to-fuel ratio measures the amount of moderator with respect to the amount of heavy metal in a unit cell. The cell chosen was a fuel pin surrounded by moderator (water). A cross sectional view of the

unit cell is displayed in Figure 6. A better thermalization of the neutron spectrum is logically observed with higher MFR.

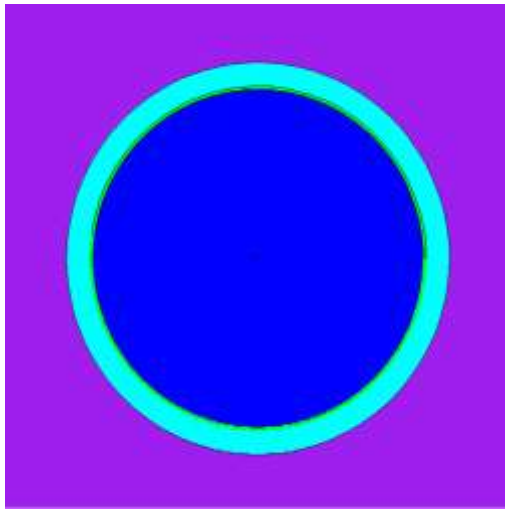

Figure 6. Unit Cell used to calculate the MFR

The energy spectrum per unit lethargy is illustrated in Figure 7. It is the energy spectrum in a fuel rod containing 4wt% ^{235}U enriched UO_2. The peak at low energies (below 1.0eV) corresponds to the thermalization of the neutrons. It means that the neutron energies are comparable to the energy of the surrounding nuclei and the latter cannot be considered at rest any longer. In this region, neutrons finally come into thermal equilibrium with the surrounding nuclei. In the slowing down region, between 1.0eV and 0.1MeV, the energy spectrum per unit lethargy is approximately constant. The spectrum peaks again in the fission region between 0.1MeV and 10MeV. Numerous depressions are observed in this region: neutrons are removed from the region after having scattered

against the oxygen atoms present in the moderator. This energy spectrum corresponds to a typical PWR energy spectrum.

These results were obtained using 3500 particles per cycle, 200 cycles and ignoring the first 60 cycle for the AP1000. The material cards used in MCNP are detailed in Appendix A.

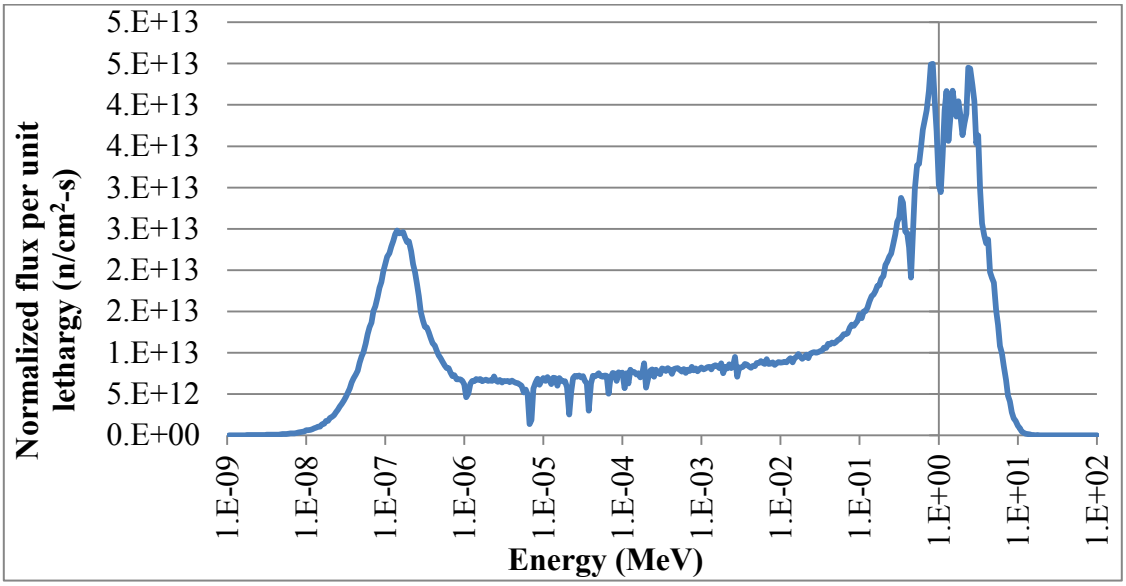

Figure 7. Energy Spectrum of the AP1000 fueled with 4wt% enriched UO_2, T_{fuel}=1200K

With this configuration, about 775kg of TRU were produced by the AP1000 at shutdown.

2.3.2 VHTR

The VHTR is a scaled-up evolutionary extension of the HTTR. This specific configuration was created for the present analysis. Therefore a large fraction of the

design was developed and scaled-up from documentation existing for the High Temperature Test Reactor (HTTR) of the Japan Atomic Energy Research Institute [41].

The VHTR prismatic core was modeled with 102 hexagonal blocks arranged in a hexagonal lattice of columns to form a cylindrical core. 17 blocks piled on top of each other form a column – the active core consisting of 13 block-high columns only. There are 66 fuel columns and 36 control columns. The fuel and control columns are placed in a configuration designing a 3 block-wide annular core with a thickness of 108cm. The outer reflector is 88cm thick and the center of the core is at 144cm from the closest fuel block.

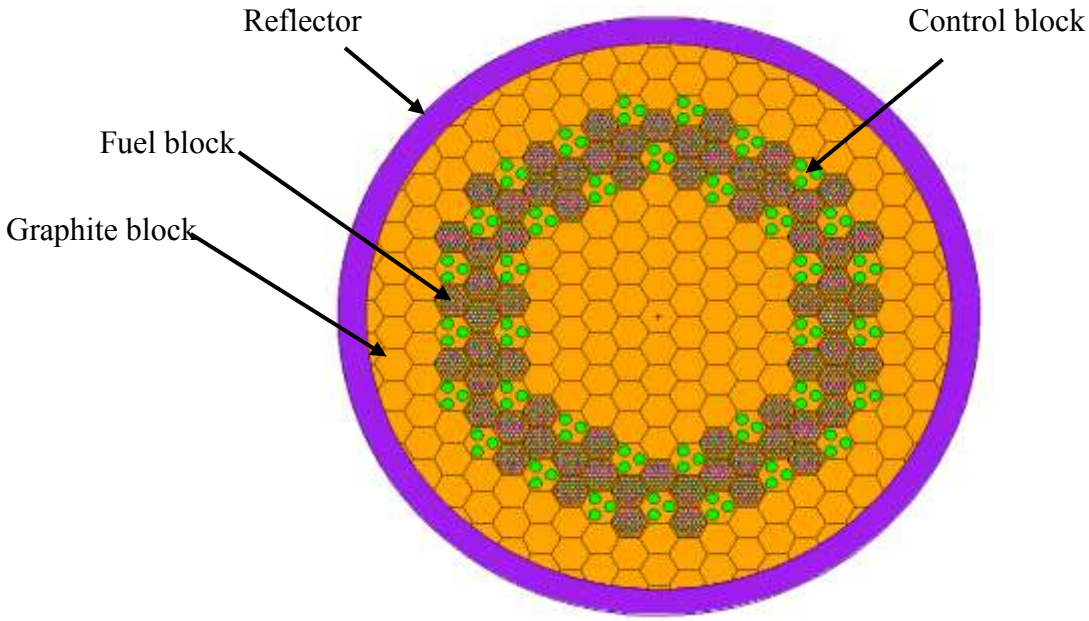

Figure 8. VHTR Core Cross Sectional View obtained from MCNP Vised

The overall radius of the core is thus 340cm. The bottom reflector is 160cm thick and the top reflector is 116cm thick. The core is 1030cm high with an active length of 754cm. A cross-sectional view of the core can be seen in Figure 8.

Each fuel block is perforated with 33 vertical boring to contain the 33 fuel compacts and their Helium coolant channel. 3 other thinner boreholes have also been drilled. Two of these holes are filled with burnable poison absorbers rods. The burnable absorber rod is composed of two sections of burnable poisons separated by 10cm of graphite. A cross sectional view and a transversal view of the fuel block are illustrated in Figure 9 and Figure 10.

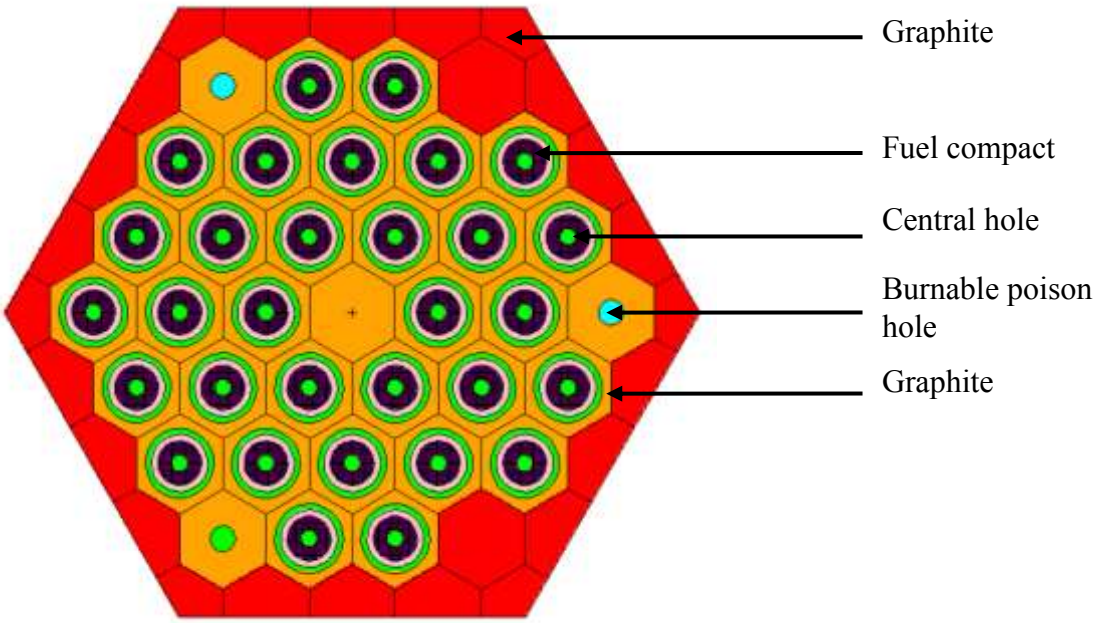

Figure 9. VHTR Prismatic Fuel Block Cross Sectional Area (obtained from MCNP VisEd)

The control rod guide blocks are also perforated to allow the control rods to be inserted through the blocks. The shutdown hole is only used for shutdown and thus is left empty from control rod during operations.

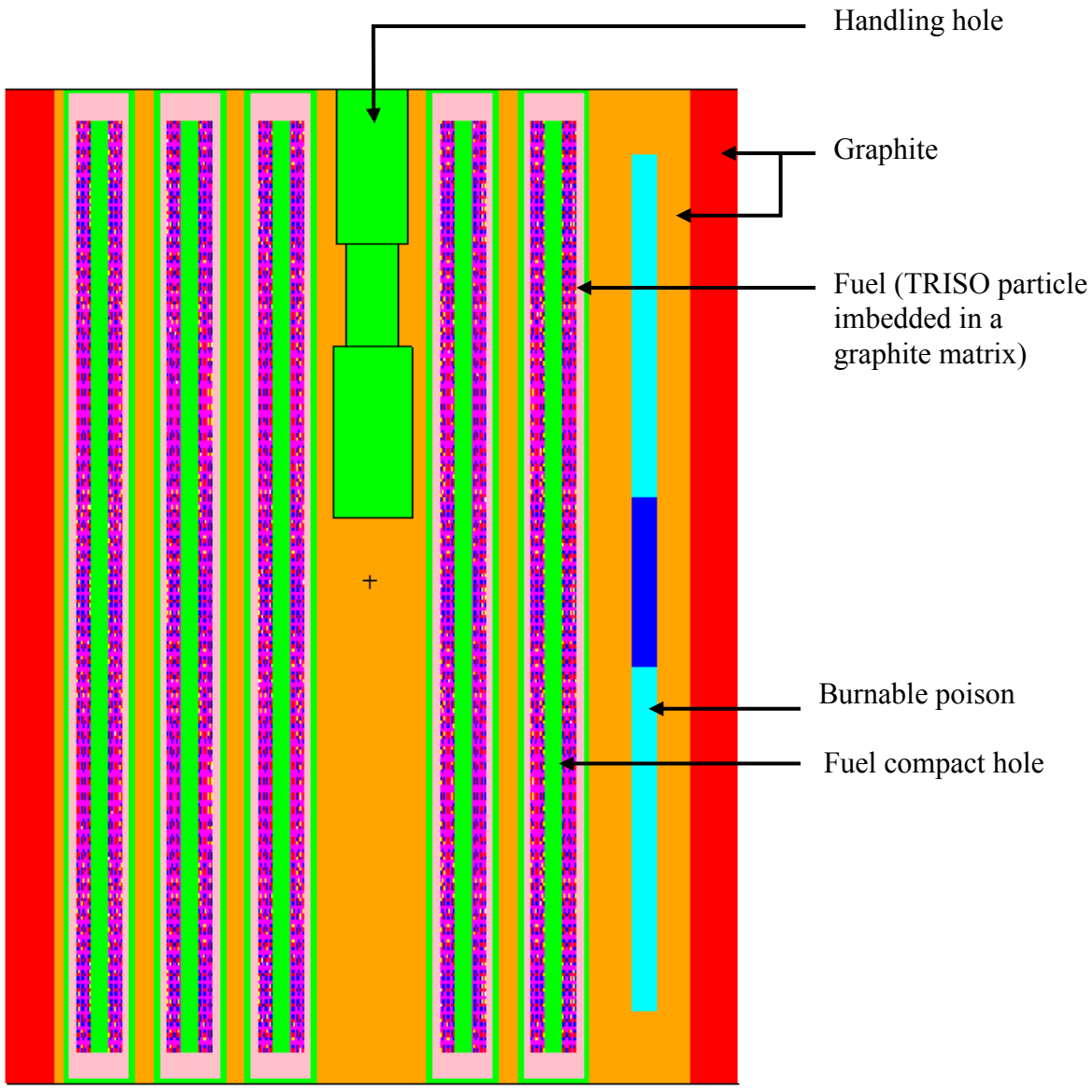

Figure 10. VHTR Prismatic Fuel Block Transversal View (obtained from MCNP VisEd)

The graphite blocks can be of two types. Some are simply solid graphite blocks and are located at the exterior of the core and inside the annular core. The role of these blocks is to reflect neutrons back in the core. They reduce neutron leakage and allow the mass of fissile material to be diminished thus cutting down the size of the reactor. It also limits the ratio of peak flux to the flux at the edge and then increases the core average power level without any changes in the maximum power. The central graphite core also flattens the radial power distribution and allows the fuel temperature to decrease in case of loss of coolant accident without substantial active heat removal [42]. The second type of graphite blocks are used as moderator blocks and are located above or below the fuel blocks (2 of them above the 13 fuel block-column and 2 of them below). These graphite blocks have also been perforated to allow coolant channels to pass through. The graphite blocks have the same dimensions as the fuel blocks. A solid graphite block is displayed in Figure 11. The graphite has been set translucent so that the handling hole can be seen.

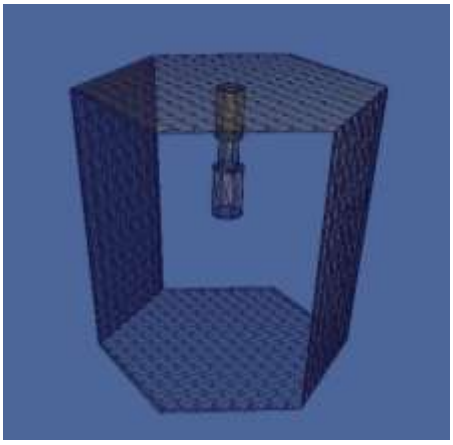

Figure 11. VHTR Replaceable Reflector Block

TRISO particles were modeled as 0.0465cm-diameter spheres having a fuel (UO_2 or ThO_2) kernel of 0.03cm in diameter. 176,515 TRISO particles were modeled per fuel compact using a square lattice array imbedded in a graphite matrix. The packing fraction was 20%. Figure 12 illustrates how the TRISO particles were modeled in MCNP and compared them to an actual TRISO particle.

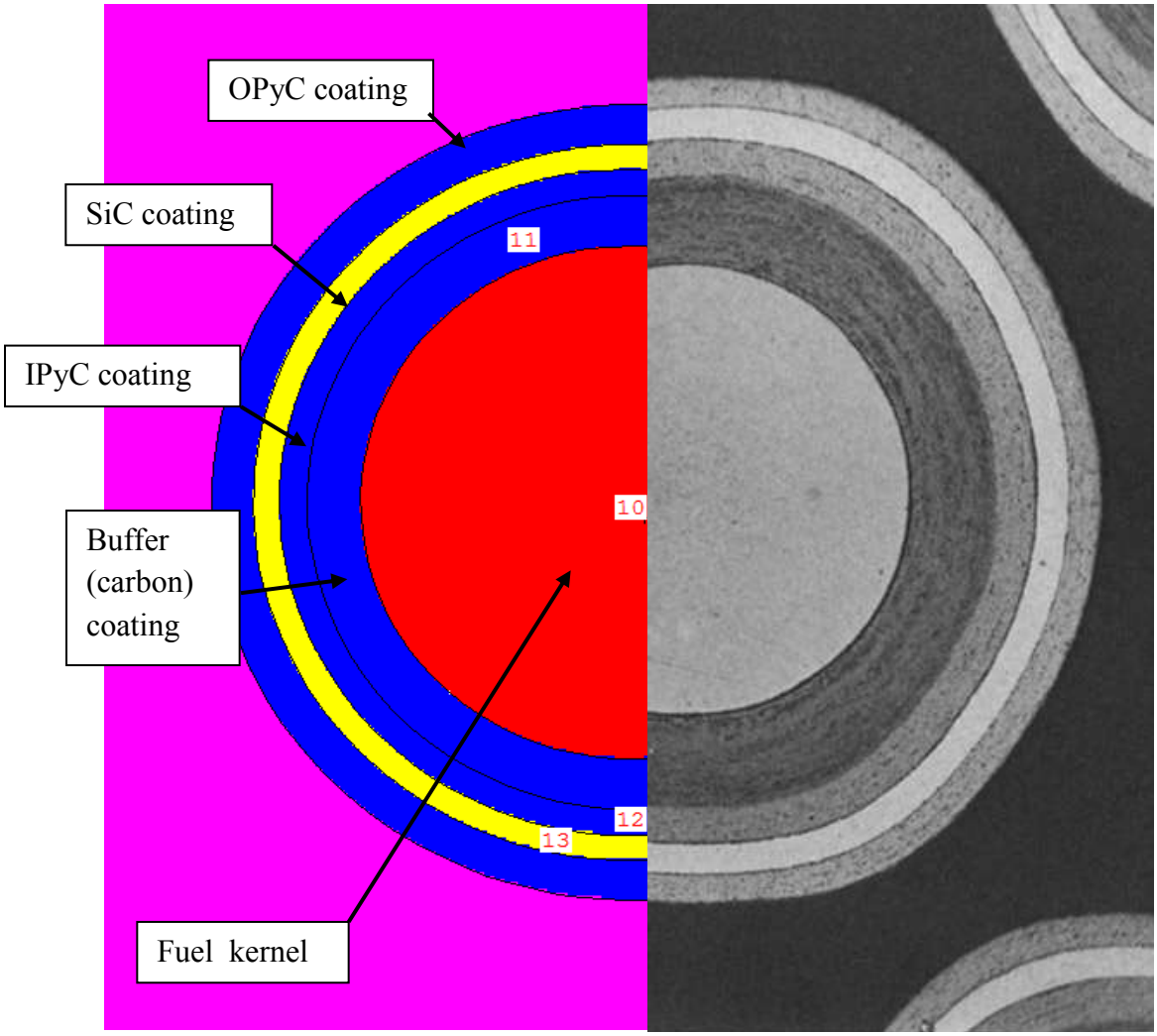

Figure 12. TRISO Particle as Modeled in MCNP (left)

The energy spectra of the VHTR fuel compact obtained from the MCNP calculations is illustrated in Figure 13.

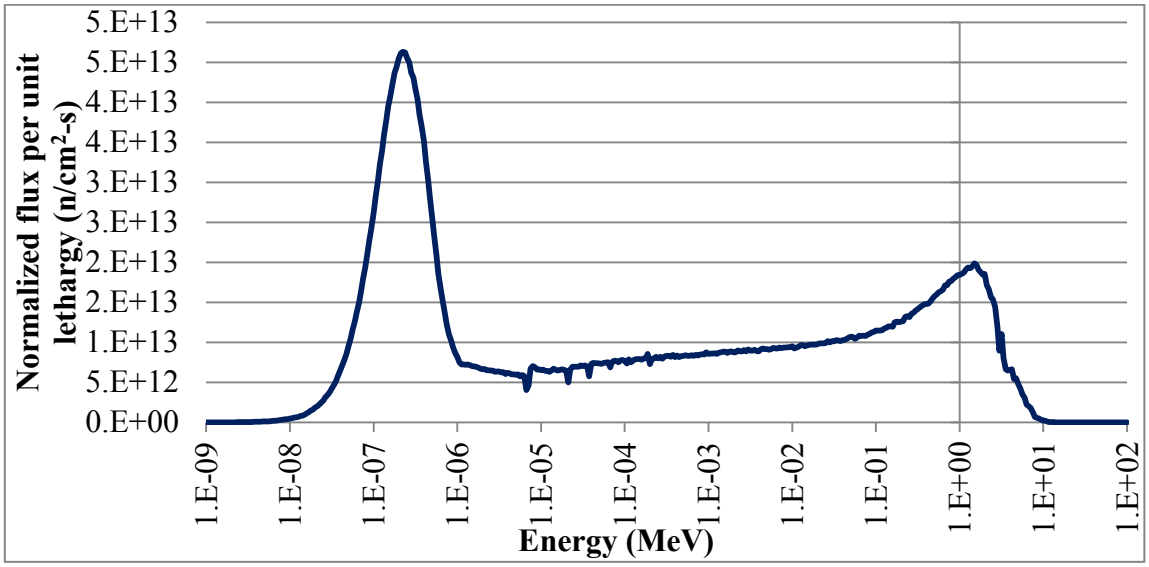

Figure 13. Energy Spectrum of the VHTR fueled with 15wt% enriched UO_2, T_{fuel}=1200K

Again, a neutron thermalization region can be observed between 0.01eV and 1.00eV, a slowing down region between 1.00eV and 0.25MeV and the fission region between 0.25MeV and 10MeV. Contrarily to the AP1000, very few depressions are to be observed in the spectrum. The VHTR spectrum is lower at higher energies and harder at low energies. Indeed the graphite in the moderator absorbs less thermal neutrons than the hydrogen in the PWR moderator and thus there are more thermal neutrons left in the reactor. The fast neutrons population (high energy neutrons) is directly proportional to the fission rate density. The fission rate density is directly proportional to the power density. Since the VHTR power density is lower than that of an AP1000, the fast

spectrum is thus lower than that of the AP1000. Both spectra were plotted in Figure 14 to stress the differences.

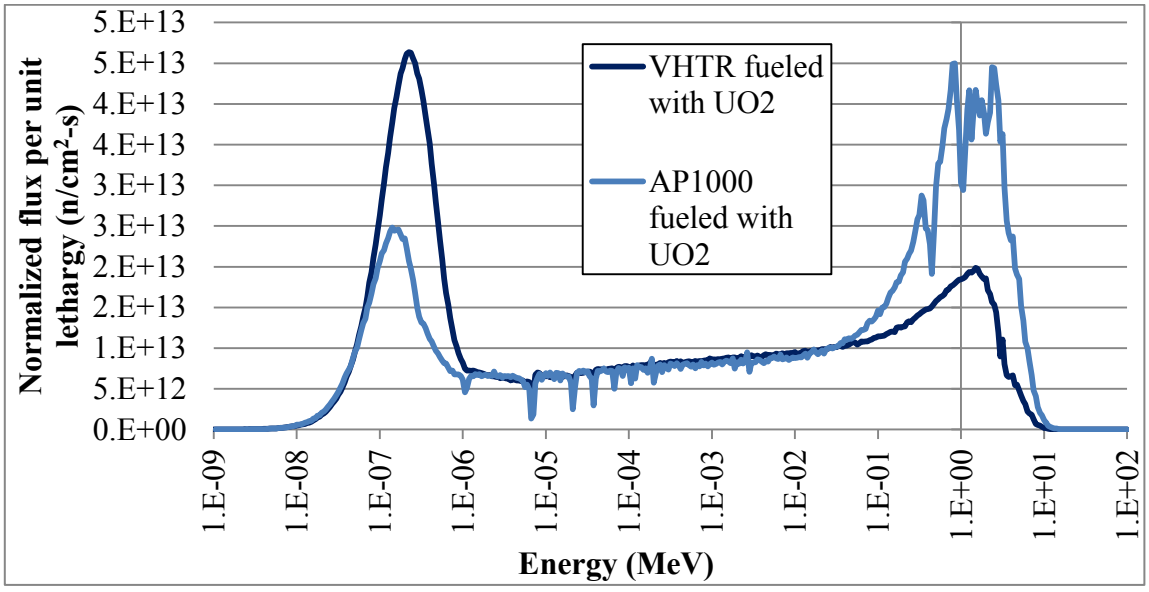

Figure 14. Energy Spectra of the AP1000 and the VHTR fueled with UO_2, T_{fuel}=1200K

To obtain the preceding results, MCNP was run using 3000 particles per cycle and 200 cycles, the first 50 being skipped. Material cards of the VHTR can be found in Appendix B.

Benchmark tests were realized in a previous study [36] and the more detailed procedure can be found in the latter reference. Not only experience-to-code comparisons were performed but also code-to-code comparisons were conducted. Experimental results for the HTTR were found in an IAEA Technical Document publication [41] and SCALE was used to model the 3D HTTR core.

These MCNP models were intensely used to produce the data presented in Chapter 3. In the latter, reactor performance characteristics and some fuel cycle metrics were quantified to improve the understanding of the AP1000 and the VHTR. Then, the transmutation capability of various AP1000-VHTR fuel cycle strategies were analyzed as well as the VHTR performances when loaded with various TRU-based fuels. The values obtained will be used as reference values for the parameters of interest and are described in Chapter 4. Creating reference values was also a necessary step to evaluate the changes in the output parameters due to variations in the input nuclear data. The quantification of their impact is presented in Chapter 5.

CHAPTER III

AP1000 AND VHTR CHARACTERISTICS

The analysis of the TRU destruction and Uranium minimization capabilities of AP1000-VHTR fuel strategies cannot be completed without first evaluating the behavioral characteristics of the AP1000 and the VHTR when fueled with conventional uranium oxide and thorium oxide fuels. Indeed the correct evaluation and interpretation of fuel cycle parameters for advanced fuel cycle strategies containing TRU-based fuels cannot be performed without first understanding the main characteristics of the selected AP1000-VHTR system.

This chapter outlines both reactors physics metrics such as the evolution of k_{eff} with time, the core lifetime, their energy spectra and fuel cycle parameters such as the TRU content at end of life. ThO_2-fueled reactors were confronted to UO_2-fueled reactors.

3.1 AP1000 AND VHTR WITH UO_2

As explained in Chapter II, the AP1000 currently under construction in China and recently licensed by the U.S. NRC have been designed for LEU fuels. To assess reactors' characteristics and compare their performances, the AP1000 and the VHTR have been first fueled with LEU. AP1000 fuel consists of 3wt% ^{235}U-enriched uranium whereas the VHTR one of 15wt%-enriched uranium. The difference lies in the core lifetime of each reactor which was chosen to be 600 days for both in order to facilitate comparison. The core lifetime is defined as the amount of time the reactor effective

multiplication factor is above 1. For the VHTR to maintain criticality for about 600 days, UO_2 had thus to be raised to 15wt%.

First, the study was focused on evaluating the impact of temperature changes in the fuel on k_{eff} and the TRU content at EOL. The TRU content is defined as the percentage of initial fuel that has turned into TRU. More precisely it is defined as:

$$\tau_{reactor} = \frac{m_{TRU}^{EOL} - m_{TRU}^{BOL}}{m_{fuel}^{BOL}} = \frac{m_{TRU}^{EOL}}{m_{fuel}^{BOL}} \quad (1)$$

where m_{TRU}^{EOL} is the mass of transuranics contained in the reactor when it is shutdown (end-of-life, EOL), m_{TRU}^{BOL} is the mass of transuranics initially in the reactor and m_{fuel}^{BOL} is the mass of fuel initially loaded in the reactor. The mass of TRU at BOL is in these cases 0 since the only fuel being loaded in the reactors is fresh UO_2.

Four temperatures were set for the fuel: 1200K, 900K, 600K and 300K – the rest of the reactor being respectively at 900K, 600K and 300K. The results for k_{eff}, and TRU content are displayed in Table 1 and Table 2.

Temperature variations affect reactors parameters in a small amount, the TRU content being the parameter the most affected. Indeed, comparatively with the value at 1200K, the TRU content at 300K is 3.0% as high in the AP1000 and 6.6% as high in the VHTR; at 600K, the transmutation efficiency is 6.8% as high in the AP1000 and 5.1% as high in the VHTR At 900K it is 2.9% as high for the AP1000 and 5.2% higher in the VHTR. In the AP1000 as well as in the VHTR k_{eff} at BOL increased with decreasing temperatures. At 300K, k_{eff} has increased by 3.8% of the 1200K value in the AP1000 and increased by 3.5% in the VHTR.

Table 1. AP1000 Reactor Parameters Obtained at 1200K, 900K, 600K and 300K.

Reactors	AP1000 (3% enriched in ^{235}U)			
temperatures (K)	1200	900	600	300
MCNP XS extension	.73c	.72c	.71c	.70c
k_{eff} at EOL	1.1174	1.12936	1.15061	1.15936
Standard deviation	0.00091	0.00079	0.00103	0.00079
k_{eff} at EOL	0.88711	0.88977	0.89069	0.88547
Standard deviation	0.00076	0.00077	0.00078	0.00075
EOL at: (days)	975.75	975.75	975.75	975.75
core lifetime (days)	610 < L << 660	610 < L < 660	610 < L < 660	610 < L < 660
mass TRU BOL (kg)	0.00	0.00	0.00	0.00
mass TRU EOL (kg)	772.8322	794.9968	825.1294	796.2384
mass BOL fuel (kg)	86056.00	86056.00	86056.00	86056.00
TRU content (%)	0.89806%	0.92381%	0.95883%	0.92526%

At the AP1000 EOL, that is a year after the reactor has become subcritical, k_{eff} are very similar whatever the fuel temperature was. At the VHTR EOL - corresponding here to the time the reactor becomes subcritical, variations in k_{eff} with respect to the value at 1200K are at worst different by 2.8% (at 600K). The core lifetime varies between 651 and 676 days. The variations with temperature of these parameters are consequently minor effects and the effect of temperature changes can be disregarded for the study.

Table 2. VHTR Reactor Parameters Obtained at 1200K, 900K, 600K and 300K.

Reactors	VHTR (15% enriched in U-235)			
Temperatures (K)	1200	900	600	300
MCNP XS extension	.73c	.72c	.71c	.70c
k_{eff} (BOL)	1.30948	1.32597	1.34239	1.35484
Standard deviation	0.00118	0.00108	0.00122	0.00119
k_{eff} (EOL)	0.95082	0.97788	0.9505	0.94497
Standard deviation	0.00082	0.00099	0.00083	0.00092
EOL at: (days)	666	651	671	676
core lifetime (days)	546 << L <636	551 < L < 601	551 < L < 641	556 < L < 646
mass TRU BOL (kg)	0.00	0.00	0.00	0.00
mass TRU EOL (kg)	33.4877	35.2441	35.1979	35.6878
mass BOL fuel (kg)	3416.50	3416.50	3416.50	3416.50
TRU content (%)	0.98018%	1.03158%	1.03023%	1.04457%

The following paragraphs will focus on the evolution of k_{eff} with time, the TRU composition after 600 days and their activity for reactors operated at 900K.

3.1.1 EVOLUTION OF THE EFFECTIVE MULTIPLICATION FACTOR OVER TIME

The effective multiplication factor is a parameter of importance in reactor physics calculations. It describes whether or not if the chain reaction in a nuclear reactor is stable and self-sustained. The AP1000 and VHTR effective multiplication factors were compared and can be seen in Figure 15. k_{eff} at VHTR BOL appears 200 milli-k higher than in that of the AP1000. Then k_{eff} drops 2.5 as fast during operation in the VHTR as

in the AP1000. The reactivity swing at shutdown is relatively the same for both reactors: +0.2milli-k per day for the PWR and +0.102milli-k per day for the VHTR. After shutdown, k_{eff} seems to decrease twice as fast in the AP1000 as in the VHTR.

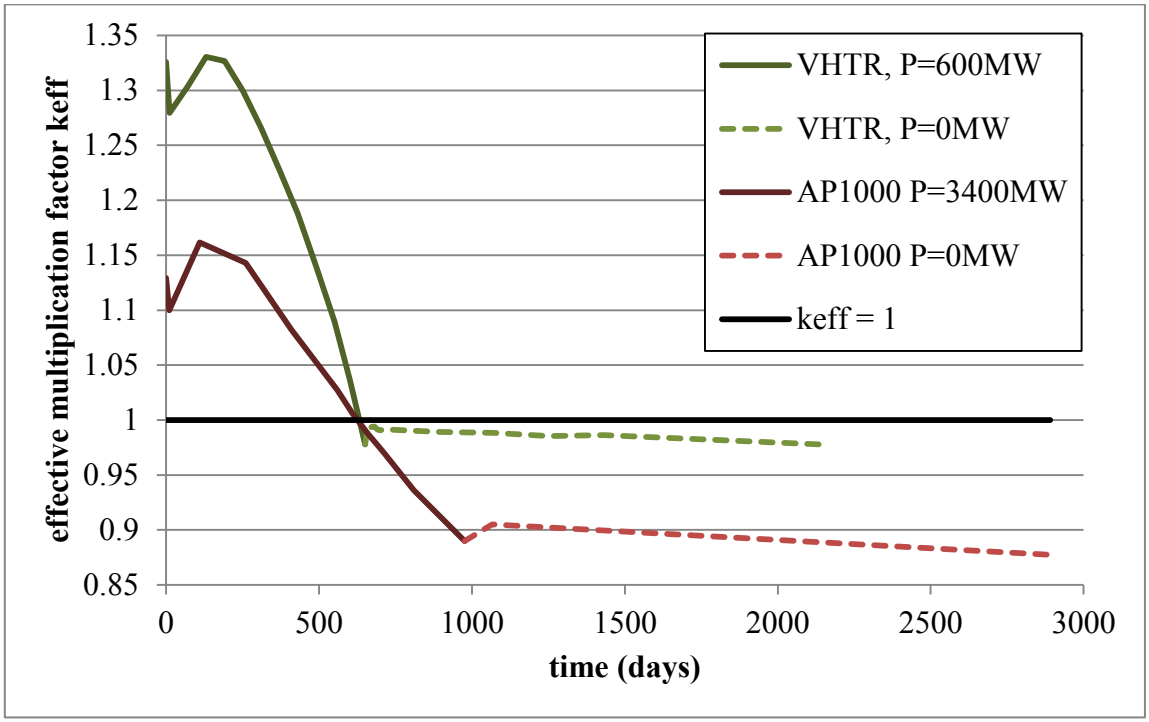

Figure 15. Evolution of the Effective Multiplication Factor for the AP1000 and the VHTR

The depletion of burnable absorbers and the depletion of fresh fuel explain the first drop in k_{eff}. The following increase is caused by the absence of burnable poisons after complete depletion which reduces the parasitic captures in the fuel, leading to more fission. However this increase is quickly stopped by the continuous depletion of fuel and the build-up of fission products capturing neutrons.

3.1.2 TRU COMPOSITION AT THE END OF THE REACTORS' LIFETIME

The identity and the amount of TRU created during reactor operation are of interest in fuel management optimization strategies. AP1000 and VHTR spent fuels were decided to be qualitatively and quantitatively compared. Differences in fuel enrichment were expected to affect the amount of TRU produced by each reactor. The mass of each nuclide contained in the spent fuel stream after approximately 600 days were plotted for both reactors on the same graph. Since 86.1T of fresh fuel are loaded in the AP1000 for 3.42T of fresh fuel in the VHTR, the mass of each nuclide was normalized per unit mass of initial fuel. The results can be seen in Figure 16. Each isotope is identified by its Z number followed by it's a number (ZAiD). For instance, the ZAiD of ^{239}Pu is 94239.

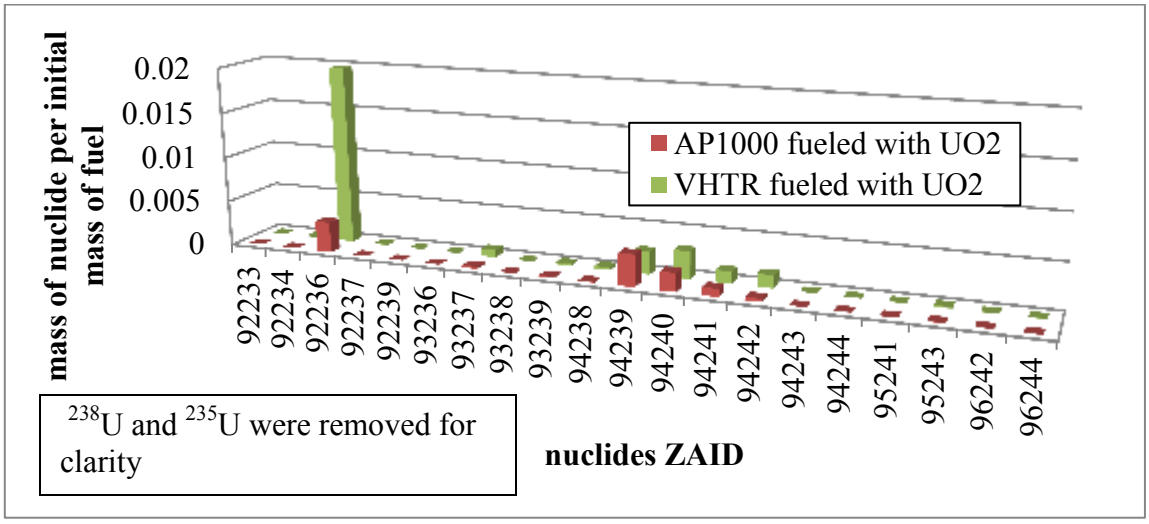

Figure 16. Normalized Mass of Nuclides Contained in the Spent Fuel Stream of an AP1000 and a VHTR

As it can be seen, both reactors produce the same streams of TRU. The major nuclides present after about 600 days are of course ^{238}U and ^{235}U (removed from Fig. 16 from clarity), ^{236}U, ^{239}Pu, ^{240}Pu, ^{241}Pu, ^{242}Pu. The amount of Pu produced per unit mass of initial fuel by both reactors is sensibly the same for ^{240}Pu, ^{241}Pu. For ^{238}Pu, ^{242}Pu, ^{243}Pu and ^{244}Pu the VHTR produces 4 to 5 times more Pu than the AP1000 per unit initial mass of fuel. It remains 3 times more ^{235}U and also almost 6 times more ^{236}U in the VHTR than in the AP1000. This can be explained by the fact that there were 5 times more ^{235}U loaded in the VHTR per unit mass of initial fuel. The only isotopes produce in slightly higher quantities by the AP1000 than by the VHTR are ^{239}Pu, ^{241}Am and ^{242}Am. The exact masses after 600 days of operation can be found in Appendix C.

Nevertheless, identifying and quantifying the nuclides present in the spent fuel of both reactors is not enough. Quantifying their activity is also of fundamental importance.

3.1.3 TRU ACTIVITY AT THE END OF THE REACTORS' CORE LIFETIME

The activity of a nuclide is a primordial parameter since it can quantify the easiness the spent fuel can be handle with for further reprocessing. Figure 17 compares the activity normalized per unit mass of initial fuel for the AP1000 and the VHTR.

The major contributors to specific activity are ^{239}U and ^{239}Np for both reactors. The specific activity coming from these isotopes in the VHTR is noticeably twice as high as in the AP1000. The specific activity of VHTR spent fuel is also 5 times as high as the AP1000 one for ^{237}U, 8 times as high as for ^{238}Np. However ^{239}U, ^{239}Np, ^{237}U and ^{238}Np have short half-lives as indicates Table 3.

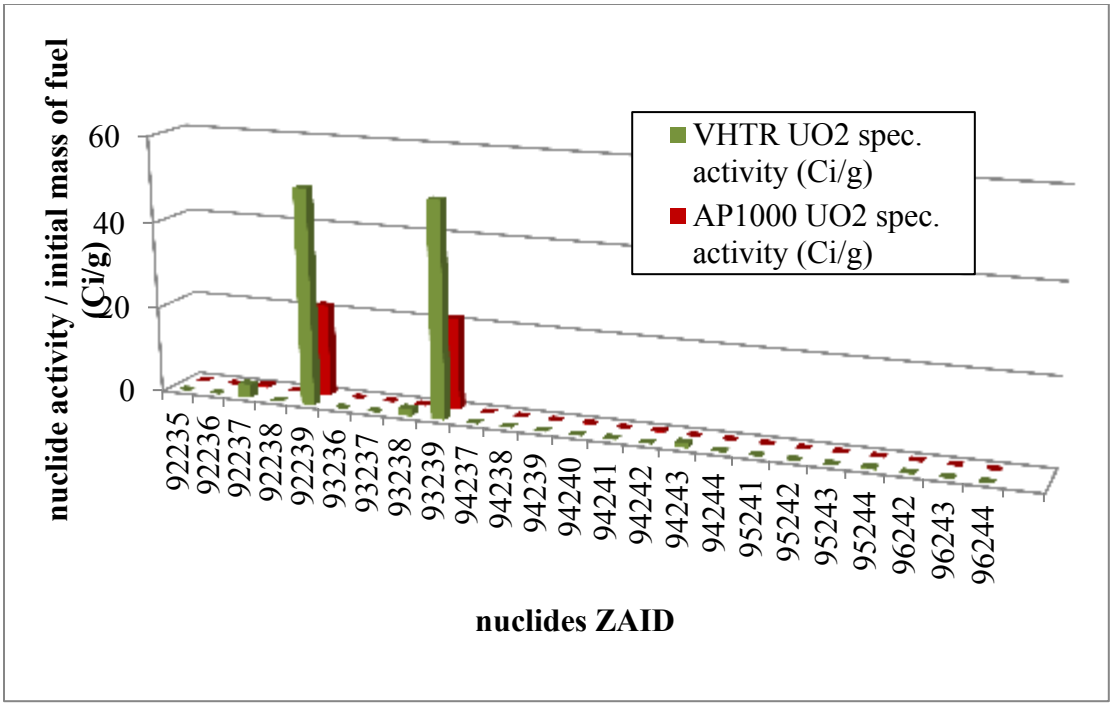

Figure 17. Specific Activities of AP1000 and VHTR Spent Fuel

Table 3. Major Contributors to Specific Activity and their Half-lives

Nuclides	^{239}U	^{239}Np	^{237}U	^{238}Np
Half-life (days)	0.0162	2.3565	6.75	2.117

The above nuclides beta decay producing ^{239}Pu, ^{237}Np and ^{238}Pu whose half-lives and specific activities are summarized in Table 4. For comparison, the specific activity of natural Uranium is 0.683μCi/g

From Figure 18, the main specific activity contributors – other than ^{239}U and ^{239}Np – differ from one reactor to another.

The total specific activities are finally 106.7 Ci/g and 43.8 Ci/g for the VHTR and the AP1000 respectively.

Table 4. Half-lives and Specific Activities of Major Contributors to Specific Activity Several Years after Shutdown

Nuclides	^{239}Pu	^{237}Np	^{238}Pu
Half-life (years)	24,110	2.144 millions	87.7
Specific activity (Ci/g)	0.063	0.0071	17.3

If it seems that the VHTR TRU will be harder to handle it has to be remembered that the VHTR contains less fuel than the AP1000. The total activity of the TRU part of the spent fuel is indeed only 364.6MCi for the VHTR and 3,771MCi for the PWR. As a consequence limitations on the quantity of TRU to handle at once and cooling down times have to be carefully defined for each reactor.

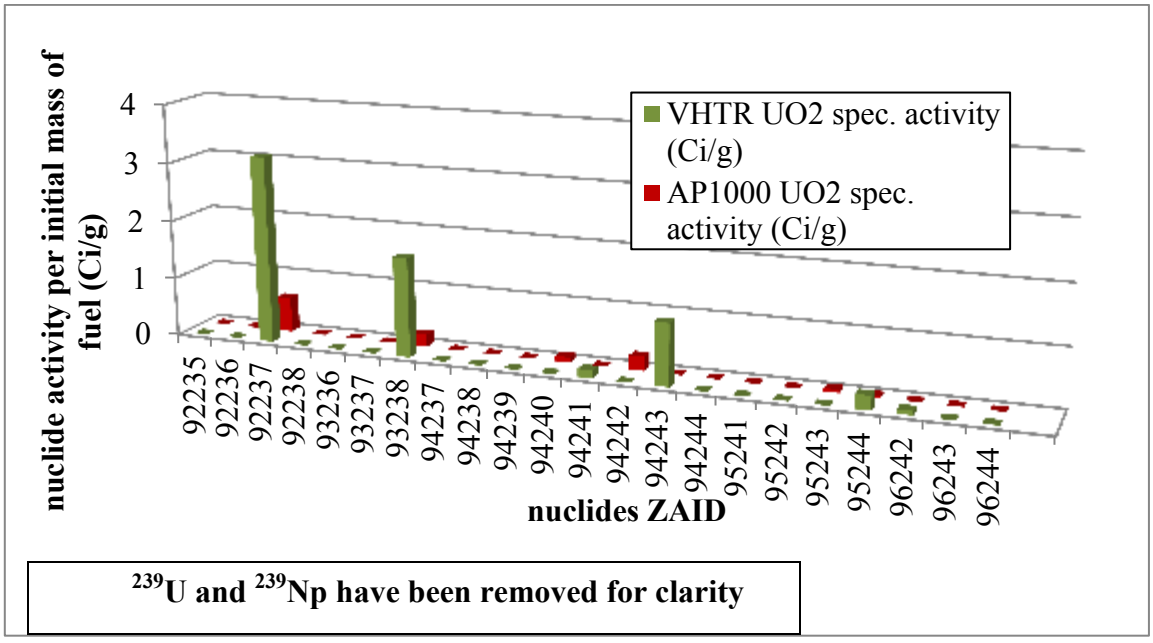

Figure 18. Specific Activities of AP1000 and VHTR Spent Fuel

3.2 AP1000 AND VHTR WITH ThO_2

With larger known resources than Uranium, Thorium has become a nuclear fuel of interest. The initiation of a research and development project in thorium-fueled molten-salt reactors (MSR) in China at the beginning of year 2011 confirms the enthusiasm expressed and justified by the rationales described in Chapter 1. For these reasons, the performance characteristics of an AP1000 reactor and a VHTR fueled with Thorium were examined. The fuel chosen was ThO_2. ThO_2 is defined as a UO_2 fuel where ^{238}U has been replaced by ^{232}Th.

Table 5. AP1000 Reactor Parameters at Different Temperatures

Reactors	AP1000 3% enriched in ^{235}U + ^{232}Th			
temperatures (K)	1200	900	600	300
Cross section extension	.73c	.72c	.71c	.70c
k_{eff} (BOL)	0.98203	0.99128	1.00455	1.01868
Standard deviation	0.00072	0.0008	0.0009	0.00076
k_{eff} (EOL)	0.89266	0.89082	0.88808	0.88214
Standard deviation	0.00069	0.00068	0.00064	0.00057
EOL at: (days)	975.75	975.75	975.75	975.75
core lifetime (days)	260 < L < 310	300 < L < 350	300 < L < 350	350 < L <400
mass TRU BOL (kg)	0.00	0.00	0.00	0.00
mass TRU EOL (kg)	40.8624	40.8135	41.0393	41.4026
mass BOL fuel (kg)	86056.00	86056.00	86056.00	86056.00
TRU efficiency (%)	0.04748%	0.04743%	0.04769%	0.04811%

As explained in detail in Chapter 1, ^{232}Th absorbs thermal neutrons and becomes ^{233}U. ^{233}U is a long-lived fissile isotope having a higher neutron yield per fission than ^{235}U or ^{239}Pu. Thus once ^{233}U has been produced in the reactor, it can be removed and used as a fuel in another reactor of a closed fuel cycle setting up a breeding cycle.

Comparatively to paragraph 3.1.A, the effect of fuel temperature changes on k_{eff} and the TRU content were studied. Variations are again minim and are presented in Table 5 for the AP1000 and Table 6 for the VHTR.

Table 6. VHTR Reactor Parameters at Different Temperatures

Reactors	VHTR 15% enriched in ^{235}U + ^{232}Th			
temperatures (K)	1200	900	600	300
Cross section extension	.73c	.72c	.71c	.70c
k_{eff} (BOL)	1.31859	1.33098	1.33896	1.34943
Standard deviation	0.00108	0.00111	0.00102	0.00117
k_{eff} (EOL)	0.99435	1.03331	1.03861	1.04082
Standard deviation	0.00088	0.00088	0.00075	0.00087
EOL at: (days)	606	586	586	586
core lifetime (days)	596 < L < 606	L > 586	L > 586	L > 586
mass TRU BOL (kg)	0.00	0.00	0.00	0.00
mass TRU EOL (kg)	3.5197	3.3357	3.3075	3.1356
mass BOL fuel (kg)	3416.50	3416.50	3416.50	3416.50
TRU efficiency (%)	0.10302%	0.09763%	0.09681%	0.09178%

However it is interesting to note the difference in TRU content between the AP1000 fueled with UO_2 and ThO_2 and the VHTRs just before subcriticality. The VHTR seems

to produce more TRU than the AP1000 whatever the fuel is. VHTRs however can also destroy TRU when used in a Deep Burn configuration (DB-VHTR) [43]. Also Th-fueled reactors produce a lot less TRU than U-fueled one. The AP1000 TRU content is divided by 100 while the VHTR TRU content is 10 times less than with UO_2. Figure 19 stresses these differences.

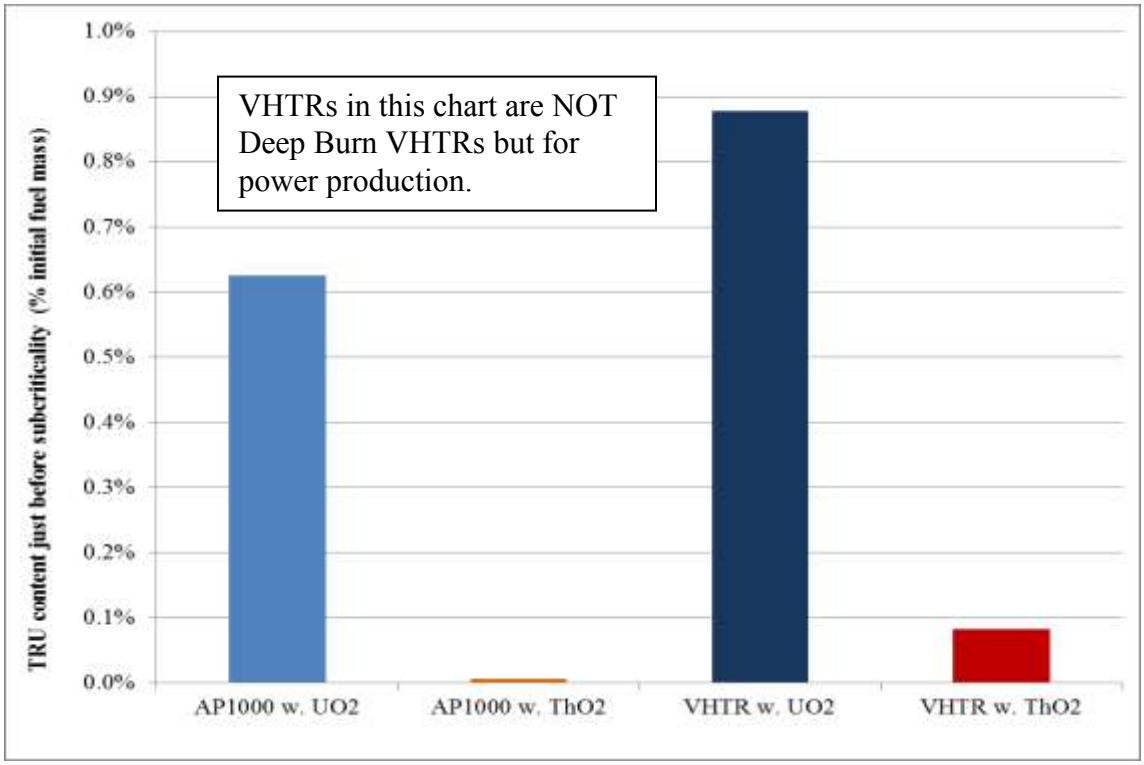

Figure 19. TRU Content in the AP1000 and the VHTR, just before Subcriticality

3.2.1 EVOLUTION OF THE EFFECTIVE MULTIPLICATION OVER TIME

Similarly to paragraph 3.1.1, the evolution of the effective multiplication factor over time was reviewed and the core lifetime of each reactor was derived from it. To facilitate

comparisons Uranium versus Thorium based fuels, the same ^{235}U enrichment was kept in the reactors. The AP1000 contains 3wt% ^{235}U enriched uranium and the VHTR is 15wt% ^{235}U enriched. The powers of the reactors were kept at 3,400MW_{th} for the AP1000 and 600MW_{th} for the VHTR. The reactors fuel temperature was kept at 900K. The results are displayed in Figure 20. Dashed lines represent the evolution after shutdown.

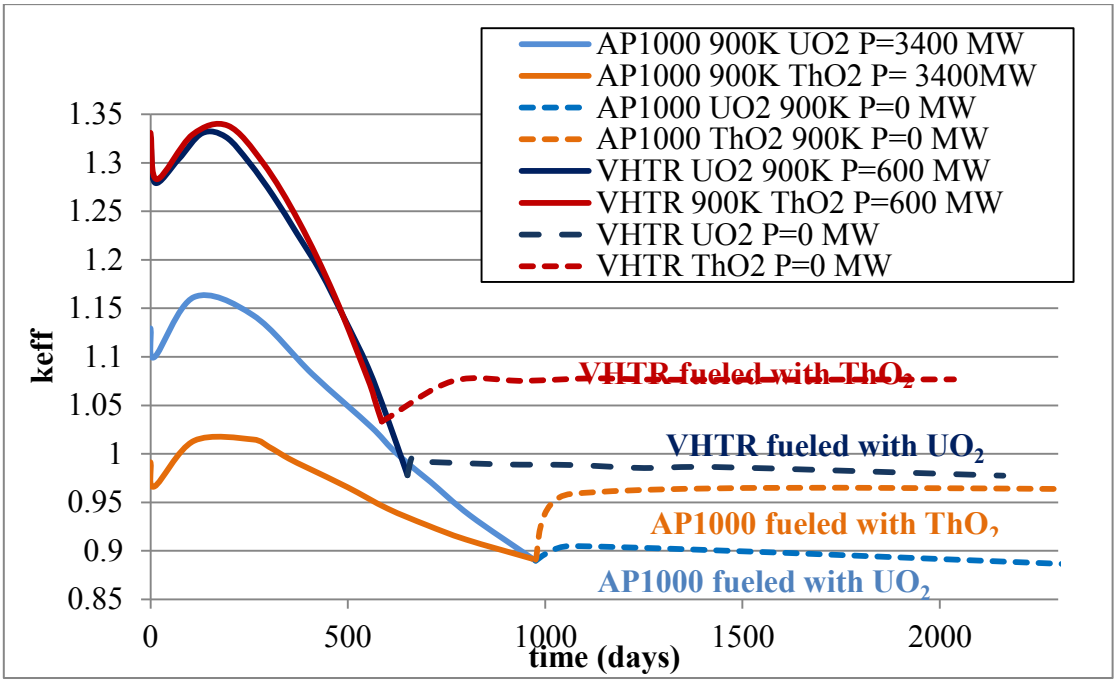

Figure 20. Time Evolution of the AP1000 and the VHTR Effective Multiplication Factor k_{eff}.

These configurations led to a core lifetime of 300 days for the AP1000 against about 600 days for the VHTR. Loaded with ThO_2, the AP1000 starts with a k_{eff} of 0.99128 ± 0.00080 and stays subcritical for a hundred days. 110 days of operations are needed for

the AP1000 to become critical with a value of 1.01340 ± 0.00073. On the other hand, the VHTR k_{eff} at BOL is 1.33098 ± 0.00111, 340milli-k above the AP1000 effective multiplication factor. Comparatively with UO_2-fueled VHTR, the ThO_2-fueled VHTR has approximately the same k_{eff} at BOL (1.33098 for ThO_2 against 1.32597 ± 0.00108 for UO_2).

After a quick drop the first 10 days of operation, k_{eff} increases during another 200 days in both the AP1000 and VHTR. This behavior is the result of several factors: the reduction of k_{eff} is caused by a high burnable poison concentration at BOL which reduce the excess reactivity of the fresh fuel. However with neutrons being produced and captured by the burnable poison, its concentration inevitably diminishes to a point where it can no longer counteract the excess reactivity of the fuel. k_{eff} thus increases until the buildup of fission products is sufficient to participate in enough parasitic captures to reduce the reactivity of the fuel. The diminution in k_{eff} is also the results of changes in the fuel composition and fuel depletion. The raise is more important for the AP1000 than for the VHTR: respectively k_{eff} increases by 24milli-k and by 7milli-k. These observations can be shown in Figure 21.

Then k_{eff} decreases in the AP1000 4.5 times slower than in the VHTR, at a rate of -0.75milli-k per day. Multiplication factor decreases because fresh fuel is being depleted and fission products are buildup, participating in parasitic captures. At EOL k_{eff} is finally 0.89082 ± 0.00068 in the AP1000. It then jumps quickly to 0.95866 ± 0.00067 in only 90 days. The ability of the reactor to gain 68milli-k in the three months following shutdown is an important feature that has to be kept in mind for safety purposes.

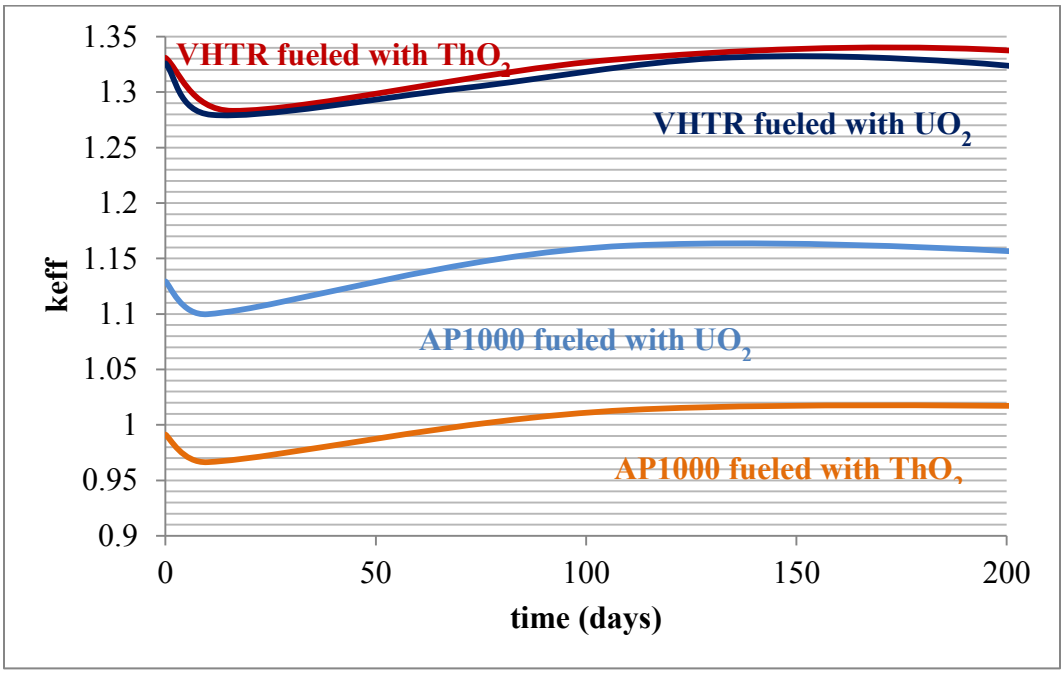

Figure 21. Rise of k_{eff} the First 200 Days

An AP1000 fueled with Thorium would have to become very subcritical to be stopped or the reactor could start again by itself. Figures 22 and 23 stress the differences in the evolution of k_{eff} after shutdown between U- and Th-fueled reactors. The VHTR gains 39milli-k in 346 days. This reactivity surge is explained by the rather long half-life of ^{233}Pa (26.967days) which spread the production of fissile ^{233}U over a longer period of time [18]. The decay chain is described below:

$$^{232}_{90}Th + {}^{1}_{0}n \rightarrow {}^{233}_{90}Th \xrightarrow[21.83\text{min}]{} {}^{233}_{91}Pa \xrightarrow[26.967d]{} {}^{233}_{92}U$$

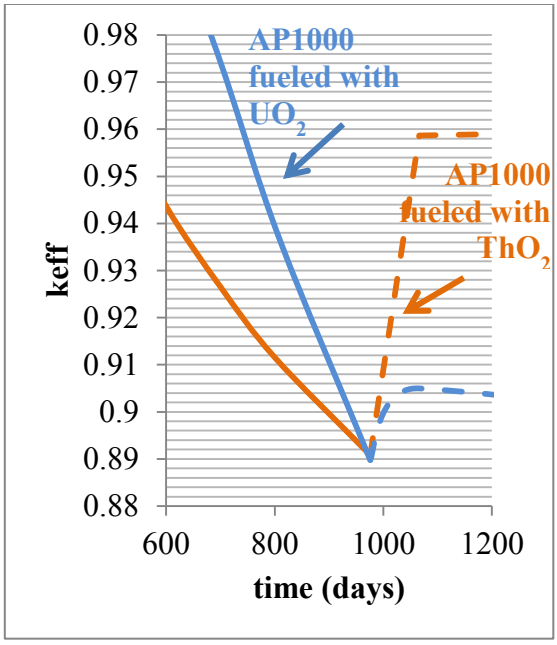

Figure 22, Variation of k_{eff} at EOL of AP1000s

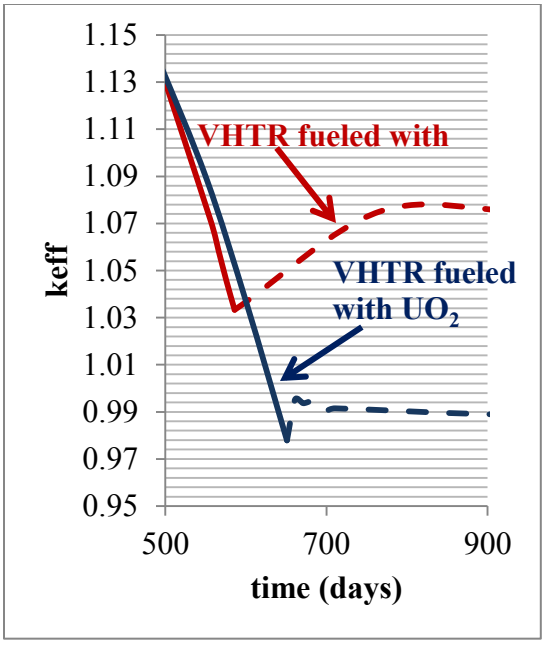

Figure 23. Variation of k_{eff} at EOL of VHTR

On the contrary of reactors fueled with UO_2, k_{eff} stabilizes after shutdown in reactors fueled with Thorium: in the AP1000, k_{eff} is only lowered by 0.46milli-k in 15 years while k_{eff} in the VHTR is depressed by 1.1milli-k in 2.5 years. These results can again be observed in Figure 20.

3.2.2 TRU COMPOSITION AT THE END OF LIFE OF THE REACTORS' CORE LIFETIME

Similarly to the comparisons in section 3.1.2 the spent fuel composition and activity of the AP1000 after 610 days were compared to those of the VHTR after 606 days. The results are shown in Figure 24.

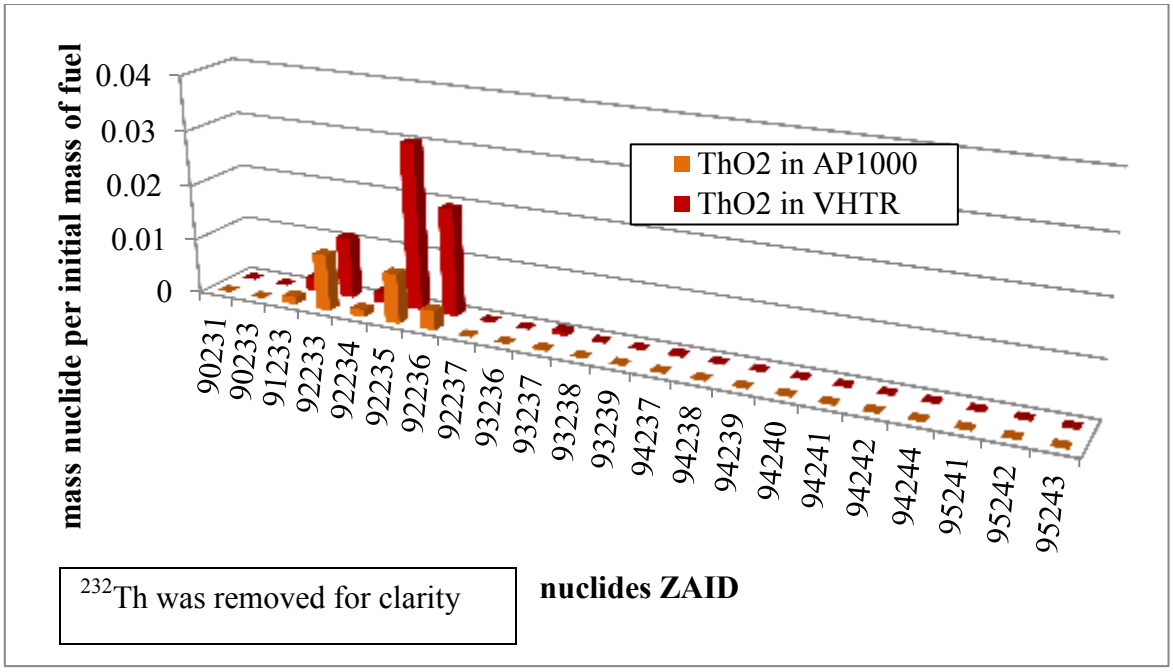

Figure 24. Normalized Mass of Nuclides Contained in the Spent Fuel of a AP1000 and a VHTR

The main nuclides present in the spent fuel after about 600 days are ^{231}Pa, ^{233}U, ^{234}U, ^{235}U, ^{236}U and ^{237}Np.

The difference in ^{235}U enrichment explains again why there remains 3 times more ^{235}U per unit initial mass in the VHTR than in the AP1000 and 6 times more ^{236}U. The other isotopes are found in relatively the same amount in both reactors. In particular, the PWR produced 869 kg of ^{233}U and the VHTR 37.6 kg after about 600 days of operation. It corresponds to 1.01% and 1.10% of the initial mass of actinides loaded into the AP1000 and the VHTR respectively. Hence both reactors have the same capability to produce ^{233}U from ^{232}Th. But more interesting is their ability to keep producing ^{233}U after the reactor has been shutdown. The AP1000 produces another 116kg of ^{233}U the

first 90 days following shutdown, i.e. an increase of 13.4% in the ^{233}U mass at shutdown. The VHTR produces another 7.8 kg of ^{233}U which corresponds to a 20.7% increase of the mass at shutdown. These particular characteristics which can be seen in Figures 25 to 26 (dashed lines representing the time evolution after shutdown) will have to be remembered and taken into account when it comes to design of proliferation-safe reactors. Indeed as explained in Chapter 2, ^{233}U can be used to produce nuclear explosive devices.

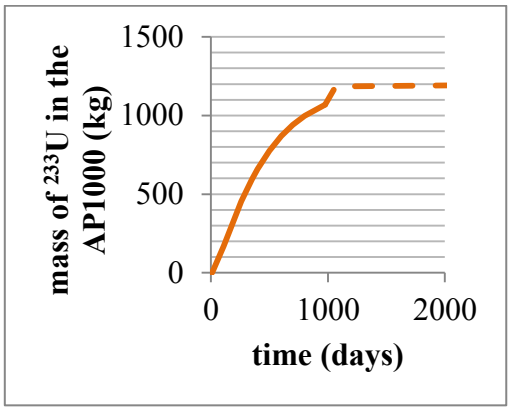

Figure 25. Build-up of ^{233}U in an AP1000 Reactor

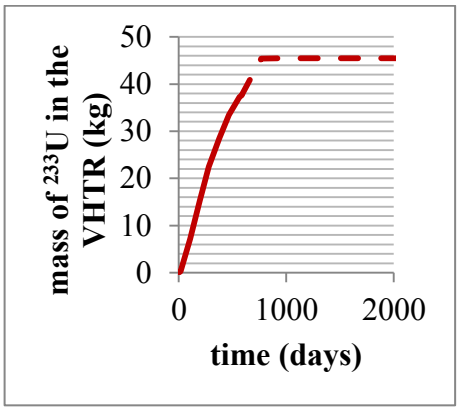

Figure 26. Build-up of ^{233}U in a VHTR

Figure 27 shows the production of ^{233}U per unit mass of initial fuel (specific mass) loaded in each reactor. It appears that the VHTR seems to produce ^{233}U faster than the AP1000. The continuous buildup per unit mass of initial fuel at shutdown equally seems more important in the VHTR than in the AP1000 initial fuel with the VHTR producing ^{233}U faster than the AP1000.

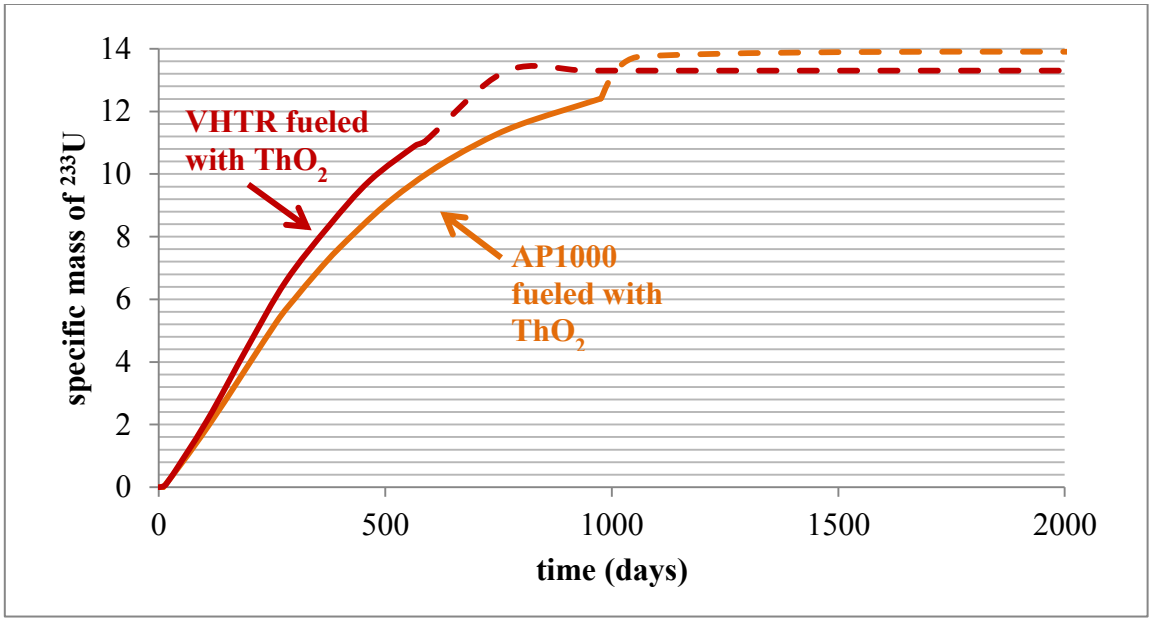

Figure 27. Evolution of the Specific Mass of ^{233}U in the AP1000 and the VHTR.

The comparison of the different TRU contents per initial mass of fuel at shutdown is featured in Figure 29 for each configuration of reactor.

Three interesting features are summarized in Figure 28. First, reactors loaded with the same fuel lead to the same TRU inventory at shutdown. Secondly, UO_2-fueled reactors produce more Plutonium than ThO_2-fueled ones. Plutonium isotopes are a burden in wastes reprocessing management as ^{239}Pu, ^{240}Pu, ^{242}Pu and ^{244}Pu have very long half-lives. Moreover ^{238}Pu is responsible for much of the short-term decay heat as a result of a relatively short half-life of 87.7 year. Decay heat hampers the quick reprocessing of spent nuclear fuel and is one of the reasons why spent fuel has to be stored in pools to remove the excess heat. The presence of ^{239}Pu is also very unwelcomed regarding non-proliferation as ^{239}Pu is the primary fissile isotope used in

nuclear weapons production. Thirdly, the fissile isotope ^{233}U is only produced with Thorium based fuels.

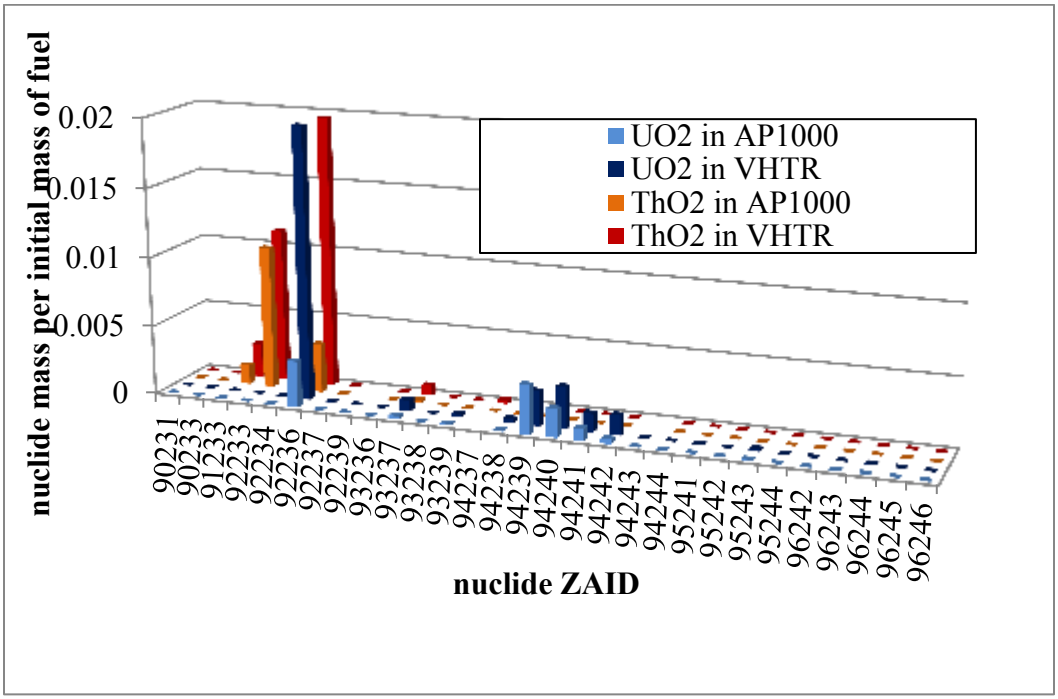

Figure 28. Used Fuel Inventory at Shutdown (^{232}Th, ^{238}U and ^{235}U have been removed for clarity)

The half-lives of all major nuclides present at shutdown are summarized in Table 7 with their specific activities. For comparison, the specific activity of natural Uranium is 0.683μCi/g. Their very long half-lives of these nuclides assure them to be still an important part of the spent fuel years later and pose a challenge regarding their containment, handling and storage.

Table 7. Major Nuclides Present in the Spent Fuel, their Half-lives and Specific Activities

Nuclide	^{231}Pa	^{233}U	^{234}U	^{235}U	^{236}U	^{237}Np
Half-life (years)	32,760	159,200	245,500	704 millions	23.42 millions	2.144 millions
Specific activity (Ci/g)	0.048	0.0098	0.0063	0.0000022	0.0000065	0.00071
Spec. activity relative to the U_{nat} one	70,278	14,349	9,224	3.22	9.51	1,040

Likewise paragraph 3.1.3, the specific activities of the TRU just before the reactors become subcritical were also evaluated and are presented in the next paragraph.

3.2.3 TRU ACTIVITY AT THE END OF LIFE OF THE REACTORS' CORE LIFETIME

At the time of shutdown, the major contributors for the activity are ^{233}Th, ^{233}Pa, ^{237}U, ^{238}Np. However ^{233}Th, ^{233}Pa, ^{237}U and ^{238}Np half-lives are respectively 21.83 min, 26.967 days, 6.75 days and 2.117 days. Therefore these nuclides will not contribute in the activity when the fuel will be handled after several years of cooling. They will have indeed beta-decayed into ^{233}Pa, ^{233}U, ^{237}Np and ^{238}Pu. ^{233}U and ^{237}Np half-lives and specific activities are summarized in Table 4 above. ^{238}Pu has a half-life of 87.7 years and a very high specific activity of 17.3Ci/g.

The major contributors to the activity at shutdown were plotted in Figure 29. ^{233}Th and ^{233}Pa were removed for clarity. The specific activity for each nuclide appears higher in the VHTR than in the AP1000.

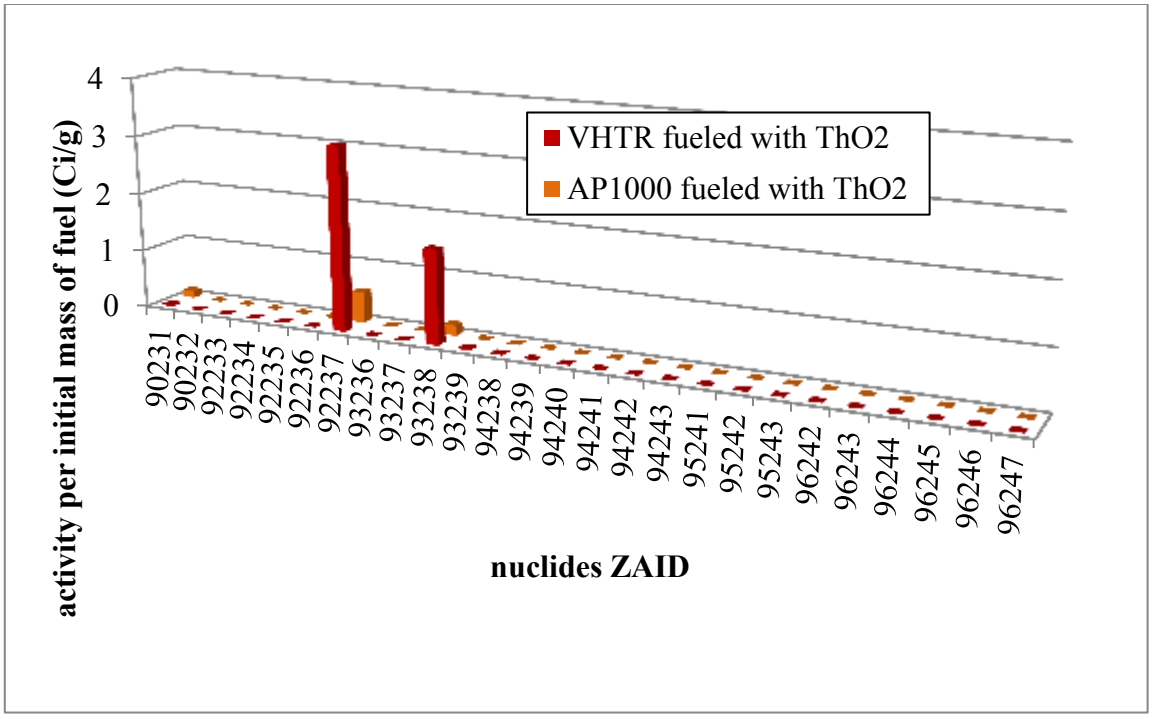

Figure 29. Used Fuel Activity per unit amount of Initial Fuel for the AP1000 and the VHTR after about 600 days (^{233}U and ^{233}Pa were removed for clarity)

Indeed the specific activity is 9 times higher for ^{238}Np in the VHTR spent fuel than in the LWR one. For ^{237}U, the specific activity is 5 times more important in the VHTR. The total specific activity is 114Ci/g for the VHTR and 59.6Ci/g for the AP1000 at shutdown. However, having a smaller core, VHTRs' total activity is considerably smaller than that of the AP1000s. The total activity of the TRU part of the spent fuel is 388MCi for the VHTR and 5,129MCi for the PWR.

Compared to UO_2-fueled reactors, the specific activities for ThO_2-fueled reactors can be considered similar – although slightly higher – as can be seen in Figure 30. ^{233}Th, ^{233}Pa, ^{239}U and ^{239}Np were removed for clarity.

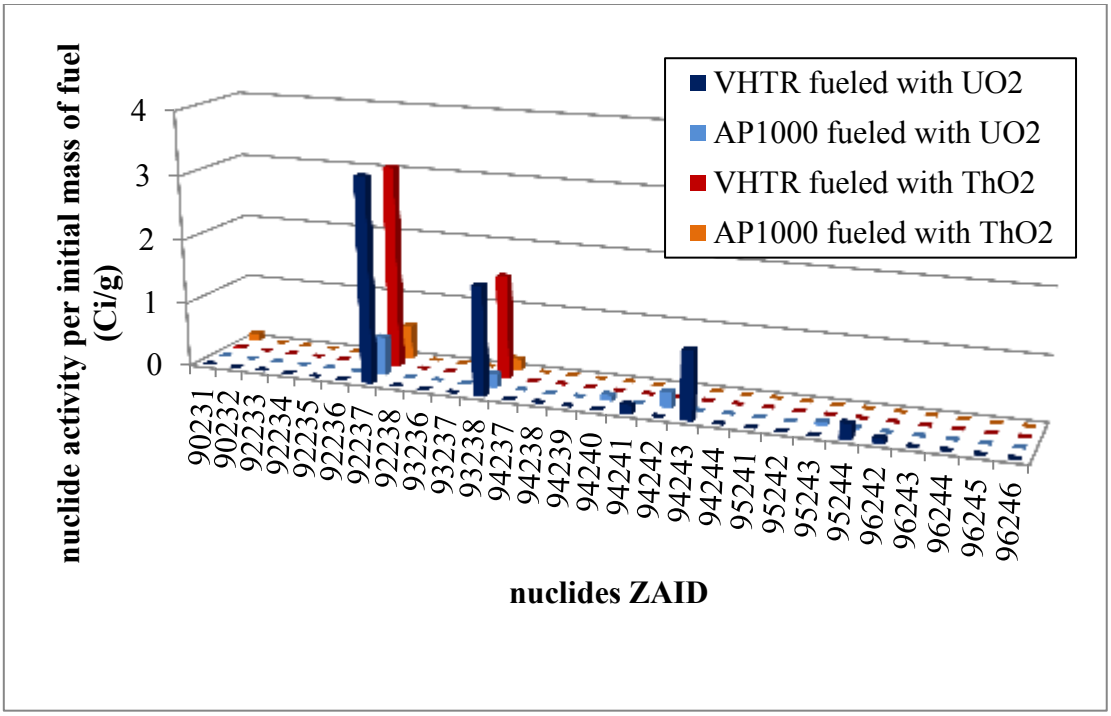

Figure 30. Used Fuel Activity at Shutdown

3.3 REACTORS ENERGY SPECTRA

The energy spectrum of each reactor is partly responsible for the difference encountered between reactors. Figure 31 represents the energy spectra corresponding to each reactor configurations. First it can be noticed that whatever the fuel, the energy spectra are similar between the two AP1000 reactors and between the two VHTRs. The spectrum is harder at low energy for VHTRs fueled with ThO_2 than for VHTRs fueled with UO_2. Spectra of reactors fueled with ThO_2 seem to suffer less from resonance absorptions than spectra from UO_2-fueled reactors. The absorption cross section of ^{238}U indeed shows resonances around 6.6eV, 10eV, 36eV, 80eV, 90eV and 100eV that do not exist in ^{232}Th.

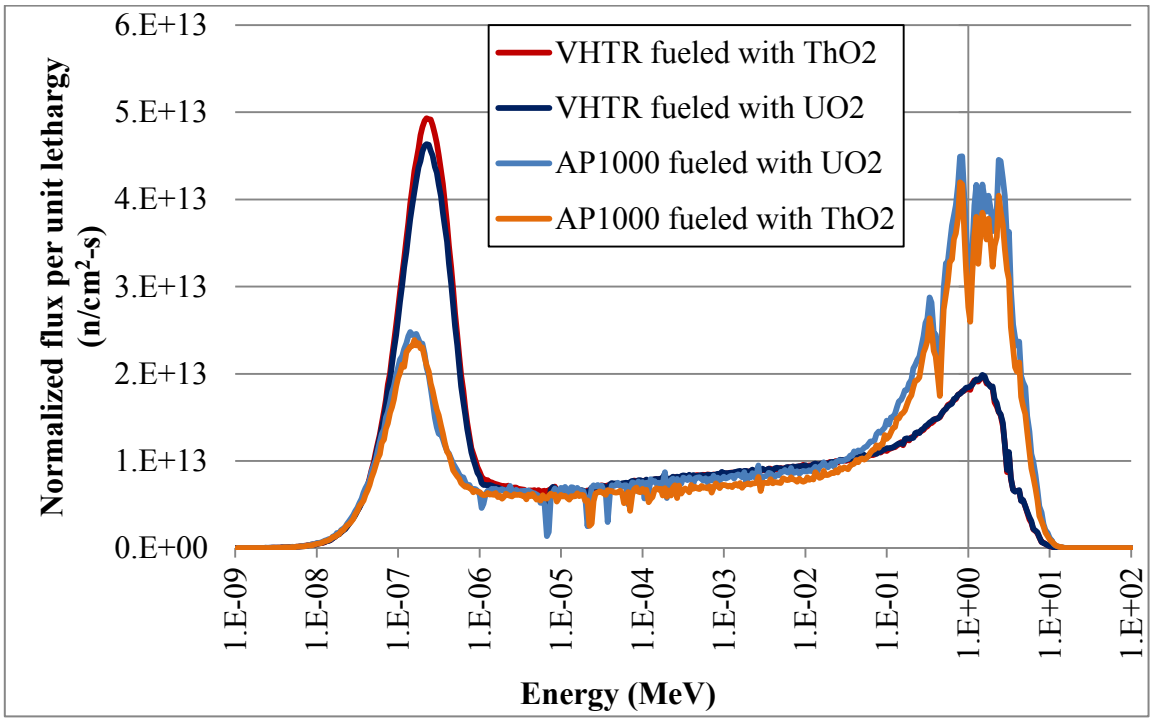

Figure 31. Energy Spectra of the AP1000 and the VHTR fueled with UO_2 or ThO_2

Before establishing reference values for the reactor parameters of interest and the fuel cycle metrics, the first step consisted in defining the performance characteristics of the AP1000 reactor and the VHTR. The evolution of the effective multiplication over time, the inventory and activity of TRU at EOL and the energy spectra were established for a 3wt% ^{235}U enriched AP1000 and a 15wt% ^{235}U enriched. These enrichments were chosen to sustain criticality for 600 days in both reactors. Performance characteristics were also constituted for Th-based fuels.

The next step consisted in producing reference cases to analyze advanced fuel cycle strategies and later allow the quantification of the impact of nuclear data variations on

fuel cycle parameters. One of these strategies was used later as a reference case to against which the altered parameters would be confronted. The next chapter describes the different reference cases chosen and quantifies the reference parameters.

CHAPTER IV

TRU-FUELED VHTR: REFERENCE CASES

After having completed the evaluation of reactors physics metrics of the AP1000 and the VHTR loaded with conventional Uranium Oxide fuel and Thorium Oxide fuel and after having estimated their TRU production capacity, the next step of this study was to establish values of reference for the same parameters when the VHTR is fueled with TRU-based fuels. One of these "reference cases" has later allowed the quantification of the impact of fission spectrum variations on the fuel cycle parameters.

First have been described the different TRU-based fuels. Secondly the evolution of the effective multiplication factor k_{eff} is being presented. Thirdly, the TRU composition and activity at EOL is being exposed. Fourthly, the TRU destruction rates have been established. Finally the energy spectra have been studied.

4.1 DESCRIPTION OF THE REFERENCE CASES FOR TRU-FUELED VHTR

In this Chapter, the VHTR's main role is to burn transuranic isotopes coming from the PWR AP1000. In the first category of reference cases, the AP1000 was fueled with UO_2 while in the second category of reference cases, the AP1000 was fueled with ThO_2. Thus the VHTR TRU destruction performances have been studied for TRU arising from a Uranium cycle or a Thorium cycle.

The UO_2-fueled AP1000 was set operational for 630 days at a power of 3,400MW(th) until k_{eff} reached a value of 0.98918 ± 0.00078. The fuel was 3wt% ^{235}U

enriched. The ThO_2-fueled AP1000 was set operational for 310 days at a power of 3,400MW(th) until k_{eff} reached a value of 1.00010 ± 0.00064. The fuel was composed of 3wt% ^{235}U and 97wt% of ^{232}Th. In both cases, the fuel temperature was 1,200K and the core temperature was 900K. Also, in the U-cycle case as well as in the Th-cycle case, a 12-year lag time was chosen between the EOL of the AP1000 and the BOL of the VHTR. This lag time is used for the PWR fuel to cool and for fabrication of the VHTR fuel. The lag time has only a low impact on the TRU destruction rate [44].

The amount of TRU in the fuel varies from 20% to 100%, with an intermediate ratio of 40%. The different cases are summarized in Table 8. Two cases using weapon-grade Pu (WgPu) instead of reactor-grade Pu (RgPu) in the fuel were also implemented for a ratio of 40% of TRU coming from a Uranium cycle. Composition of the U-cycle TRU-based fuels can be found in Appendix D.

Table 8. TRU-based VHTR fuel Reference Cases

Fuel in AP1000	Fuel in VHTR	
UO_2	100% TRU	
	20% TRU	80% ThO_2
		80% UO_2
	40% TRU	60% ThO_2
		60% UO_2
		60% UO_2 with WgPu
ThO_2	100% TRU	
	20% TRU	80% ThO_2
		80% UO_2
	40% TRU	60% ThO_2
		60% UO_2

The evolution over time of the effective multiplication factor k_{eff} and consequently the VHTR core lifetime when fueled with TRU have been studied and the results are exposed in the next paragraph.

4.2 EVOLUTION OF THE EFFECTIVE MULTIPLICATION FACTOR OVER TIME

VHTRs fueled with transuranic isotopes arising from a ThO_2-fueled AP1000 cannot sustain criticality even when the fuel is completed with UO_2 or ThO_2. The effective multiplication factor at BOL of a VHTR fueled with 20% and 40% of TRU arising from a Thorium cycle can be seen in Appendix E. Therefore only VHTRs fueled with TRU arising from U-cycle have been studied in the present research.

4.2.1 USING TRU CONTAINING REACTOR-GRADE PLUTONIUM

The transuranic isotopes mentioned in this section exclusively contain isotopes coming from the AP1000 reactor. No external Plutonium has been added.

The effective multiplication factors of VHTRs fueled with 20% then 40% of TRU, completed either by UO_2 or ThO_2, are illustrated in Figure 32 along with the evolution over time of a VHTR solely fueled with TRU (100% TRU). For comparison, the k_{eff} evolution of a UO_2-fueled VHTR has been added. Dashed lines correspond to the evolution after shutdown.

Firstly, adding TRU to the fuel lowers the effective multiplication factor at BOL. The multiplication factor of a fuel containing exclusively TRU is reduced by 14%. When

the VHTR is fueled with 20% TRU + ThO_2, k_{eff} at BOL is reduced by 16%. The lowest effective multiplication factor at BOL is obtained for a VHTR fueled with 40% of TRU + UO_2 with a value of 1.07146 ± 0.00071, 20% lower than the value obtained in the UO_2-fueled VHTR.

Secondly, increasing the fraction of TRU in the fuel increases the core lifetime. Indeed when the core contains only TRU, a lifetime of 2220 days is observed. When the fuel contains 20% of TRU + UO_2, the lifetime of an UO_2-fueled VHTR has been stretched by 36%, from 610 days to 830 days. When the fuel contains 40% of TRU complemented by UO_2, the core lifetime has been extended by 53% to 930 days.

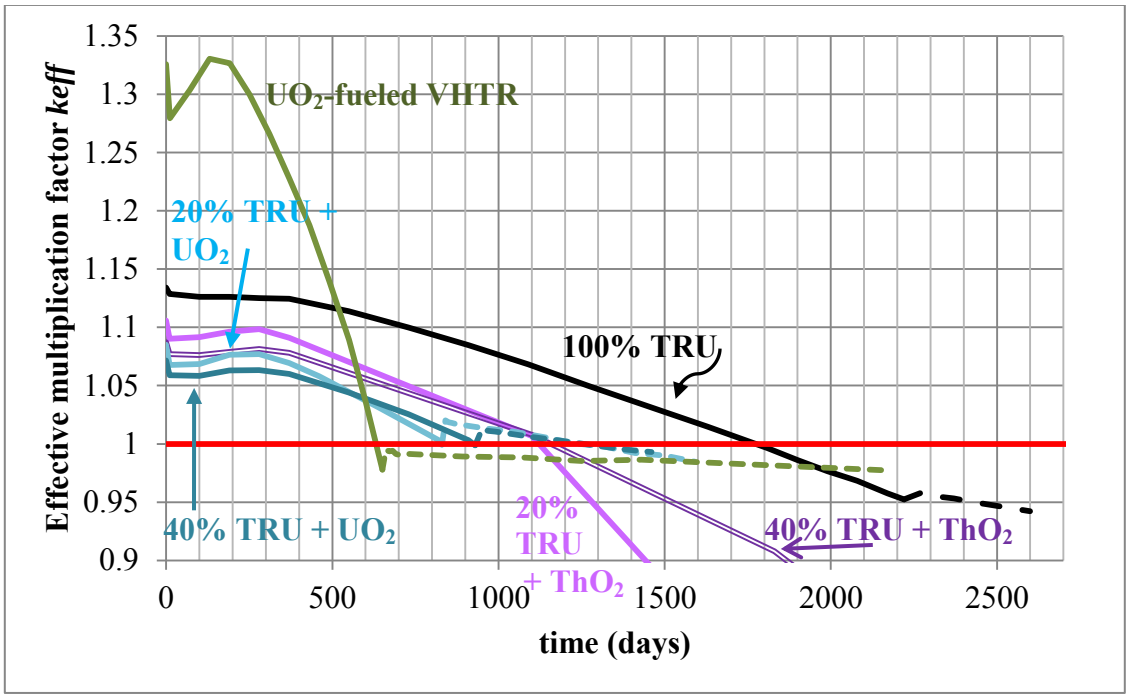

Figure 32. Evolution of k_{eff} for VHTRs loaded with TRU-based fuels, TRU arising from U-cycle

Thirdly, when the fuel complement is switched from UO_2 to ThO_2, the core lifetime is increased. With a TRU content of 20%, the core lifetime is extended by 33% from 830 days to 1100 days. With a TRU content of 40%, the core lifetime is stretched from 930 days to 1150 days, i.e. a 24% extension. Table 9 summarizes these observations.

Table 9. BOL k_{eff} and Core Lifetime for VHTR with TRU-based Fuels

Amount of TRU arising from a UO_2-fueled AP1000	Complement	k_{eff} at BOL	Core lifetime (days)
20%	UO_2	1.08508 ± 0.00066	830
	ThO_2	1.10574 ± 0.0005	1100
40%	UO_2	1.07146 ± 0.00071	930
	ThO_2	1.08719 ± 0.00075	1150
100%	none	1.13419 ± 0.00066	2220

The evolution of the multiplication over time and consequently the core lifetime depend on the consumption rate of fissile material and the rate of parasitic capture. Figure 33 illustrates the evolution of fissile content in each of these scenarios over time. The fissile content has been defined as the total mass of the following isotopes: ^{233}U, ^{235}U, ^{239}Pu, ^{241}Pu, ^{243}Pu, ^{243}Cu and ^{245}Cu. The fission cross sections of these isotopes can be seen in Appendix F. It appears that the more TRU in the fuel, the more fissile material is present. However, from Figure 32, the more TRU in the fuel, the lower k_{eff}. It indicates that the more TRU are added in the core, the more parasitic capture occur. Additionally, for the same amount of TRU, ThO_2-completed fuels appear to show less neutron losses by parasitic captures. They indeed have a high k_{eff} for the same amount of fissile material

(Fig. 33). Extension of the core lifetime in VHTRs containing ThO_2 is also explained by the buildup of ^{233}U over time as illustrated in Figure 34.

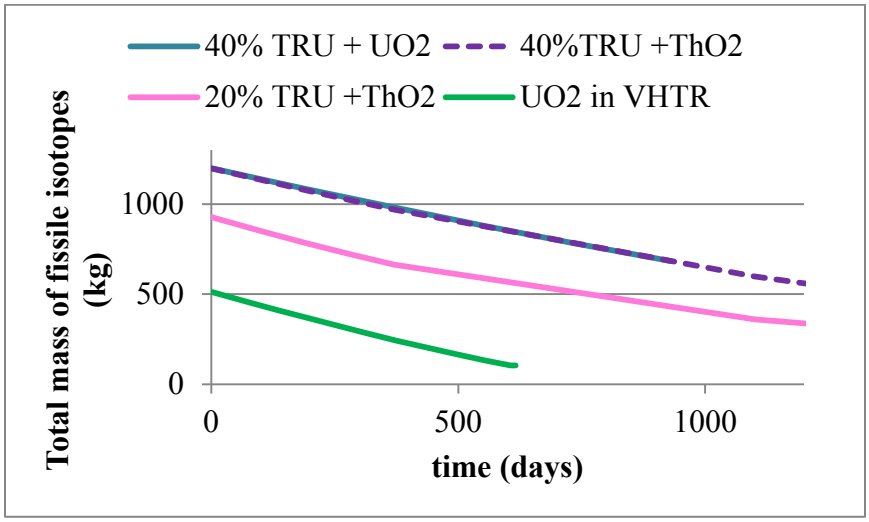

Figure 33. Evolution of the Total Mass of Fissile Isotopes during Reactor Operation. The isotopes included are ^{233}U, ^{235}U, ^{239}Pu, ^{241}Pu, ^{243}Pu, ^{243}Cu and ^{245}Cu.

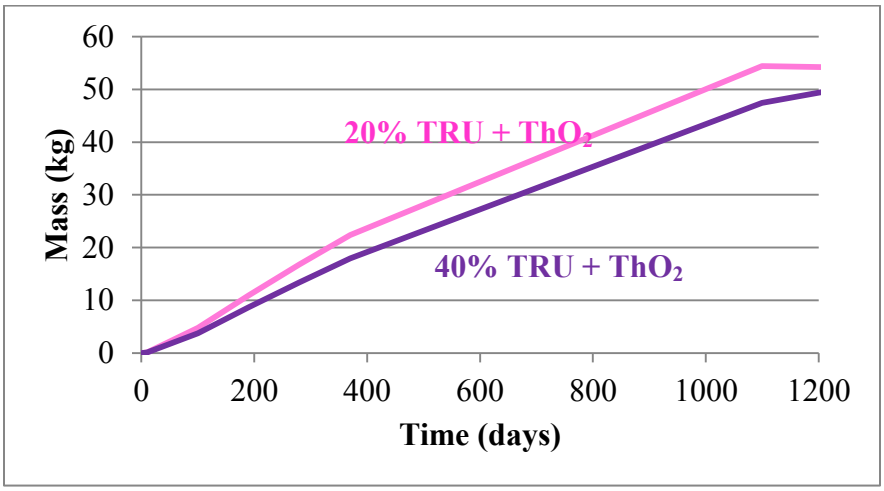

Figure 34. Evolution of the Mass of ^{233}U with time in VHTRs.

Another important observation is the increase of k_{eff} after shutdown. Similarly to a UO_2-fueled VHTR, in all cases where the reactor has been stopped when k_{eff} was very close to 1, the reactor has become supercritical again. This remark stresses the importance of having enough negative reactivity in the core to maintain it subcritical during shutdowns. Table 10 illustrates the importance of these k_{eff} jumps at EOL. The gain in the multiplication at EOL is not available (n/a) as the reactors complemented with Thorium were shutdown a long time after they had become subcritical.

Table 10. k_{eff} Increase after Shutdown

Amount of TRU arising from a UO_2-fueled AP1000	Complement	k_{eff} at EOL	Max k_{eff}	Gain in k_{eff}
20%	UO_2	0.99930 ± 0.00068	1.02023 ± 0.00072 after 10 days	0.02723
	ThO_2	1.00677 ± 0.00082	n/a	n/a
40%	UO_2	0.99885 ± 0.00067	1.01262 ± 0.00069 after 20 days	0.01377
	ThO_2	1.00793 ± 0.00074	n/a	n/a
100%	none	0.95223 ± 0.00059	0.95781 ± 0.00058 after 50 days	0.00558

To summarize, when TRUs are added to the fuel, the reactor core lifetime is extended and the effective multiplication factor decreases much more smoothly than in an UO_2-fueled VHTR.

4.2.2 USING TRU CONTAINING WEAPON-GRADE PLUTONIUM

The observations detailed in this section exclusively concern TRU fuels where the reactor-grade plutonium isotopes have been replaced by weapon-grade plutonium (WgPu). The composition of TRU-based fuels containing WgPu can be found in Appendix G.

First, the evolution of k_{eff} over time for VHTRs loaded with TRU-based fuels containing RgPu is compared to the evolution of k_{eff} when the reactors are fueled with TRU containing WgPu. Figure 35 illustrates the differences in evolution of k_{eff} over time. The effective multiplication factor of a TRU fuel containing WgPu is translated by 172 milli-k for the VHTR fueled with 40% TRU + UO_2.

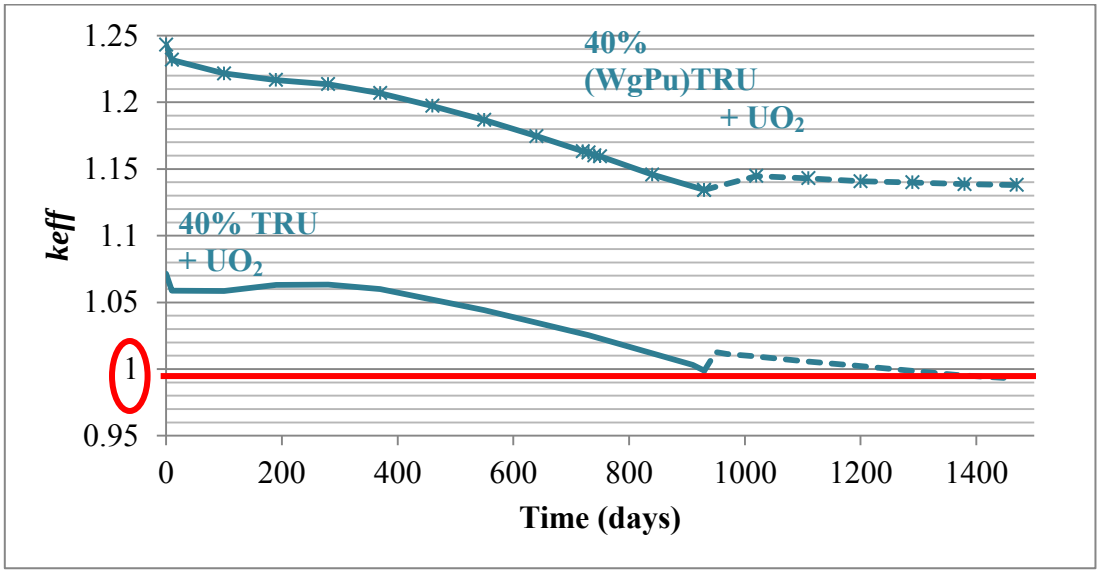

Figure 35. Evolution of k_{eff} for VHTRs loaded with 40%TRU +UO_2 Fuels Containing WgPu instead of RgPu. TRU arise from U-cycle

To sum up, during the VHTRs lifetime, fuels with 40% of TRU containing WgPu have an effective multiplication factor 16.0% higher than the same fuel containing RgPu. The reduction over time is very similar in both cases. Therefore VHTRs fueled with WgPu should have a longer core lifetime. Extra negative reactivity must be added to such cores to balance the supercriticality at BOL.

The presence of WgPu seems to lower the amplitude of k_{eff} jump at shutdown. However more cases should be run with more burnup steps before and after shutdown to draw reliable conclusions. Table 11 compares k_{eff} jumps after shutdown for VHTRs fueled with TRU containing WgPu against VHTRs fueled with regular TRU.

Table 11. Summary of k_{eff} Variations for VHTRs Fueled with 40% TRU.

Comple-ment	Pu type	k_{eff} *at BOL*	k_{eff} at EOL	Max k_{eff} (days after shutdown)	Gain in k_{eff} after shutdown
UO_2	Rg	1.07146 ± 0.00071	0.99885 ± 0.00067	1.01262 ± 0.00069 (20 days)	0.01377
	Wg	1.24317 ± 0.00071	1.13424 ± 0.00066	1.4470 ± 0.00072 (90 days)	0.0105

The next step was to establish the composition of the fuel at EOL for each reference case and determine the destruction rate achieved by each fuel cycle strategy.

4.3 VHTR TRANSURANICS TRANSMUTATION PERFORMANCES AND FUEL CYCLES OPTIONS

4.3.1 TRU COMPOSITION AT THE END OF THE VHTR CORE LIFETIME

Figure 36 presents the specific mass of TRU left in the VHTR when the latter is shutdown. For consistency with Chapter 3, the specific mass has been used and defined as the mass of each nuclide left per unit initial mass of fuel. ZAiD identifies each isotope by its atomic number Z followed by its mass number A. For instance, ^{235}U is designed by 92235.

The main isotope left at shutdown is ^{238}U when TRUs are completed with UO_2 and ^{232}Th when TRUs are completed with ThO_2. ^{235}U is also present in a significant amount, as well as ^{236}U, in all cases. As expected, VHTRs containing ^{232}Th produced important quantities of ^{233}U. The masses of each of these isotopes have been summarized in Table 12. The total mass of the main Pu isotopes (from ^{238}Pu to ^{242}Pu) can also be found in Table 12.

Table 12. Mass in kg of the principal isotopes left in the VHTRs at EOL

Isotopes	Mass (kg)			
	20% TRU		40% TRU	
	ThO_2	UO_2	ThO_2	UO_2
^{235}U	193.6	236.4	190.3	207.8
^{236}U	45.36	34.97	26.28	22.75
^{233}U	54.40	trace	47.43	trace
Pu	325.1	441.6	879.2	1,021

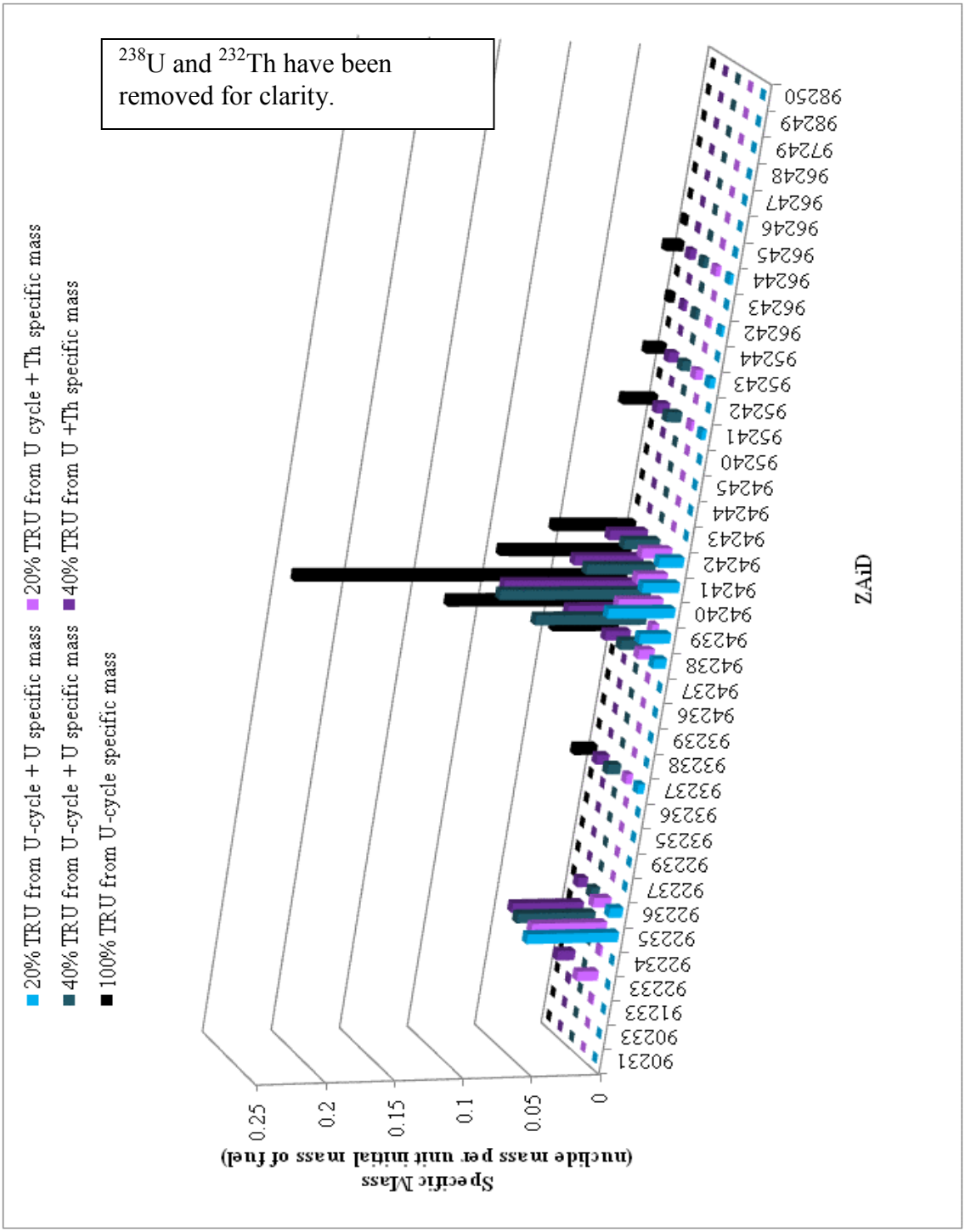

Figure 36. Isotopic Specific Mass of VHTR Used Fuels

As it can be seen from Table 12 and Figure 34, using 20% of TRU instead of 40% of TRU leaves 1.2 times more ^{233}U at EOL.

The amount of ^{236}U left at EOL in the VHTR fueled with 40% of TRU +ThO_2 is reduced by a factor of 1.7 compared to the quantity left when only 20% of TRU is used. The production of ^{236}U in ThO_2 fuels was described in Figure 2. It comes from the parasitic capture of a neutron in ^{233}U, then in ^{234}U, and finally in ^{235}U.

Finally, replacing UO_2 by ThO_2, reduces the production of Pu isotopes. In the 20% TRU cases, the total mass of Pu is reduced by 26% when ThO_2 is used instead of UO_2. In a VHTR fueled with 40% of TRU, the mass of Pu is reduced by 14%.

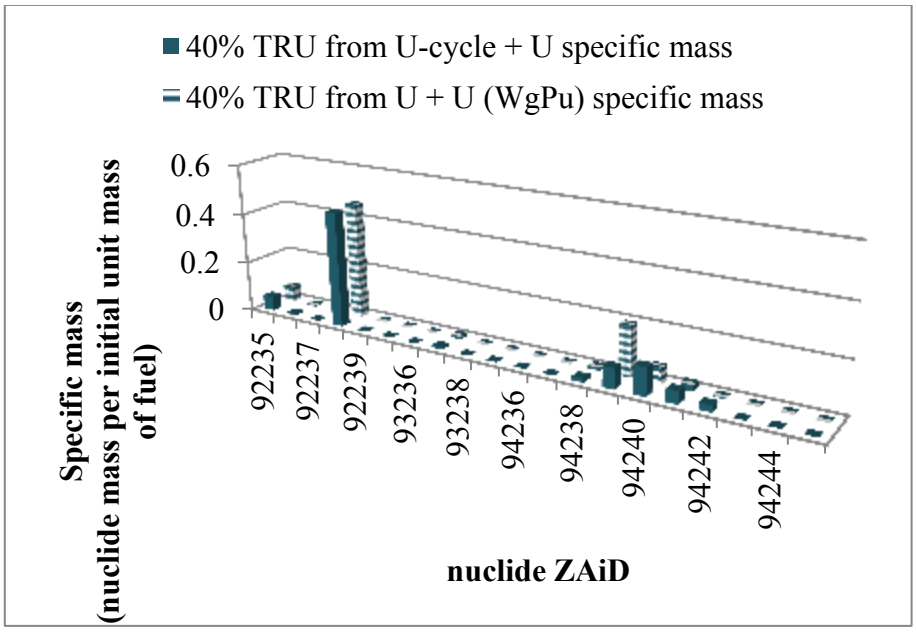

Figure 37. Specific Mass of Pu at EOL. WgPu TRU Fuels against RgPu Fuels

A similar trend can be observed when WgPu is used. If UO_2 is added, the fuel will contain 1.14T of Pu at EOL. Using WgPu instead of RgPu, the mass of ^{239}Pu is left at EOL is more than 5 times more significant in the case where 40% of TRU is used. On the contrary, the mass of ^{238}Pu has been reduced by 1.16 and the mass of ^{242}Pu by 2.52. Figure 37 illustrates these observations.

The Plutonium destruction rates and more generally the TRU destruction rates, as well as the transmutation efficiencies of each scenario, are detailed in the next section.

4.3.2 TRANSMUTATION EFFICIENCIES AND FUEL CYCLES OPTIONS

As explained in Chapter 3, the transmutation efficiency of a cycle was defined as its ability to incinerate transuranic isotopes relatively to the initial amount of fuel loaded in the first reactor of the cycle (Eq. 2). The TRU destruction rate D_{TRU} corresponds to the VHTR ability to reduce the initial mass of TRU that was loaded in it as a fuel. It can be defined as:

$$D_{TRU} = \frac{m_{TRU}^{EOL} - m_{TRU}^{BOL}}{m_{TRU}^{BOL}} \quad (2)$$

where m_{TRU}^{EOL} is the mass of TRU at EOL in the VHTR and m_{TRU}^{BOL} the mass at BOL.

In the present section both parameters have been established for each fuel cycle scenario. These parameters have been used to rank the scenarios depending on three objectives they could fulfill. One objective could be to reprocess AP1000 wastes faster than they are produced. Another objective could be the incineration of as much TRU as possible at the end of the VHTR lifetime. Another objective – and the last one studied herein – could be the reduction of ^{235}U consumption while reprocessing.

VHTR reprocessing rate

To determine which configuration could reprocess AP1000 wastes faster than they are produced, the number of wastes batches produced by the AP1000 per year was derived from the core life characteristics chosen in Chapter III. Since the AP1000 was set to run for 600 days approximately, 1 batch of wastes is created every 600 days, i.e. 0.61 batch per year

The number of AP1000 batches of wastes a VHTR could reprocess per year was calculated as follow:

$$\dot{N}_{VHTR} = \frac{B}{L} * 365.25 \tag{3}$$

where B is the number of AP1000 TRU batches the VHTR can be loaded with, L the core lifetime of the VHTR in days. $\dot{N}_{VHTR}$ unit is batch per year of VHTR operation.

B was simply calculated as:

$$B = \frac{m_{VHTR}^{BOL}(TRU)}{m_{AP1000}^{EOL}(TRU)} \tag{4}$$

where *m(TRU)* is the mass of TRU either at EOL or BOL depending on the superscript, in the AP1000 or the VHTR depending on the subscript.

Finally the number N of AP1000 wastes batches that can be processed every 600 days – i.e. every time a new batch of TRU is created by the AP1000 – is given by:

$$N = \frac{\dot{N}}{0.61} \tag{5}$$

The results are shown in Table 13 below. Only VHTRs fueled either 100% of TRU or 40% of TRU completed by UO_2 can process more AP1000 wastes than created. For

instance, one VHTR fueled with 100% of TRU can reprocess the wastes created by 1.64 AP1000. On the other hand 3 VHTRs fueled with 20% of TRU + 80% of ThO_2 are necessary to process the wastes produced by one AP1000.

Table 13. TRU Processing Rate for each VHTR Configuration

Fuel in VHTR (TRU from U-cycle)		Core lifetime (days)	VHTR Rate of AP1000 batch processing (batch per year)	AP1000 Rate Production of TRU batch (batch per year)	# of TRU batches that can be processed every 600 days
100% TRU		2220	1.00	0.61	1.64
20% TRU	80% ThO_2	1100	0.20	0.61	0.33
	80% UO_2	830	0.48	0.61	0.80
40% TRU	60% ThO_2	1150	0.50	0.61	0.82
	60% UO_2	930	0.89	0.61	1.46
	60% UO_2 with WgPu	[930]	0.95	0.61	1.57

VHTR TRU destruction rate

If the objective of the fuel cycle is to incinerate as much TRU as possible, the TRU destruction has to be measured. Table 14 summarized these values for the different VHTR scenarios.

Table 14. Transuranics Destruction Rates

Fuel in VHTR (TRU from U-cycle)		AP1000-VHTR cycle Transmutation Efficiency (%)	TRU mass left at VHTR EOL as a percentage of AP1000 initial UO_2 mass (%)	VHTR TRU Destruction Rate (%)
100% TRU		-2.18	2.92	-35.2
20% TRU	80% ThO_2	0.29	0.45	-88.9
	80% UO_2	0.16	0.58	-85.7
40% TRU	60% ThO_2	-0.42	1.16	-72.2
	60% UO_2	-0.59	1.33	-68.2
	60% UO_2 with WgPu	-0.71	0.82	-67.7

The highest transmutation and TRU destruction rates are obtained for a VHTR fueled with 20% of TRU completed with ThO_2 or UO_2. For the same amount of TRU, the reactor containing ThO_2 obtains higher TRU destruction rates. The results observed in paragraph 3.2.2 where the Pu inventory was lowered in a VHTR fueled with only 20% of TRU and completed by ThO_2 seems to be confirmed while looking at the destruction rates. Interestingly a reactor fueled solely with TRU obtains the lowest TRU destruction rates.

Whatever the VHTR fuel loading, the transmutation efficiency fluctuates between -0.29% and 2.18%. The final mass of TRU left at the VHTR's EOL therefore fluctuates between 0.45% and 2.92% of the mass of initial UO_2 loaded in the AP1000.

^{235}U consumption reduction using VHTR

Uranium resources consumption minimization is one of the challenges of nuclear fuel cycles optimization. ^{235}U consumption rate per day of VHTR and per percentage of initial amount of ^{235}U in the fuel are presented in Table 15 for the different loadings of the VHTR. The use of ThO_2 to complement the fraction of TRU in the VHTRs fuel instead of UO_2 does not significantly reduces the consumption of ^{235}U. Aside from the 100% TRU fuel case which produces approximately 1kg of ^{235}U in 6 years, the fuel containing 40% of TRU and WgPu, complemented by 60% of UO_2 has the lowest consumption of ^{235}U per day at a value of 0.026%/day. With RgPu, this consumption is increased to 0.034%. Replacing UO_2 by ThO_2 slightly lowers the consumption by 0.002%. Therefore ThO_2 fuels, made of ^{235}U and the fertile isotope ^{232}Th to replace ^{238}U, do not lower the daily consumption of Uranium-235. However, implementing ThO_2

fuels in a nuclear system would reduce Uranium resources consumption by producing the fissile isotope ^{233}U.

Table 15. ^{235}U Daily Consumption Rate for each Fuel Cycle Strategy per Initial Amount of ^{235}U

Fuel in VHTR (TRU from U-cycle)		^{235}U consumption per day as a percentage of initial ^{235}U mass (%/day)
100% TRU		*1.122kg produced*
20% TRU	80% ThO_2	0.049
	80% UO_2	0.050
40% TRU	60% ThO_2	0.032
	60% UO_2	0.034
	60% UO_2 with WgPu	0.026

Table 16 below summarized the results established in paragraph 4.3. A fuel containing simply transuranic isotopes appears to reach a TRU destruction rate of 35% at the fastest rate and while sparing ^{235}U resources. However the metallurgy of such fuels seems to be an unknown and such fuels are unlikely to be produced. A transuranic fuel containing 40% of TRU complemented by ThO_2 appears as a good compromise. It reduces the inventory of TRU in the VHTR by 72.2% – the mass of TRU left at VHTR EOL representing only 1.16% of the initial mass of LEU fuel loaded in the AP1000 – and has the lowest ^{235}U daily consumption (WgPu excepted). However, 2 VHTRs would be necessary to reprocess the TRU produced by one AP1000 if no other reprocessing mean is implemented in parallel.

Table 16. Summary of Fuel Cycle Strategies Performances

Rank	Fastest reprocessing rate	Best TRU destruction rate	Lowest ^{235}U consumption per day
First	100% TRU	20% TRU + 80% ThO_2	100% TRU
Second	40% TRU with WgPu + UO_2	20% TRU + 80% UO_2	40% TRU (WgPu) + UO_2
Third	40% TRU + UO_2	40% TRU + ThO_2	40% TRU + ThO_2
Worst	20% TRU + ThO_2	100% TRU	20% TRU + UO_2

4.3.3 TRU ACTIVITY AT THE END OF THE VHTR CORE LIFETIME

Similarly to Chapter 3.2.3, the specific activity of the TRU left at EOL of the VHTR was analyzed and can be seen in Figure 38.

First the main isotopes contributing to the activity are ^{239}U and ^{239}Np, for UO_2-complemented fuels and ^{233}Th and ^{233}Pa for ThO_2-complemented fuels. In all cases, the activity is also caused by ^{238}Np – especially present in UO_2-complemented fuels and the when the fraction of TRU is increased – by ^{241}Pu, by ^{243}Pu, by ^{244}Am and by ^{242}Cm.

Table 17. Total Activity in the VHTRs at EOL

TRU fraction	Complement	Total Activity (Ci)
100%		1.910e8
20%	ThO_2	2.214e8
	UO_2	2.999e8
40%	ThO_2	2.151e8
	UO_2	2.815e8

The total activities of these fueling strategies have been summarized in Table 17. The least active fuel is the one made of TRU exclusively. Replacing UO_2 by ThO_2,

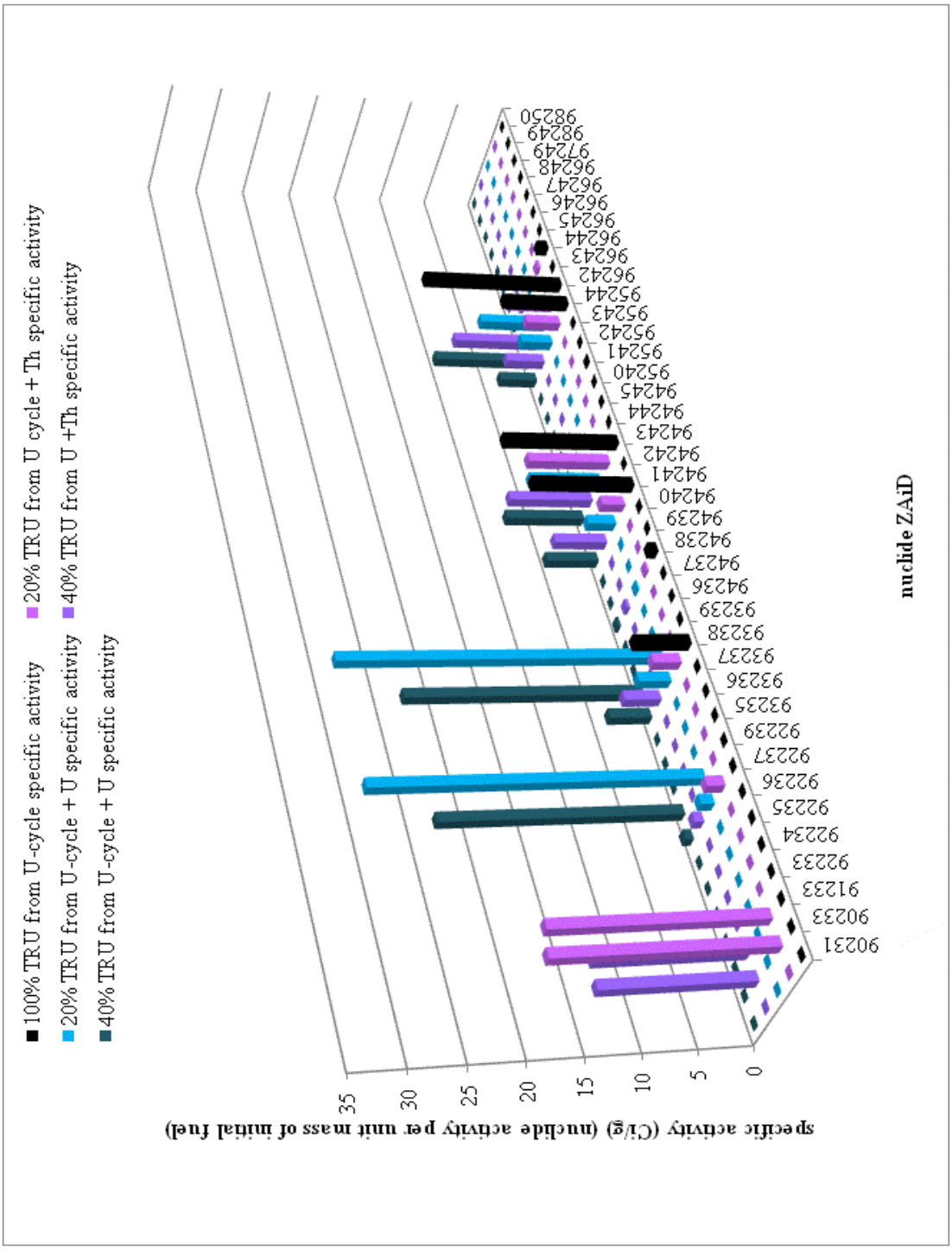

Figure 38. Specific Activity per Isotopes at EOL for Different VHTRs Fuel Loadings

reduces the total activity. Indeed for the 20% TRU case, the activity has been reduced by 26% while for the 40% TRU case, the activity has been reduced by 25%.

In a summary, the handling of TRU-fuels completed by ThO_2 after one reprocessing, immediately after shutdown, appears easier than the handling of TRU-fuels supplemented with UO_2.

Figure 39 represents the specific activities of VHTRs loaded with 40% of TRU completed either by Thorium or Uranium oxides and containing either RgPu or WgPu.

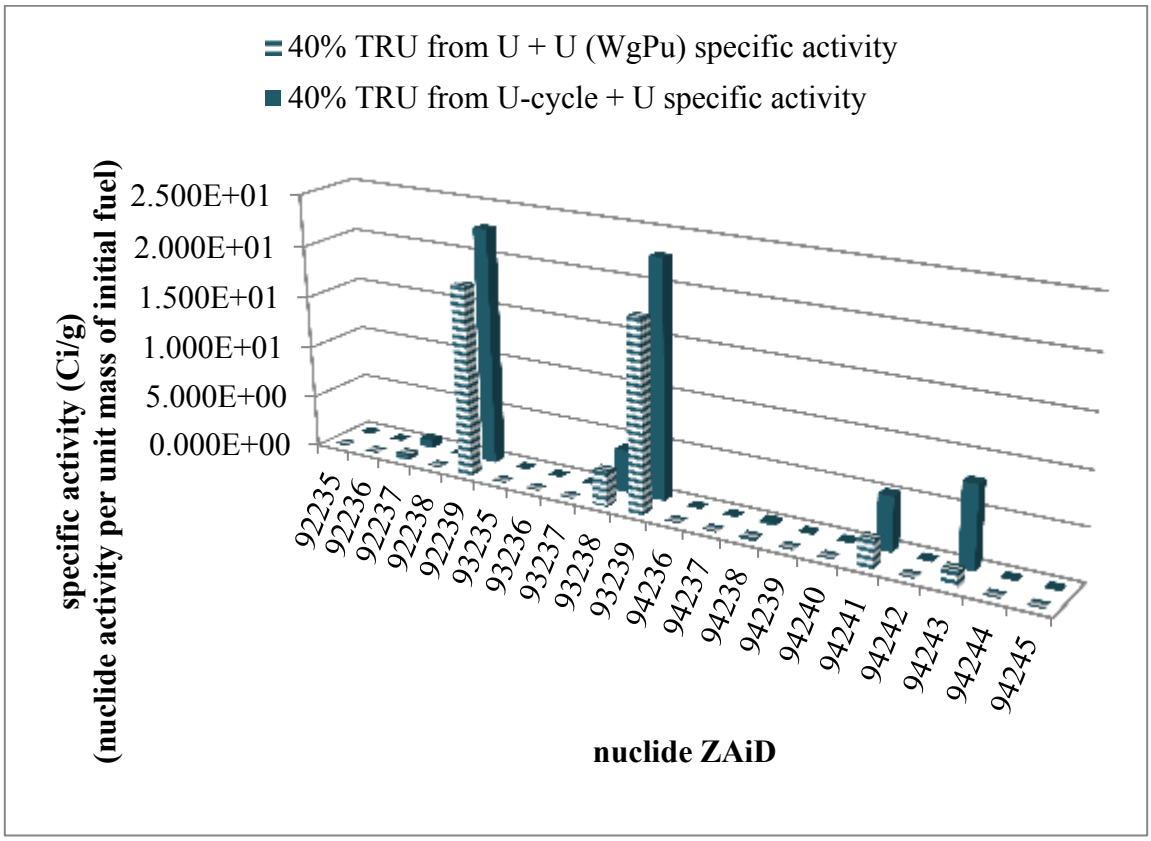

Figure 39. Comparison of the Specific Activity of the Inventory at EOL

It appears that fuels containing WgPu are less active after having spent the same amount of days in the reactors. There is indeed less ^{238}Pu in WgPu.

Most of the differences observed between the different fuel loading configurations are related to fuel differences. The next and last paragraph summarizes the effect of different fuels loadings on the VHTR spectra.

4.4 VHTR ENERGY SPECTRA

Likewise Chapter 3.2.4. the normalized flux per unit lethargy was evaluated for several VHTR fuel loadings. Evident variation of the spectrum relatively to a UO_2-fueled VHTR is to be seen in the thermal region of the flux: the thermal peak is inexistent for VHTR loaded with TRU-based fuels. Indeed neutrons are being removed by absorption in ^{237}Np, ^{241}Am, ^{240}Pu and ^{242}Pu. The absorption of a neutron by ^{237}Np yields ^{238}Pu (a strong alpha emitter) after several days. ^{241}Am becomes ^{242}Am after absorbing a neutron. ^{240}Pu and ^{242}Pu respectively become ^{241}Pu and ^{243}Pu both fissile isotopes. These features are illustrated in Figure 40. The radiative capture cross sections of ^{237}Np, ^{241}Am, ^{240}Pu and ^{242}Pu can be seen in Appendix H.

The energy spectrum of a VHTR fueled with 40% of TRU +UO_2 against the energy spectrum of the same reactor loaded with the same fuel mix but containing WgPu is plotted in Figure 41. The ratio in between the two fluxes is plotted in Figure 42.

In a fuel containing WgPu, neutrons at energies below 0.5eV seems less likely to be absorbed as their higher energy spectrum can testify. Also the resonance in the absorption cross section of ^{240}Pu affects less significantly the flux of a VHTR containing

WgPu since it contains less ^{240}Pu than RgPu. A depression around 2.6eV, observed in the spectrum of a VHTR fuel containing RgPu, is absent from the spectrum of a VHTR containing WgPu.

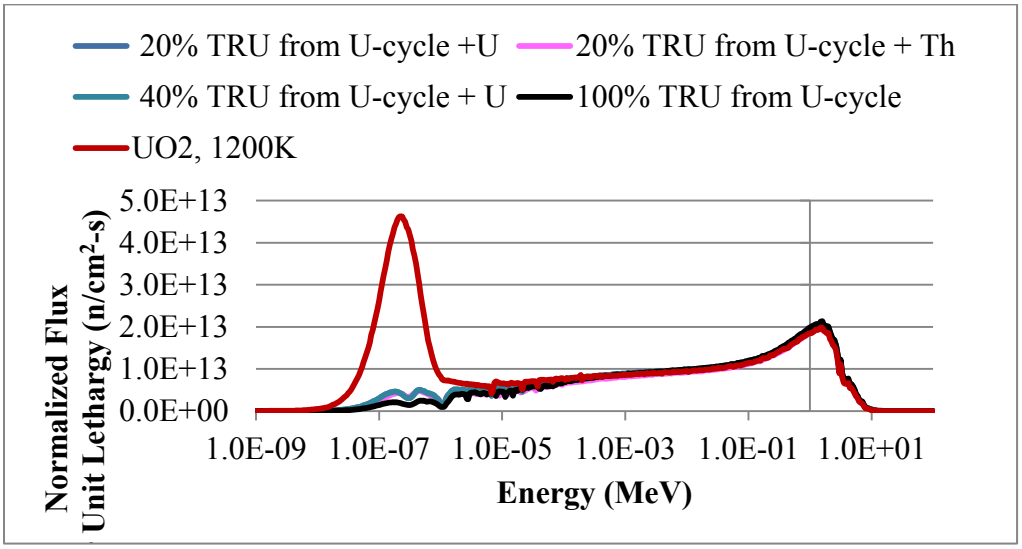

Figure 40. Normalized Flux per Unit Lethargy for the different VHTR Fuel Loading Configurations

This depression certainly corresponds to a resonance in the ^{232}Pu capture cross section. The absence of the depression in the spectrum of a VHTR containing WgPu can be explained by the lower amount of ^{232}Pu in the core. This depression is not visible in the fuel containing WgPu. At energies above 10eV, the two spectra are very similar. Again, these observations prove that the energy spectrum of a reactor is dependent of the fuel composition.

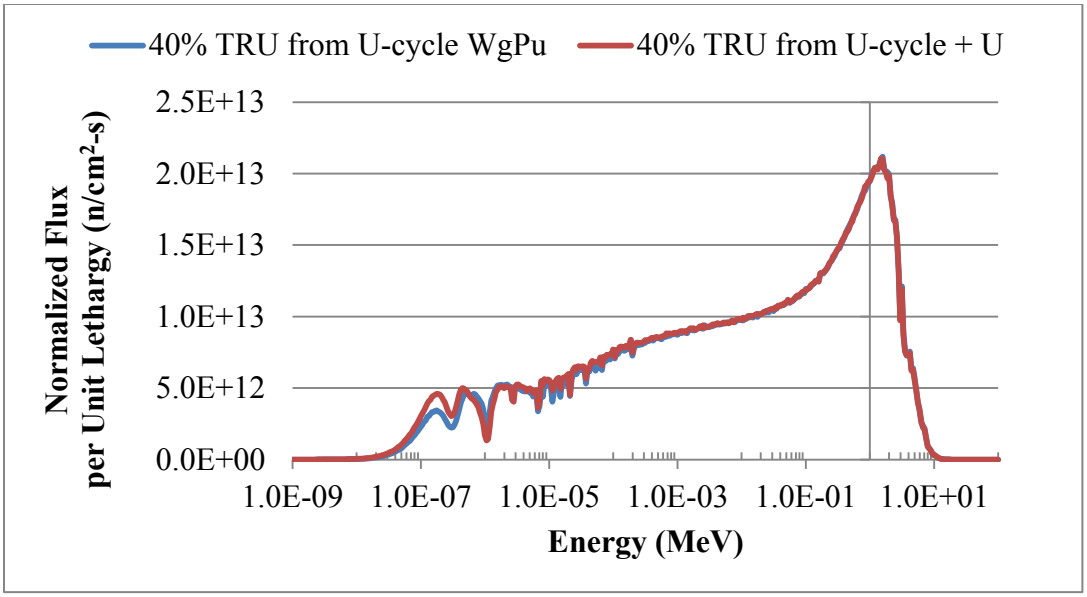

Figure 41. Normalized Flux per Unit Lethargy for VHTRs TRU-based fueled containing WgPu or RgPu.

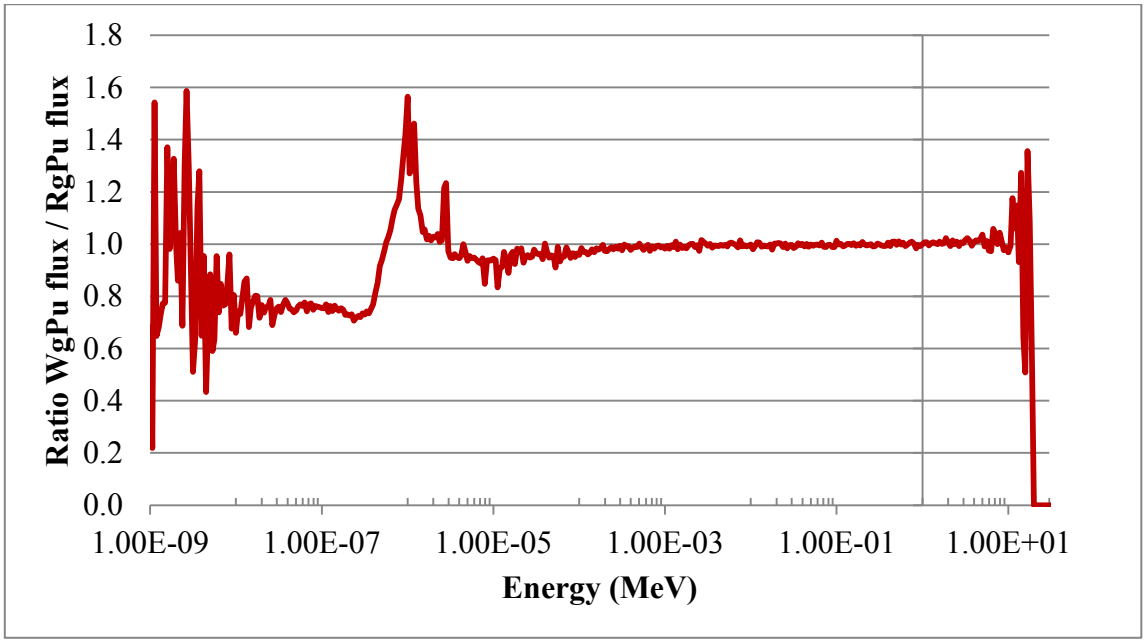

Figure 42. Ratio of the Energy Spectrum from a VHTR containing WgPu to the Energy Spectrum of a VHTR containing RgPu

After having analyzed various advanced AP1000-VHTR fuel cycle strategies and established values of reference for the effective multiplication factor, the TRU inventory at EOL, the transmutation efficiency and the energy spectra of the VHTRs when the latter is loaded with TRU-based fuels, the next and final step of the study was to perturb the prompt neutron fission spectrum and quantify the impact of these variations on the fuel cycle parameters.

CHAPTER V

NUCLEAR DATA VARIATION IMPACT ON NUCLEAR ENERGY SYSTEM EVALUATIONS – FISSION SPECTRUM CASE

5.1 CURRENT DISCREPANCIES IN NUCLEAR DATA

The first step of this work consisted in gathering data proving the existence of discrepancies among nuclear data. Four nuclear data libraries were compared to ENDF/B-VII.0 considered the reference library for the study. Indeed it was presumable the most complete version of the evaluated file with the most recent evaluations at the time of the study. The four libraries were ENDF/B-VI.8, JEFF-3.1, JENDL-3.3 and CENDL-3.1. ENDF/B-VI.8 corresponds to the US evaluated nuclear datafile released in 1990 in the ENDF-6 format. JEFF-3.1 is the European evaluated nuclear data library of the OECD Nuclear Energy Agency. It was finalized in 1992, released in 1993 and has been continuously updated since its release. JENDL-3.3 is the Japanese evaluated nuclear data library, released in 1989, significantly updated in 1994 and continuously updated since the release. A new version was released in 2010, JENDL-4.0, after the comparisons were made. CENDL-3.1 is the Chinese version of the evaluated nuclear data library and was issued in 1991, supplemented in 1993 and 1995 and revised in 1997. All libraries are now edited in the ENDF-6 format. This format, developed and first used in the United States, is now used worldwide to encode nuclear data evaluations.

The effort was limited to three nuclear properties: the microscopic fission cross section σ_f, the microscopic radiative capture cross section σ_γ and the neutron fission spectrum χ. The microscopic cross sections give a measure of the probability that a particular interaction will occur per target nucleus, per unit flux of incident neutrons and per second. The neutron fission spectrum χ represents the energy distribution of neutrons emitted after a reaction of fission. As detailed in Chapter 5.2, these nuclear data are repeatedly used in criticality and reactor design calculations and fuel cycles optimization.

^{241}Am, ^{242m}Am, ^{237}Np, ^{242}Cm, ^{244}Cm, ^{235}U and ^{238}U were the isotopes retained for the fission cross sections comparison, while the isotopes chosen for the radiative capture cross sections and the fission spectrum comparisons were reduced to ^{235}U, ^{238}U and ^{239}Pu. ^{235}U and ^{238}U were chosen since they are the main constituents of the fresh fuel UO_2 and thus the main contributors to the production of TRU. ^{238}U is the main contributor in the production of TRU by producing ^{239}Pu through a neutron capture followed by beta-decays. Figure 43 presents the different transmutation and decay schemes starting from Uranium. Even if the possibilities seem numerous, upon removal from a typical LWR, the TRU elements have the approximate composition of 90% Pu, 5% Np, 4% Am, and 1% Cm. Moreover it has to be noted that the fuel contains roughly 95% uranium, 4% fission products, and only 1% TRU at EOL [44].

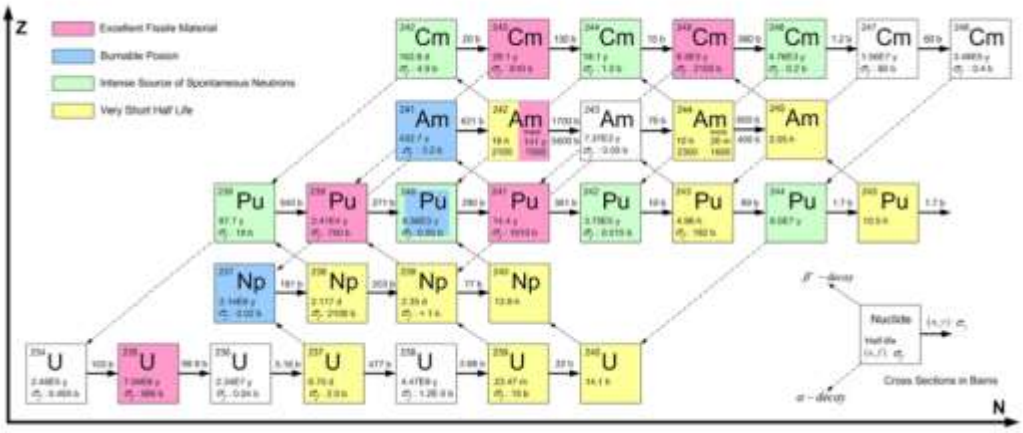

Figure 43. Transmutation and Decay Schemes [44]

The discrepancies among libraries were emphasized by plotting the three ratios:

$$\frac{\sigma_f \; from library \, i}{\sigma_f \; from \, \mathrm{ENDF \backslash B-VII.0}} \tag{6}$$

$$\frac{\sigma_\gamma \; from library \, i}{\sigma_\gamma \; from \, \mathrm{ENDF \backslash B-VII.0}} \tag{7}$$

$$\frac{\chi \; from library \, i}{\chi \; from \, \mathrm{ENDF \backslash B-VII.0}} \tag{8}$$

where i stands for a particular database other than ENDF\B-VII.0, σ_f is the fission cross section, σ_γ is the radiative capture cross section and χ the fission spectrum. JANIS-3.1, a very user-friendly JAva-based Nuclear Information Software developed by the NEA (Nuclear Energy Agency), was used to retrieve the data and plot the ratios. However the ratios presented herein were plotted in Excel for more clarity. The fission cross section was retrieved choosing MF=3 and MT=18. The couple (MF=3, MT=102) was used to plot the radiative capture cross section and the couple (MF=5, MT=18) for the prompt

neutron fission spectrum. The methodology and the models used to evaluate nuclear data from the experimental data can be found in the descriptive comments preceding the contents of each ENDF6-fornatted file and is not fully described herein. With JANIS-3.1, the heading of the file can be retrieved using MF=1 in the ENDF search window.

Only the analyses of the neutron fission spectrum will be detailed below.

5.1.1 FISSION SPECTRUM OF URANIUM-235

The first ratios studied are ENDF/B-VI.8 to ENDF/B-VII.0 and JEFF-3.1 to ENDF/B-VII.0 for ^{235}U. They are plotted together in Figure 44 along with the ratio CENDL-3.1 to ENDF/B-VII.0. Since ENDF/B-VI.8 and JEFF-3.1 are based on the same evaluations, the values of the ratio are the same. CENDL-3.1 evaluation being extremely close to those of ENDF/B-VI.8 and JEFF-3.1, the observations detailed above are equally valid for CENDL-3.1 values.

ENDF/B-VI.8 and JEFF-3.1 evaluations have been established for outgoing neutron energies from 10eV to 30MeV. The neutron incoming energy was chosen to be 2MeV, the average neutron energy. The discrepancies with respect to the reference library are 2% or less for energies below 3.08MeV. For energies in the range [6.1MeV; 9.2MeV[the ratio is 1.05 or higher meaning that the values in ENDF/B-VI.8, JEFF-3.1 and CENDL-3.1 are 5% higher than in the reference library. Only for energies above 9.2MeV are the discrepancies higher than 10%. At 0.7MeV, the most probable neutron energy, the ratio is 0.986 and at 2MeV the ratio is 0.997. Therefore, the prompt neutron fission spectra of ^{235}U from the libraries ENDF/B-VI.8, JEFF-3.1 and CENDL-3.1 are in good agreement with the reference library except for energies above 9.2MeV. ENDF/B-

VI.8 and JEFF-3.1 evaluations of the energy spectrum are both based on calculations by D.Madland using Madland-Nix formalism.

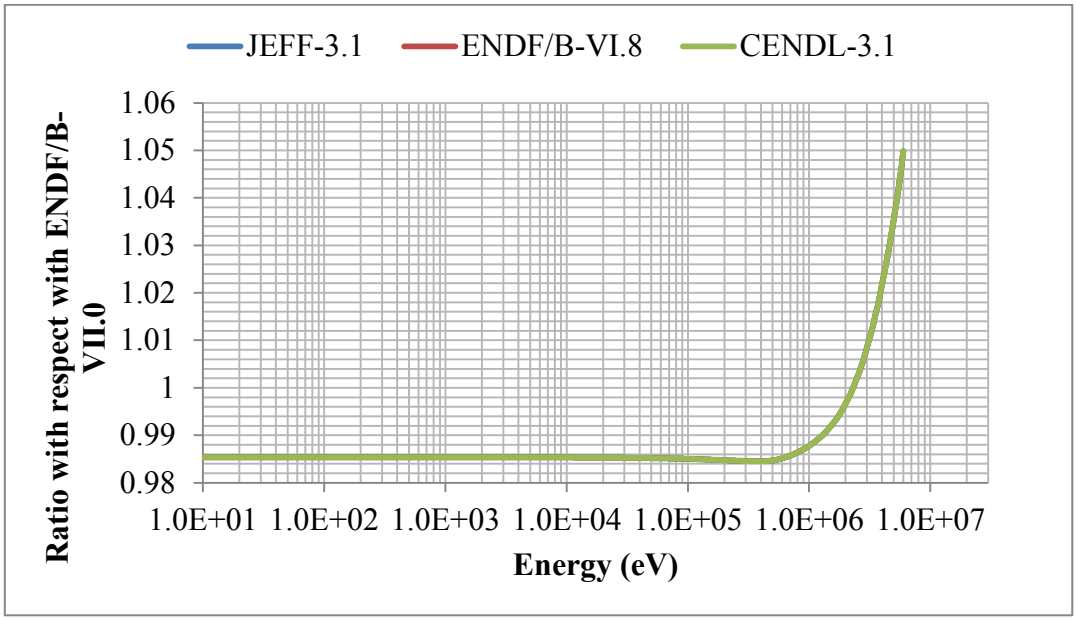

Figure 44. ^{235}U Prompt Neutron Fission Spectrum Ratio ENDF/B-VI.8, JEFF-3.1 and CENDL-3.1 vs. ENDF/B-VII.0

Although the evaluation in JENDL-3.3 library starts at 0.01eV, the ratio has been plotted only from 10eV – energy at which the evaluation starts in the ENDF/B-VII.0 library. For energies between 22keV and 5.8MeV, the discrepancy with respect to ENDF/B-VII.0 is below 5%. For energies in the range [61keV; 4.9MeV], the discrepancies are even contained in a 2% range. Only for energy below 76eV is the ratio above 1.10, i.e. the discrepancies are above 10%. The discrepancies become higher than 15% for energies above 8.5MeV. Again, the prompt neutron fission spectrum of ^{235}U evaluated in JENDL-3.3 is in good agreement with the reference evaluation.

Additionally, at 0.7MeV, the ratio is 0.978 and at 2MeV the ratio equals 1.03. These observations are illustrated in Figure 46.

To summarize, the prompt neutron fission spectrum evaluations of ^{235}U are in good agreement for energies above 61keV and below 3.08MeV, regardless of the library. For ENDF/B-VI.8, JEFF-3.1 and CENDL-3.1 this range can be extended to 10eV. Evaluations of the prompt neutron fission spectrum are only discrepant for energies above 8.5MeV, regardless of the library.

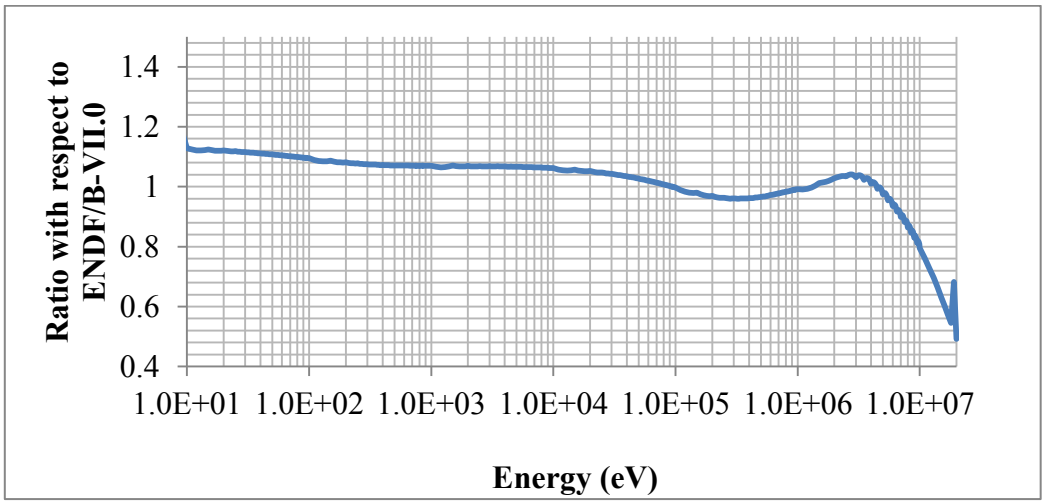

Figure 45. ^{235}U Prompt Neutron Fission Spectrum Ratio JENDL-3.3 vs. ENDF/B-VII.0

5.1.2 FISSION SPECTRUM OF URANIUM-238

Similarly to ^{235}U, the following ratios of the prompt neutron fission spectrum of ^{238}U have been derived: CENDL-3.1 to ENDF/B-VII.0, JEFF-3.1 to ENDF/B-VII and JENDL-3.3 to ENDF/B-VII.0. They can be observed in Figure 46. ENDF/B-VI.8 to

ENDF/B-VII.0 is not represented as ENDF/B-VI.8 library contained only 2 points at 0eV and 37eV for the prompt neutron fission spectrum of ^{238}U.

JEFF-3.1 evaluation is in very good agreement with the reference evaluation. Indeed from 10eV to 17.8MeV, the amplitude of the discrepancies is 2% or less. From 17.8MeV to 2MeV, JEFF-3.1 values are at worst 3.6% higher than the reference ones. At 0.7MeV, the ratio is 0.99994 and at 2MeV the ratio is 0.99927. The prompt fission neutron multiplicity and spectra for ^{238}U in JEFF-3.1 were calculated using the BRC improved Los Alamos model from Vladuca and Tudora.

The evaluation in CENDL-3.1 varies by up to 2% from the reference evaluation for energies from 7.2keV to 150keV and from 1.5MeV to 2.5MeV. In the range [150keV;1.5MeV], the amplitude of the discrepancies can be up to 7%. This energy range excluded, from 10eV to 3MeV the evaluation is by 5% discrepant at maximum. For energies above 4.3MeV, the amplitude of the discrepancies reaches 10% and more; above 6.8MeV it becomes higher than 15%. No value has been evaluated at 0.7MeV and 2MeV. However the ratio at 0.67MeV is 0.937. These features can be seen again in Figure 46.

The JENDL-3.3 evaluation is also in good agreement with the reference evaluation: from 10eV to 6MeV, the amplitude of the discrepancies is contained in a 2% range. Above 6MeV, the ratio decreases to 0.80189 at 20MeV, i.e. JENDL-3.3 value being 20% lower than the ENDF/B-VII.0.

To sum-up, the prompt neutron fission spectrum evaluation of ^{238}U are in very good agreement with the reference library except at energies above 3MeV regardless of the

library and in the range [0.15MeV;1.5MeV] for the Chinese evaluation. However no prompt neutron fission spectrum was available in the ENDF/B-VI.6 library except two data points at 0eV and 37MeV. Fission spectra for ^{235}U and ^{238}U are derived in a similar manner in JENDL-3.3.

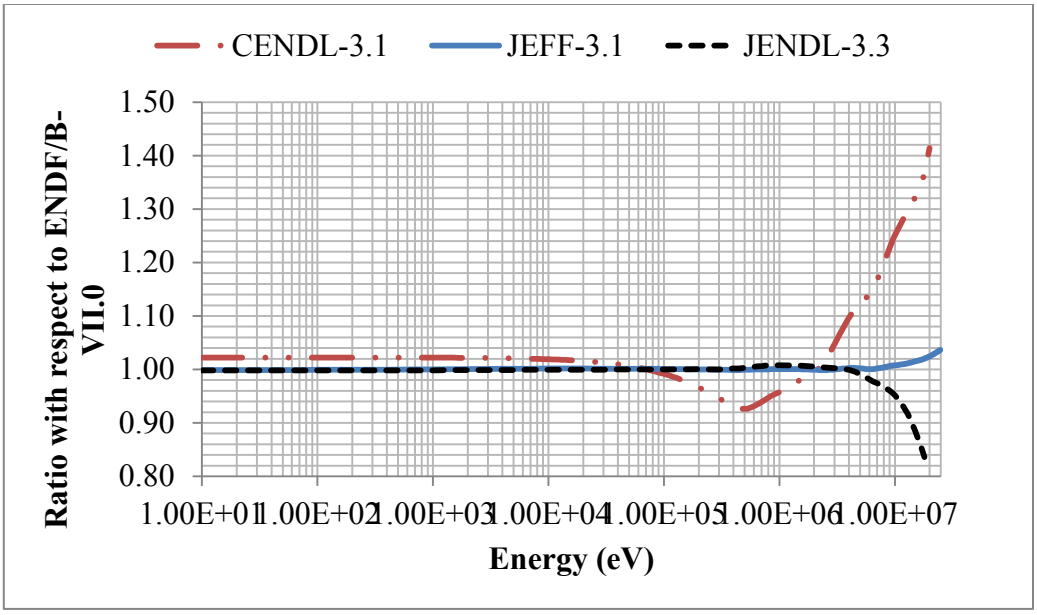

Figure 46. ^{238}U Prompt Neutron Fission Spectrum Ratio JEFF-3.1, CENDL-3.1 and JENDL-3.3 vs. ENDF/B-VII.0

5.1.3 FISSION SPECTRUM - PLUTONIUM-239

The same methodology was used to quantify the discrepancies among libraries for the prompt neutron fission spectrum of ^{239}Pu. The ratios are plotted together in Figure 47.

ENDF/B-VI.8 contains evaluations from 1eV to 25MeV whereas ENDF/B-VII.0 library contains values from 10eV to 30MeV. Thus the ratios have only been evaluated

from 10eV to 25MeV. For energies below 150keV, the amplitude of the discrepancies is 10% or more. The amplitude goes down to 5% and less between 300keV and 9.9MeV. In the range [350keV;8.7MeV], the amplitude is 2% and lower. After 9.9MeV the ratio keeps decreasing from 0.958 to 0.587, i.e. ENDF/B-VI.8 values are up to 41.3% lower than the reference values. To sum up, ENDF/B-VI.8 evaluation of the prompt neutron fission spectrum of ^{239}Pu is only in very good agreement with the reference library in the range [350keV; 8.7MeV]. At 0.7MeV and 2MeV the ratios equal respectively 0.962 and 0.971.

The evaluation of the prompt neutron fission spectrum in JEFF-3.1 is also discrepant with respect to ENDF/B-VII.0. Indeed, the amplitude of the discrepancies is less than 2% only from 1.1MeV to 2MeV. It is less than 5% between 700keV and 6.6MeV. The amplitude of the discrepancies is above 10% for energies below 200keV and above 6.7MeV. After 8.2MeV the discrepancies relatively to the reference library is 15% or more. At 2MeV the ratio is 1.02, but at 0.7MeV, the ratio is 0.954, .i.e. JEFF-3.1 value is discrepant by more than 5%. JEFF-3.1 neutron energy distributions from fission are based on the Los Alamos model, with multiple chances (first, second, third, fourth and fifth chance), and upgraded by G.Vladuca and A.Tudora.

The prompt neutron fission has been established at 46 energy points between 0 and 10eV in the JENDL-3.3 library. The ENDF/B-VII.0 library only contains values for the points 0eV and 10eV. Therefore the derivation of the ratio has been started at 10eV. The Japanese evaluation is not in better agreement with the reference library than the European one. Indeed, at 10eV and for energies in the ranges [200keV; 350keV] and

[9MeV; 20MeV] the values of the prompt neutron fission spectrum in JENDL-3.3 are discrepant from ENDF/B-VII.0 by more than 10%. Only in between 200eV and 65keV as well as in between 1MeV and 2MeV are the values within 5% of the reference one. At last, only in the range [10keV, 65keV] ∪ [1.5MeV; 2MeV] is the amplitude of the discrepancies 2% or lower. Between 65keV and 1MeV the ratio goes from 0.949 to 0.893. In JENDL-3.3 the fission spectra for ^{239}Pu was computed similarly than the prompt neutron fission spectrum of ^{238}U and of ^{235}U.

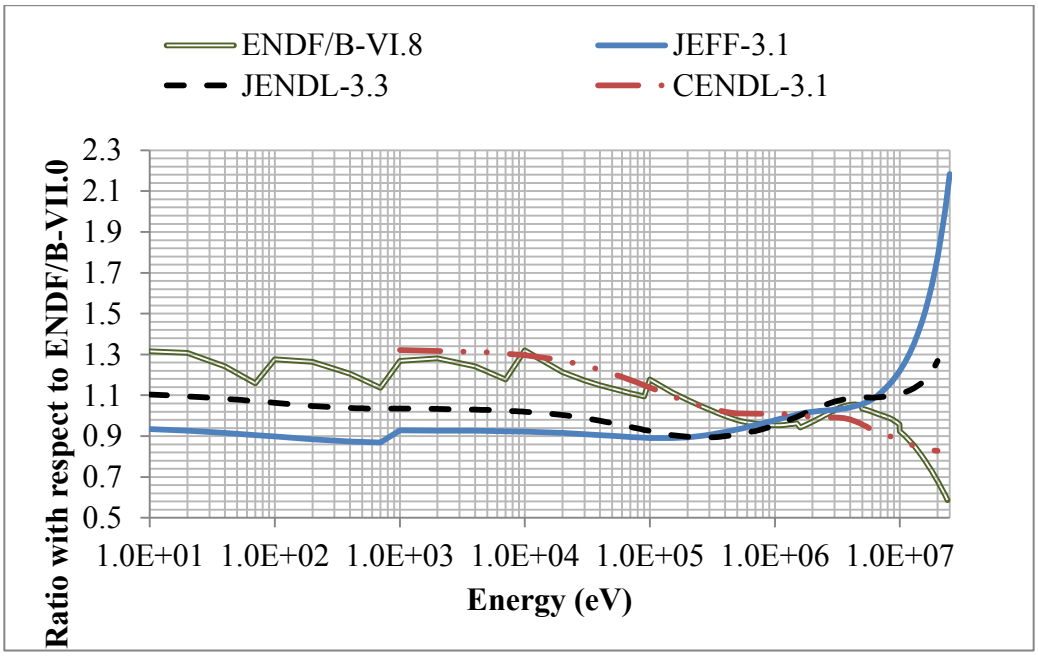

Figure 47. ^{239}Pu Prompt Neutron Fission Spectrum Ratio ENDF/B-VI.8, JEFF-3.1, CENDL-3.1 and JENDL-3.3 vs. ENDF/B-VII.0

Finally values in the CENDL-3.1 library are discrepant by only 2% or less in the range [400keV; 4MeV]. The amplitude increases to 5% in the energy range [250keV;

5.2MeV]. At 0.7MeV and at 2MeV the ratios respectively equal 1.00942 and 0.99422. The discrepancies are above 10% for energies lower than 100keV and above 8.4MeV.

In summary, the evaluations of the prompt neutron fission spectrum of ^{239}Pu do not agree with the reference library. All libraries agree only in the range [1MeV; 2MeV].

5.2 FISSION SPECTRUM VARIATION

Nuclear data, such as fission spectrum, constitute input parameters at numerous points of the nuclear fuel cycle and are part of the associated calculations. Fuel cycle performance data are thus very likely to be sensitive to their variations. For instance, material and Doppler fuel worths in a FBR have been shown to be affected by discrepancies among nuclear data libraries [45]. Existing measured prompt fission spectra are in many cases discrepant and current theoretical models leave the differences unexplained. Some biases in k_{eff} have been found in mixed-oxide fuel benchmarks, while in other cases similar biases appear to be removed by finely adjusting the evaluated data files [46]. The Consultants' Meeting on "Prompt Fission Spectra on Major Actinides" held at the IAEA Headquarters in Vienna in November 2008 has thus expressed a "*strong requirement for an international effort to explore and resolve these difficulties and recommend prompt fission neutron spectra and uncertainty covariance matrices for the actinides over the neutron energy range from thermal to 20 MeV*". Indeed, less experimental data for the fission spectrum are currently available below 1MeV and above 5MeV than for the rest of the spectrum. This lack of experimental data can be explained in part as follow. Low energy neutrons usually deposit less energy than the

threshold energy required to be detected, resulting in a reduction of the detection efficiency at low energies. High energy-neutrons are also less likely to be detected since their mean free path increases with increasing energy in the high-energy range. The detection efficiency at high-energies is thus similarly reduced [47]. Because reactor calculations codes rely on these experimental data or on their best evaluations, it is necessary to measure the impact of fission spectrum uncertainties on reactors parameters of paramount importance in fuel cycles design. In particular it is important to quantify how much the variations of the intermediate part of the energy spectrum (in the thermalization region) will affect the transmutation of TRU in graphite-moderated cores like that of a VHTR.

5.3 FISSION SPECTRUM VARIATION METHODOLOGY

5.3.1 DESCRIPTION AND USE OF THE ENDF FORMAT

The ENDF Evaluated Nuclear Data Formats have been developed in the U.S., first for national use. These formats encode nuclear data evaluations to be used in research or in the nuclear industry. Evaluating nuclear data consists in formatting experimental data into a computer-readable file able to describe nuclear reaction cross sections, energy and angle distributions (such as the fission spectrum), radioactivity data, thermal scattering data and other quantities to be used in neutron or photon transport calculations, the evolution of radioactivity in time in some particular materials, etc… Consequently, the data contained in the libraries must be described for all energies. However, experimental data do not always exist for the whole energy range. In these cases, nuclear model code

calculations are used to extend or interpolate the available data from the experimental ones. Making the file computer-readable also puts strong conditions on the formatting of the file and what can be included in it. An excerpt from the ^{235}U ENDF/B-VII file containing the fission spectrum is presented in Appendix I.

ENDF/B corresponds to the name of the library in which the evaluated nuclear data files are stored. Several versions were released, each new ENDF/B versions containing either new features (such as photon production information) or improvements in the data evaluations. Extensions for fast reactors or fusion applications started being included in ENDF/B-IV and ENDF/B-V. As the use of ENDF formats became more and more popular around the world, the ENDF formats were decoupled from the ENDF\B libraries so that the ENDF formats could encode more easily nuclear data libraries from Europe, Russia or Japan [48].

ENDF files can be retrieved online from the National Nuclear Data Center (NNDC) at the Brookhaven National Laboratory which contains U.S. ENDF/B libraries. The part of the ENDF tape corresponding to ^{235}U was thus retrieved from the NNDC website. Each ENDF tape gathers several materials and is structured by MAT number locating a material, MF number locating a file in a specific material and MT number locating a section of the MF file. ^{235}U is stored under MAT=9228. The neutron fission spectrum as a function of energy is stored in the ENDF file 5 section 18 (MF=5, MT=18). Significations of MF and MT numbers are given in Appendix J.

The neutron fission spectrum in File 5 is expressed as normalized probability distributions vs. energy. The distribution is normalized to 1 as follow:

$$\int_0^{E_{max}} p(E \rightarrow E')dE' \quad (9)$$

Where E_{max} is the maximal energy until which the spectrum has been evaluated. Equation 9 can be broken down into partial energy distributions expressed below:

$$p(E \rightarrow E') = \sum_{k=1}^{NK} p_k(E) g_k(E \rightarrow E') \quad (10)$$

where the p_k are the fractional probabilities for each of the partial distributions g_k at energy E. The partial distributions can be represented using one of six different distribution laws such as a simple Maxwellian fission spectrum, an energy-independent Watt spectrum, a Madland-Nix fission spectrum, a general or not evaporation fission spectrum or an arbitrary tabulated function. The latter was representing the partial distributions of ^{235}U.

The normalized probabilities distributions corresponding to the neutron fission spectrum of ^{235}U were then retrieved from the ENDF tape along with the corresponding energies. These distributions were modified as detailed in the next sections so as to alter the fission spectrum and allow the quantification of nuclear data variations on nuclear energy system evaluations.

5.3.2 MODIFICATIONS

The first variation consisted in representing a step fission spectrum. The modified spectrum can be seen in Figure 48 along with the unaltered fission spectrum retrieved from the NNDC website. The step function was the first alteration operated on the spectrum as it was the simplest modification to perform and to test.

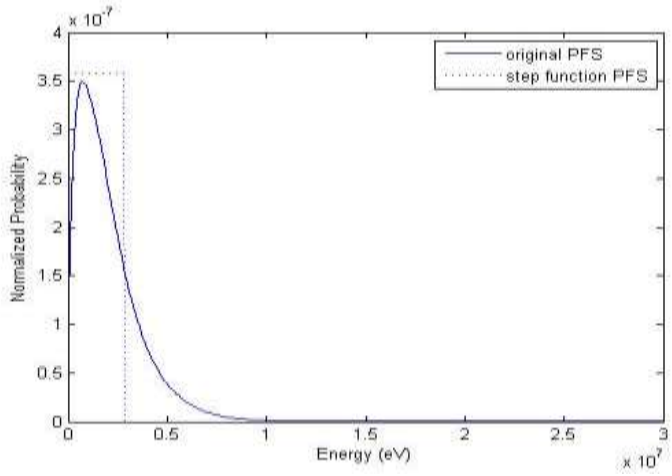

Figure 48. Original ^{235}U Prompt Neutron Fission Spectrum against the Computed Step Prompt Neutron Fission Spectrum

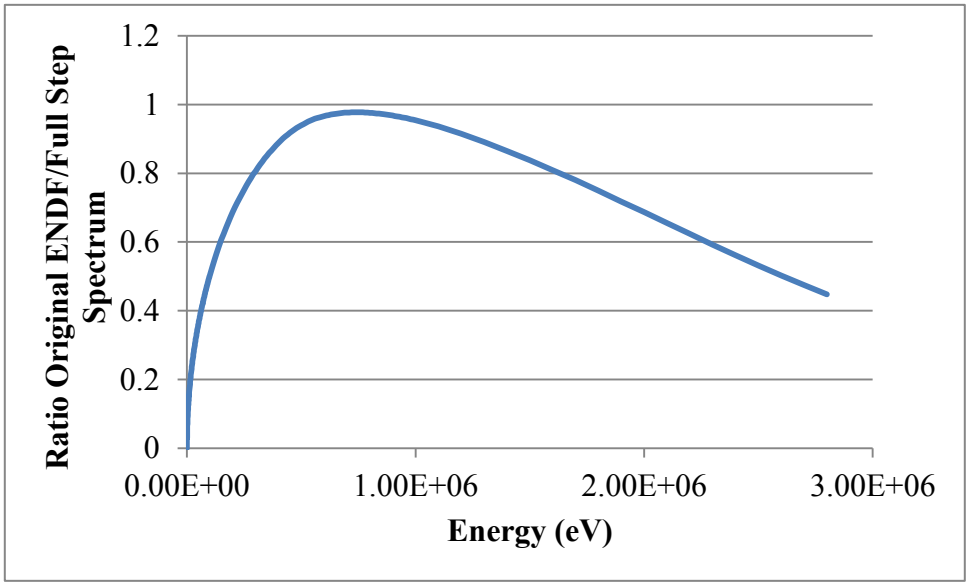

Figure 49. Ratio of the Original Prompt Neutron Fission Spectra (PNFS) by the altered one

The second and third variations consisted in altering the front or the tail of the spectrum. The front and the tail of the spectrum were replaced by a step as can be seen in Figure 50.

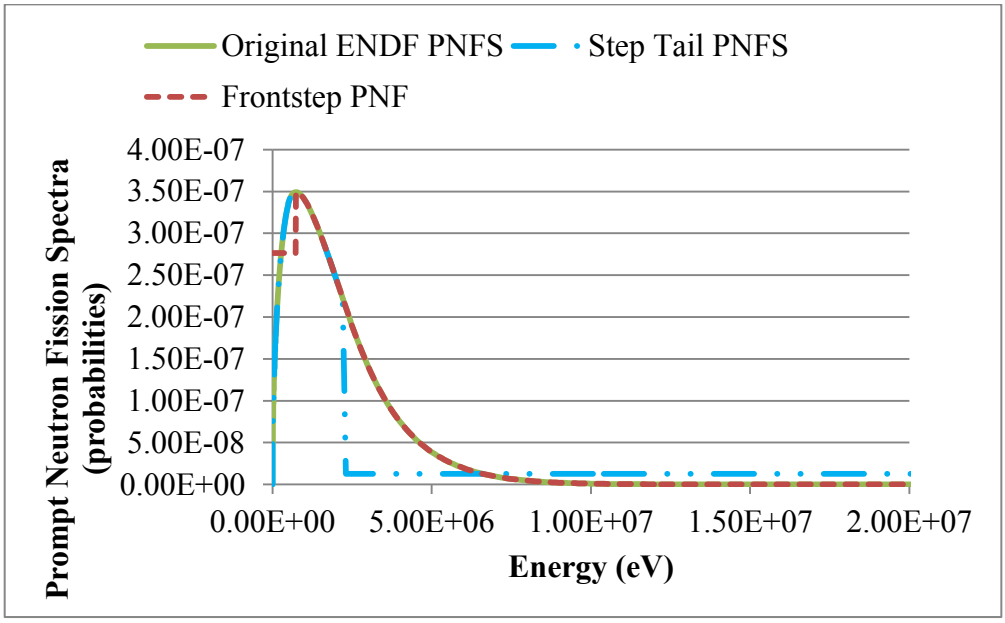

Figure 50. Original and Altered Prompt Neutron Fission Spectra

Finally the distribution was increased by 2% over the whole energy range. This marginal change is not illustrated as the 2% variation would not visible.

Figure 51 displays the ratios of the original spectrum divided by the altered spectrum. Evaluations of the spectrum at low or high energies are usually poor because difficult to make. However, if variations of the front end of the spectrum do not cause variations in the reactor and fuel cycle performance parameters, these evaluations appear sufficient. Nevertheless reassessing these evaluations may still be necessary in shielding

calculations, nuclear materials detection or fuel cycle assessments related to non-proliferation.

When using a step for the front of the spectrum, only values lower or equal to 730keV were modified. The original value was at worst 26% higher than the modified spectrum at 730keV. When replacing the end of the spectrum by a step function, only values greater or equal to 2.3MeV were modified. In this case, the original value can be up to almost 17 times more important (at 2.3MeV).

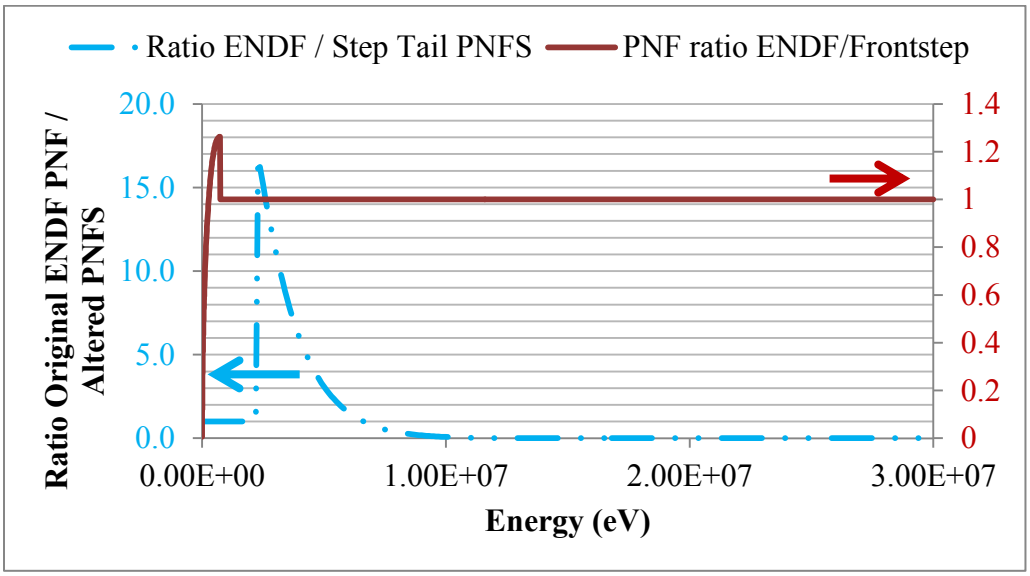

Figure 51. Ratio of the Original Prompt Neutron Fission Spectra by the Modified Fission Spectrum

NJOY, modular nuclear data processing code, was used to convert these altered ENDF files into MCNP-readable files. A brief description of this code and how it was used is described in the next section.

5.3.3 PRESENTATION AND USE OF NJOY, NUCLEAR DATA PROCESSING CODE

NJOY was first developed to read evaluated data stored in ENDF format, transform the data and create new libraries to be used in various research or nuclear industry related applications. The code is based on modules, each module performing a specific task [49]. For the purpose of the research, only the modules described herein were used.

MODER converts ASCII files (such as ENDF files) into special NJOY blocked-binary format files in order to fasten the processing of the files by the other modules. The module also converts the binary formatted files into ASCII files again. *RECONR* is the module used to produce a PENDF formatted file mandatory for the use of *BROADR* and *ACER*. Indeed these two modules require linearly interpolated piecewise functions. PENDF stands for Piecewise ENDF format. The *BROADR* module was used to bring temperature dependence to the pointwise cross sections generated by the *RECONR* module. It brings the spectrum at the right temperature (900K instead of 0K). The physical changes in the spectrum between 900K and 0K are negligible but this step was necessary before calling the *ACER* module. The latter is the reason why NJOY was chosen for the study. This module converts the altered ENDF formatted library into an ACE formatted library used by the Monte Carlo code MCNP. Two outputs are generated: the first output contains the ACE library and the second a line to be copied in the xsdir file – the MCNP's index file for data. A complete list of NJOY modules can be found in Appendix K. The NJOY script written for the purpose of this research is shown in Table 18.

Table 18. NJOY Script Used to Prepare New MCNP Libraries

Moder	MODER reads what has been saved under tape20 and produces an ENDF binary-formatted output called tape21
20 -21	
Reconr	RECONR reads tape21 and creates an output saved under tape 22.
-21 -22	
'attempt #1 to build pendf file'	Comment, the new pendf tape will be labeled 'attempt#1 to build pendf file'
9228 1/	^{235}U is the material to be reconstructed
.001/	0.001 is the fractional reconstruction tolerance used when resonance-integral error criterion is not satisfied
'endf6 library for 235U - step function #1'	Comment
0/	No user energy grid point
Broadr	BROADR needs both tape21 and tape22 and outputs tape23
-21 -22 -23	
9228 1 0 1 0/	^{235}U is the material to be processed, only 1 final temperature, no restart, bootstrap, starting temperature =0K
0.005/	0.005 is the fractional tolerance for thinning
900./	900K is the final temperature
0/	No other material to process with BROADR
Acer	ACER reads tape 21 and tape23 and creates tape31 containing the ACE formatted library and tape32 containing the single line to be copied into the xsdir MCNP file
-21 -23 0 31 32	
1/	Acer run option = fast data
'test acer script#1'/	Comment
9228 900./	^{235}U is the material to be processed at 900K
0/	No detailed photons
/	Skip card7
Moder	MODER finally reads tape23 again and converts it into an ASCII formatted file again, tape24
-23 24	
Stop	End of script

In order for the MCNP input to use the newly created library, the library extension of ^{235}U in the input material card had to be changed with the number corresponding to this new particular library. The new xsdir file had also to be called in the command line. Changes in the MCNP material card can be seen in Figure 52.

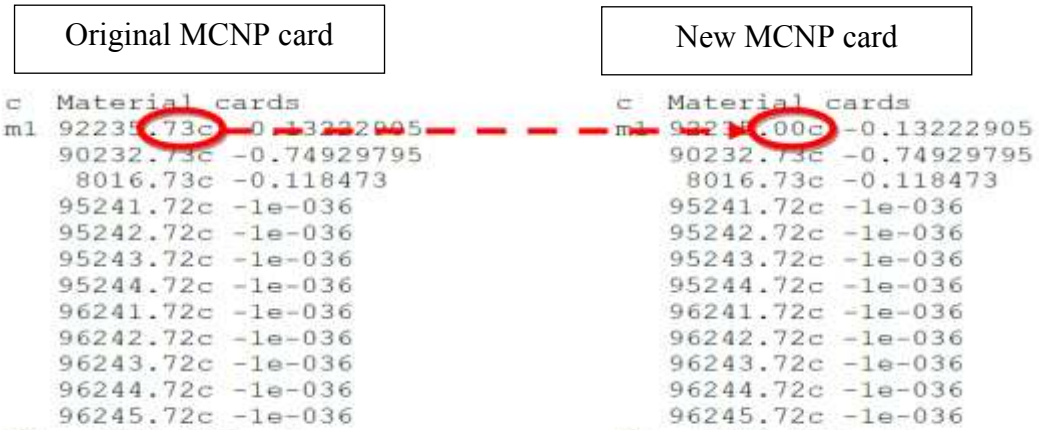

Figure 52. Changed Operated in the Material Card following a Change in the Libraries Used

5.4 IMPACT OF FISSION SPECTRUM VARIATIONS ON VHTR AND FUEL CYCLE CHARACTERISTICS

The estimation of the impact of these prompt neutrons fission changes on the VHTR metrics and the fuel cycle performance in TRU elimination was assessed by computing the ratio of the value obtained using a modified spectrum divided by the value obtained using the original spectrum. First are presented the effects of these changes on the effective multiplication factor, secondly on the VHTR energy spectrum, thirdly on the

Xenon concentration, fourthly on the isotopic composition and activity at EOL and finally on the transmutation efficiency and TRU destruction rates.

5.4.1 EFFECTIVE MULTIPLICATION FACTOR

Replacement of the complete spectrum by a step function

The ratio of the effective multiplication factor obtained using a step function as the prompt neutron fission spectrum over the original effective multiplication factor is plotted in Figure 53 for a reactor fueled with 40% +UO_2.

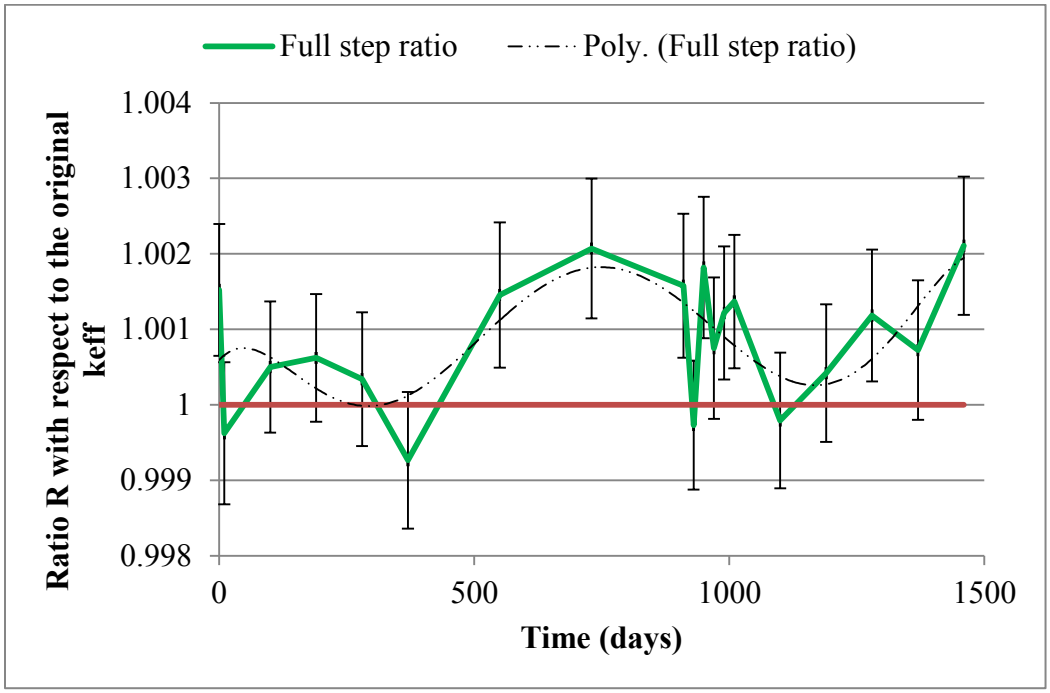

Figure 53. Ratio of the Effective Multiplication factor k_{eff} using the Modified Spectrum to the Effective Multiplication Factor Using the Original Spectrum

. Error bars calculated from MCNP standard deviations are included to separate variations resulting from the fission spectrum alteration from variations attributed to MCNP. A polynomial of degree 6 has been used as a trendline.

The values obtained for k_{eff} using such an altered spectrum are very close from the original values. Indeed, the ratio is comprised between 0.9993 and 1.0021. Most of the variations are furthermore included within the MCNP uncertainties. Only ratios after 550 days, 730 days, 910 days, 950 days, 990 days, 1010 days, 1280 days and 1460 days of operation can be said to differ using a step function fission spectrum. The complete values of k_{eff} along with the associate standard deviations can be found in Appendix L.

Replacement of the front of the spectrum by a step function

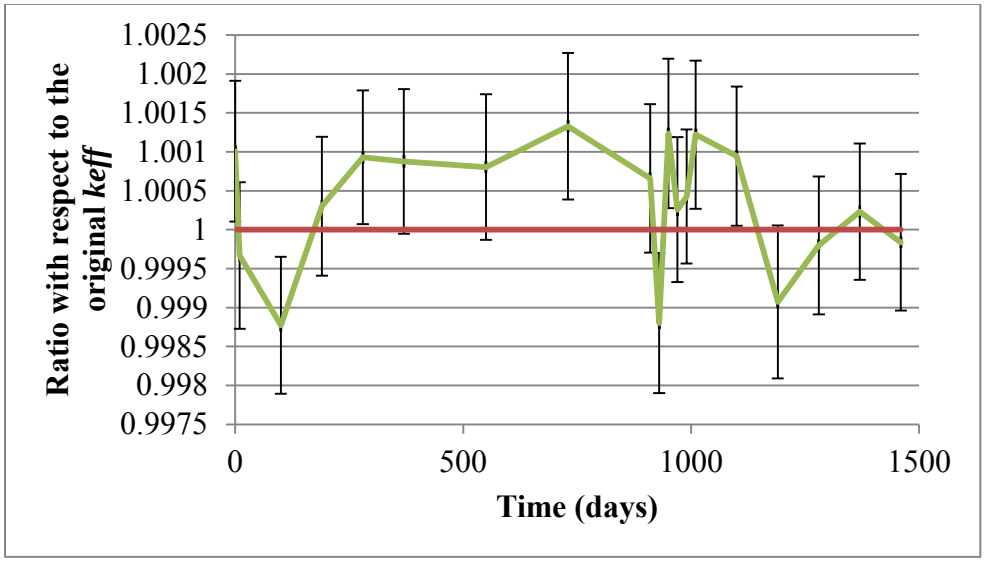

Figure 54. Ratio of the Effective Multiplication factor k_{eff} using the Front-Modified Fission Spectrum to the Effective Multiplication Factor Using the Original Spectrum

Again the replacement of the front of the spectrum by a step function does not affect significantly the evolution of the multiplication factor.

The variations are contained in the range ± 0.15%. Furthermore, for all values except 6 (100 days, 280 days, 730 days, 950 days, 1010 and 1100 days) , their respective uncertainty makes it possible for these values to equal 1. Consequently the core lifetime has not been modified. These observations are displayed in Figure 54. k_{eff} values and their respective uncertainties can be found in Appendix L.

Replacement of the tail of the spectrum by a step function

The replacement of the tail of the spectrum is the only modification that leads to obvious changes in the effective multiplication factor. Indeed the ratio is for all values lower than 1 and the uncertainties associated with the values are small enough to conclude that the ratio is different from1. The effective multiplication factor is at best 1.3% lower than the original value and at worst 1.7% lower. These variations in the effective multiplication factor are still reasonable given that the change in the tail of the prompt neutron fission spectrum was significant. However it proves that changes in the tail of the spectrum affect the effective multiplication factor.

It also affects the VHTR core lifetime: indeed the reactor clearly becomes subcritical after 910 days with k_{eff} being equal to 0.98666 ± 0.00068. In the reference case k_{eff} only reached a value of 1.0052 ± 0.00059 at EOL. Additionally, in the reference case, the jump in k_{eff} made the VHTR slightly supercritical for another 350 days. On the contrary, with such a modified tail fission spectrum, the VHTR stays subcritical after shutdown. k_{eff} values and standard deviation are summarized in Appendix L.

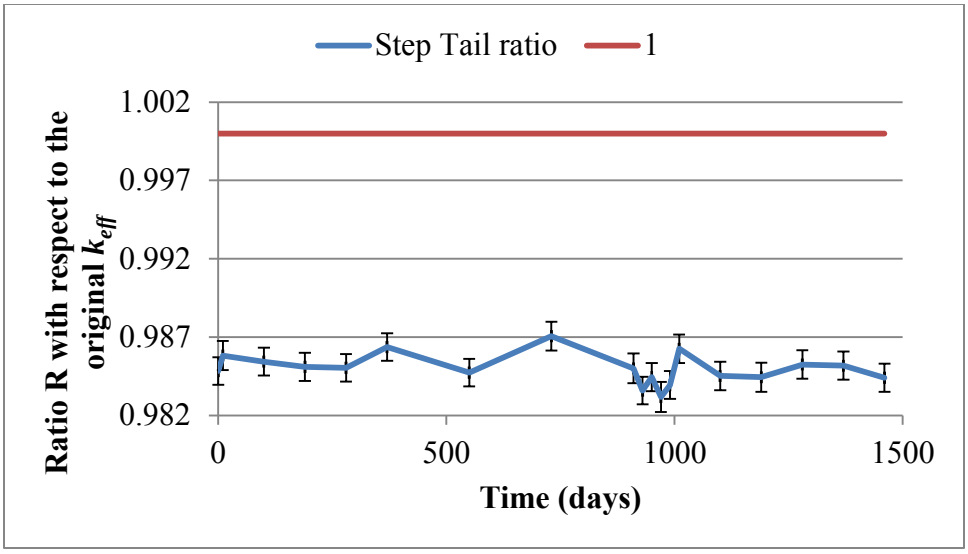

Figure 55. Ratio of the Effective Multiplication factor k_{eff} using the Tail-Modified Fission Spectrum to the Effective Multiplication Factor Using the Original Spectrum

2% increase over the whole energy range

The last modification consisted in increasing the probabilities of the prompt neutron fission spectrum by 2% over the whole energy range. Figure 56 depicts the ratio of the effective multiplication factor obtained after having modified the spectrum to the effective multiplication factor obtained using the original spectrum. The range of the variations is ± 0.2%. However only 7 out of 19 values have uncertainties low enough to conclude that k_{eff} has been modified by the change in the prompt neutron fission spectrum distribution. Three values have been lowered by less than 0.2% after 100 days, 190 days and 930 days of reactor operation. Four values have been raised (at 910 days, 1010 days, 1190 days and 1460 days) by less than 0.2%. In summary, increasing the

distribution has only a very negligible on the evolution of the effective multiplication factor.

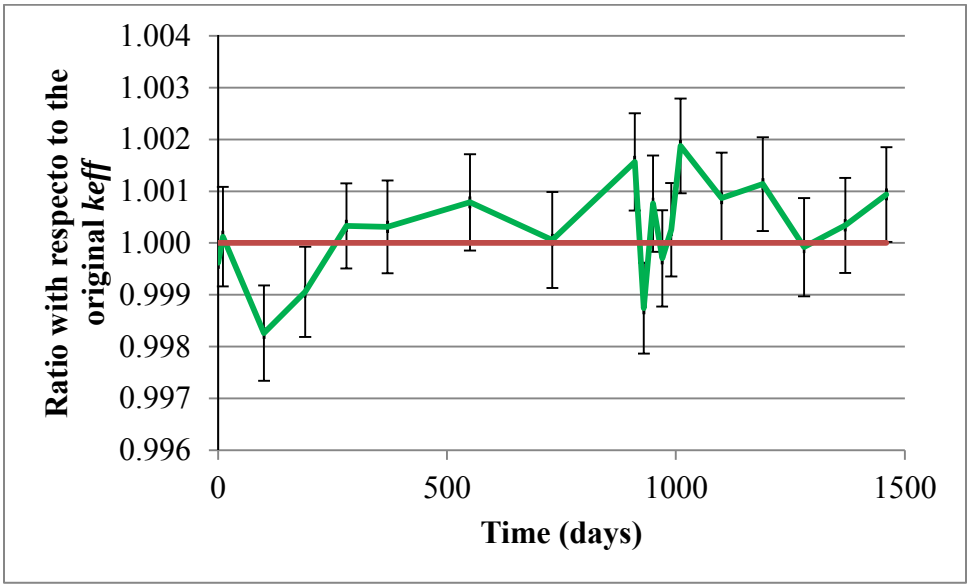

Figure 56. Ratio of the Effective Multiplication Factor obtained using a 2%-Modified Spectrum to that obtained using the Original Spectrum

5.4.2 ENERGY SPECTRA

The impacts of prompt neutron fission spectrum modifications on the energy spectrum of the VHTR have been established in the paragraphs below – first for a complete replacement of the prompt neutron fission spectrum by a step function, secondly by the replacement of only the front of the spectrum, thirdly by the replacement of the tail of the spectrum and finally by a 2% increase.

Replacement of the complete spectrum by a step function

A few variations are to be observed in the energy spectra ratio and can be seen in Figure 57 to Figure 59.

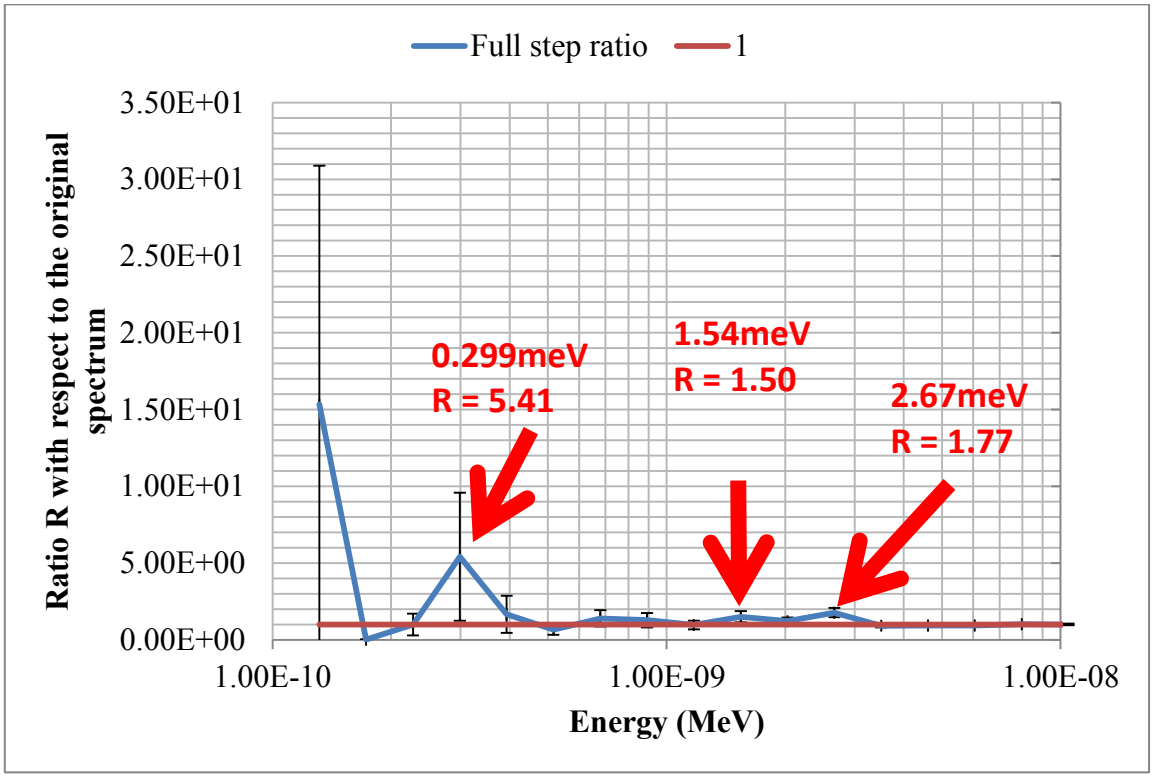

Figure 57. Ratio of the VHTR Energy Spectrum using the Modified Spectrum to the VHTR Energy Spectrum Using the Original Spectrum (energy below 10meV)

Only three points at low energies (0.299meV, 1.54meV and 2.67meV) appear to have been modified following a change in the fission spectrum. The variations range from a 540% increase to a 50% increase.

From 10meV to 1MeV the ratios are extremely close to 1. Most of them vary by only 2% from the original value. Out of 68 datapoints between 10meV to 1MeV, 32 have

small enough associated uncertainties to conclude that the variation in the energy spectrum is related to the alteration of the fission spectrum. Changing the latter has thus affected almost half of the datapoints between 10meV and 1MeV by 2% at worst.

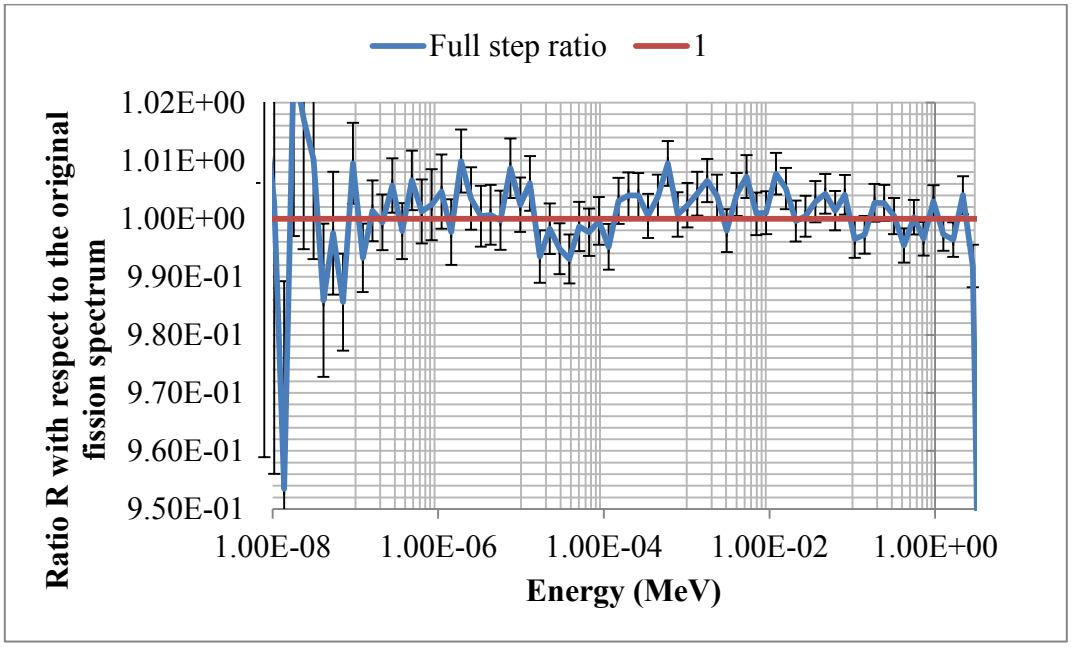

Figure 58. Ratio of the VHTR Energy Spectrum using the Modified Spectrum to the VHTR Energy Spectrum Using the Original Spectrum (energies between 10meV to 1MeV)

More substantial variations are to be observed between 3.75MeV and 14.7MeV where the ratios are clearly below 1 with minute uncertainties. The energy spectrum obtained using an altered fission spectrum is by 8% to 12% lower than the original energy spectrum. For higher energies, the uncertainties associated with each ratio are too significant to draw any conclusions.

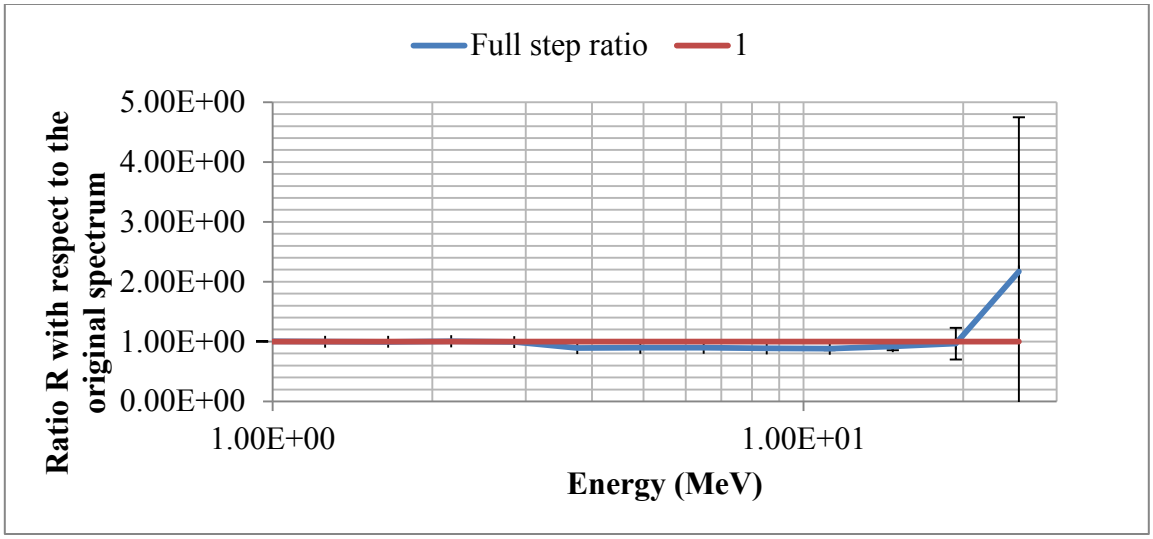

Figure 59. Ratio of the VHTR Energy Spectrum using the Modified Spectrum to the VHTR Energy Spectrum Using the Original Spectrum (energies above 1MeV)

To sum up, between 0.1meV and 10meV only a fifth of the energy spectrum datapoints have been certainly affected by the change in fission spectrum. The discrepancy varies between 50% and 540%. Between 10meV and 1MeV, almost half of the datapoints have been affected but the variation is reasonably contained in a 2% range. From 3.75MeV to 14.7MeV, the altered fission spectrum is 8% to 12% lower than the original VHTR's energy spectrum.

Replacement of the front of the spectrum by a step function

From 0.1meV to 10meV, the ratio oscillates between 4.55 and 0.723. However the uncertainties associated with the values of the ratio are high enough to prevent any conclusion to be drawn – except at 2.67meV where the ratio equals 1.63 ± 0.275. Figure 60 illustrates the preceding remarks.

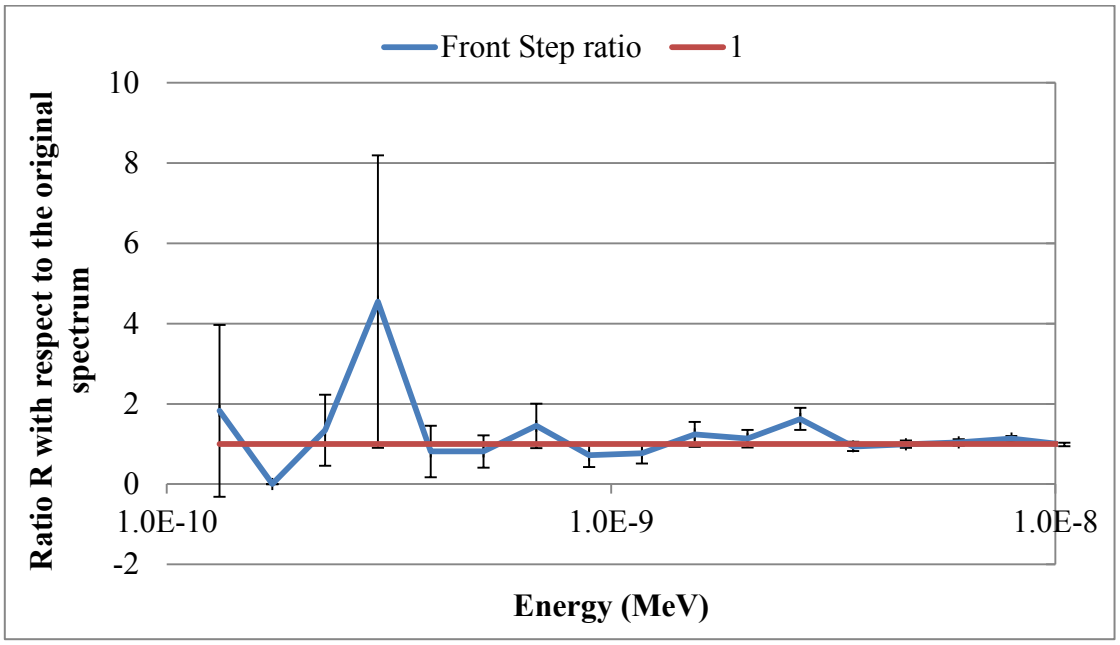

Figure 60. Ratio of the VHTR Energy Spectrum using the Front-Modified Spectrum to the VHTR Energy Spectrum Using the Original Spectrum (energies between 0.1meV and 10meV)

From 100meV to 10MeV, most variations are included in a ± 1% variation range and some of the associated uncertainties are small enough to conclude that the change in the fission spectrum impacted the VHTR energy spectrum. The latter has surely been modified for 20 energy datapoints out of 77 as illustrated in Figure 61. Nevertheless these variations are minor. The impact of fission spectrum variations on the mass of TRU and consequently on the fuel cycle ability to burn TRU are very likely to be negligible.

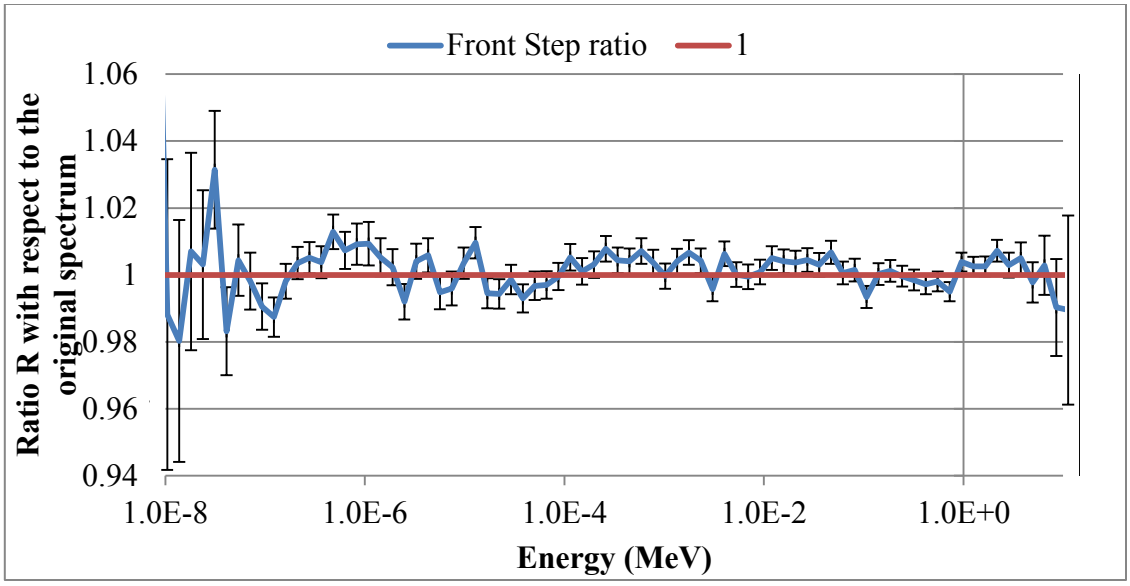

Figure 61. Ratio of the VHTR Energy Spectrum using the Front-Modified Spectrum to the VHTR Energy Spectrum Using the Original Spectrum (energies between 10meV and 10MeV)

Replacement of the tail of the spectrum by a step function

Between 0.1meV and 10meV, the ratio oscillates between 0.728 and 5.55, most values being in a 2% variation range. Except for E=1.54meV and E=6.06meV where the ratio respectively equals 1.37 ± 0.328 and 1.0000 ± 0.0763, the uncertainties are such that it cannot be concluded that these changes come from changes in the fission spectrum. However, from 50meV to 2MeV it becomes clear that variations in the tail of the fission spectrum affect the VHTR energy spectrum. Indeed the ratio decreases up to 0.956 ± 0.00284 at E=1.65MeV. Thus, modifying the tail of the spectrum can reduce the energy spectrum by up to 5%. These observations are visible in Figure 62 to Figure 63.

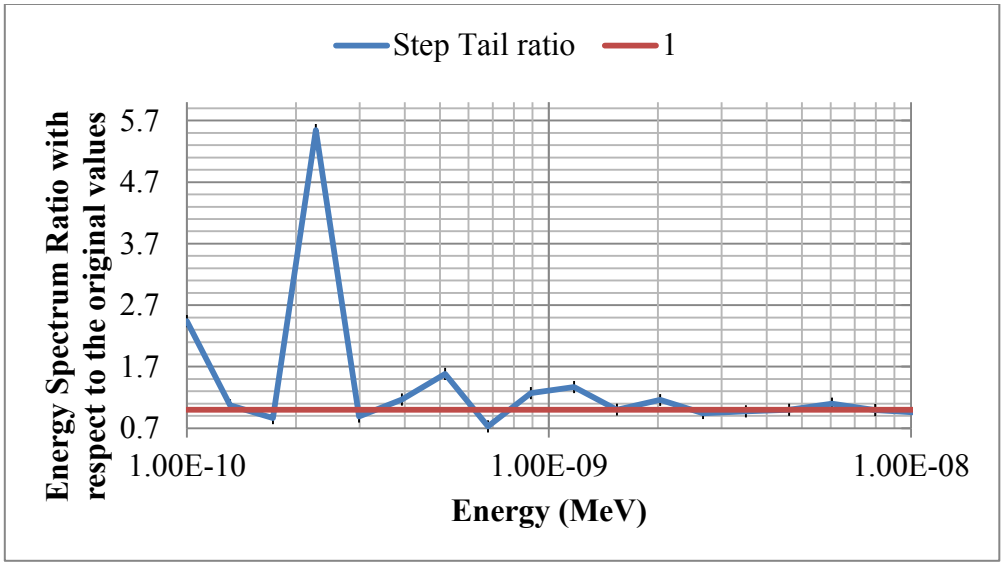

Figure 62. Ratio of the VHTR Energy Spectrum using the Tail-Modified Spectrum to the VHTR Energy Spectrum Using the Original Spectrum (energies between 0.1meV and 10meV)

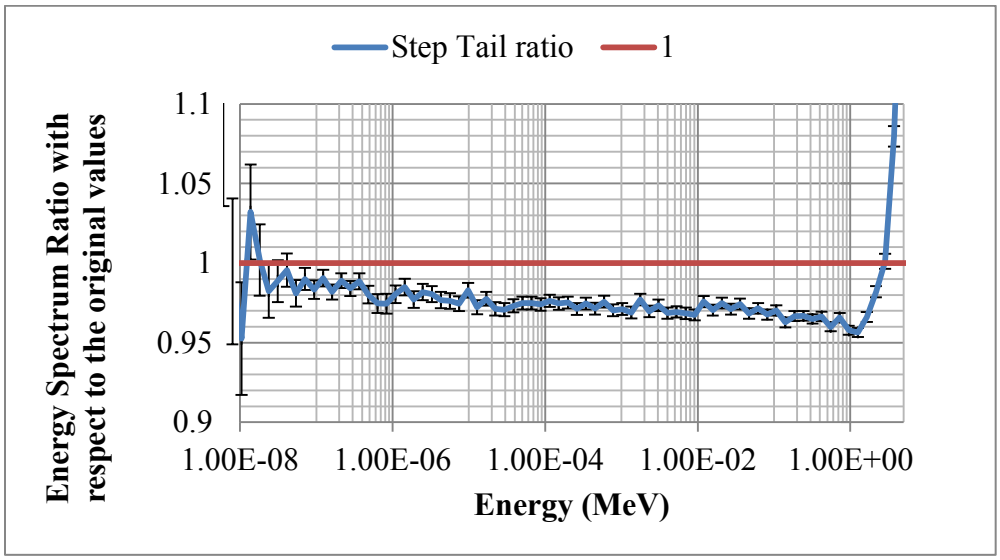

Figure 63. Ratio of the VHTR Energy Spectrum using the Tail-Modified Spectrum to the VHTR Energy Spectrum Using the Original Spectrum (energies between 10meV and 1MeV)

From Figure 64 it can be seen that at high energy the ratio is particularly high. However the uncertainties are extremely important and no conclusion can be drawn about the effect of fission spectrum variation at high energies.

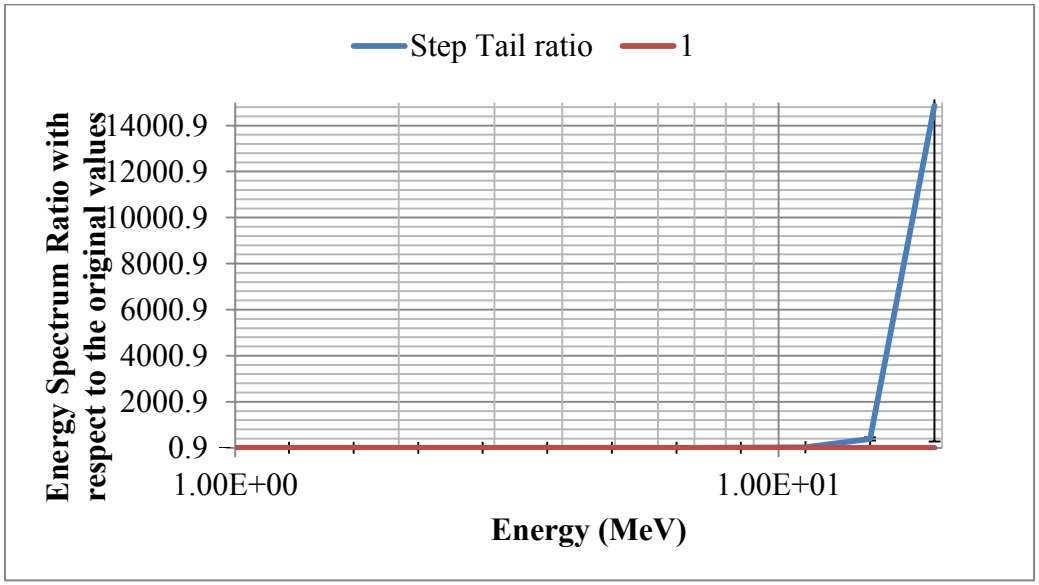

Figure 64. Ratio of the VHTR Energy Spectrum using the Tail-Modified Spectrum to the VHTR Energy Spectrum Using the Original Spectrum (energies between 1MeV and 10MeV)

2% increase over the whole energy range

Again a 2% increase leads to very negligible modification in the energy spectrum. Out of 94 values, 16 have been increased and only 11 have been lowered. Between 1eV and 10 MeV, the variations are within a [-0.1%, +0.2%] range. These observations can be seen in Figure 65. Only two values for energies below 0.01eV have been modified by 50% as testified Figure 66. For energies above 10MeV, the energy spectrum is more

affected by the change in the fission. Figure 67 illustrates this feature: at 14.7MeV the ratio is 1.12 and at 25.5MeV the ratio is only 0.107.

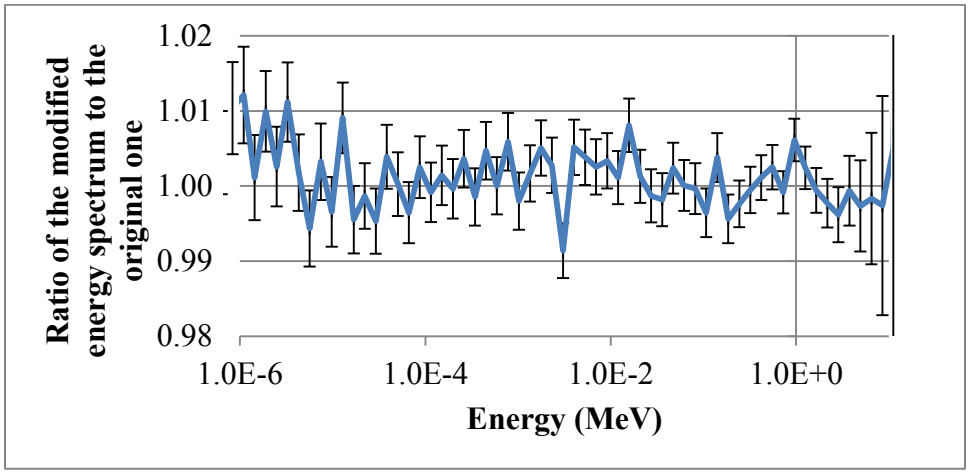

Figure 65. Ratio of the VHTR Energy Spectrum using the 2%-Modified Spectrum to the VHTR Energy Spectrum Using the Original Spectrum (energies between 1eV and 10MeV)

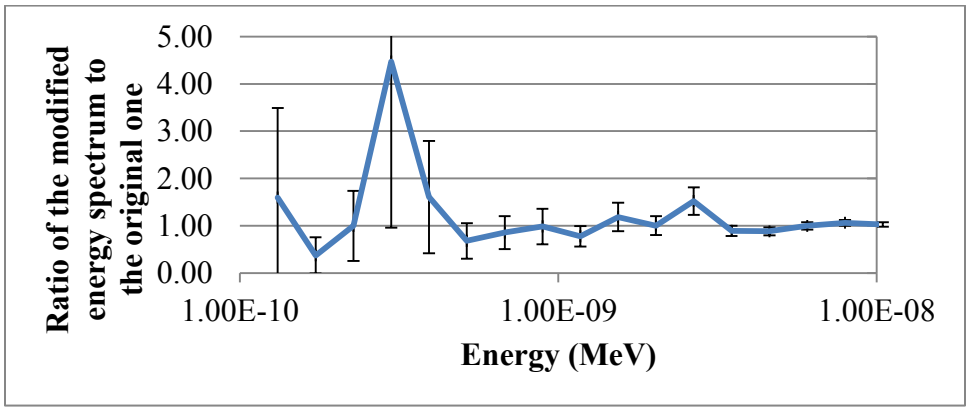

Figure 66. Ratio of the VHTR Energy Spectrum using the 2%-Modified Spectrum to the VHTR Energy Spectrum Using the Original Spectrum (energies between 0.1meV and 0.01eV)

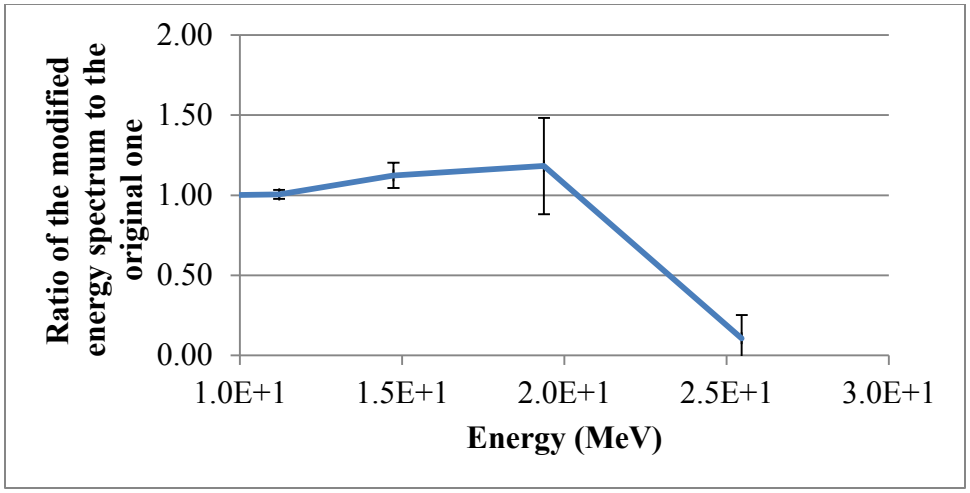

Figure 67, Ratio of the VHTR Energy Spectrum using the 2%-Modified Spectrum to the VHTR Energy Spectrum Using the Original Spectrum (energies between 1MeV and 30MeV)

To sum up, except at high energies, the 2% variation has little impact on the VHTR energy spectrum.

5.4.3 ^{135}XE BUILDUP

The variations in the mass of Xenon with respect to the original mass are summarized in Table 19. A positive entry means a reduction of the mass while a negative entry indicates an increase of the mass of Xenon comparatively with the mass obtained using the original ENDF spectrum. As it can be seen, the variations in the fission spectrum may have affected the mass of Xenon by a maximum of 0.3%. The importance of the variations is not related to the amount of modifications in the fission spectrum.

Table 19. Percentage of Reduction in the Mass of ^{135}Xe Comparatively to the Reference Mass

Time	Original mass	Full Step	Front Step	Tail Step	2%
0.00E+00	0.00E+00	n/a	n/a	n/a	n/a
1.00E+01	1.06E+01	0.283%	0.000%	0.095%	0.095%
1.00E+02	1.03E+01	0.000%	-0.097%	0.000%	0.195%
1.90E+02	1.01E+01	0.198%	-0.198%	-0.099%	0.099%
2.80E+02	9.93E+00	0.080%	-0.211%	-0.010%	0.171%
3.70E+02	9.76E+00	-0.041%	-0.041%	0.164%	0.000%
5.50E+02	9.13E+00	0.044%	-0.153%	0.011%	0.219%
7.30E+02	8.72E+00	0.126%	0.046%	0.207%	-0.011%
9.10E+02	8.22E+00	0.291%	-0.085%	-0.073%	0.243%
9.30E+02	8.62E+00	-0.046%	-0.046%	0.081%	0.000%

5.4.4 ISOTOPIC COMPOSITION AND ACTIVITY AT EOL

Table 20 summarizes the mass and activity ratios per isotope with respect to the reference values.

When the fission spectrum is entirely replaced by a full step function the variations are within a 2% range except for ^{236}Np, ^{236}Pu and ^{237}Pu. The mass and activity of ^{236}Np are 7% lower than the reference value, the mass and activity of ^{236}Pu 9.45% lower and the mass and activity of ^{237}Pu 7.3% lower than the reference values. However the mass of these three isotopes were minim in the reference case. Consequently these variations are insignificant.

When the front of the spectrum is changed into a step function, similar observations can be noticed. Only the mass and activity of ^{236}Pu – found in trace amount in the reactor – are outside the 2% variation range. Consequently a small alteration of the front of the spectrum does not affect the masses and activities at EOL.

When the tail of the spectrum is replaced by the step function chosen, variations in the masses and activities at EOL are more consequent. Indeed the mass and activity ratios of ^{233}U approximately equal 262. In this modified case, 8g of ^{233}U are to be found in the VHTR at EOL and the modified activity approximately equals 76.07mCi. The ratios of the mass and activity of ^{236}Np approximate 7.2 while those of ^{236}Pu are almost equal to 523. There is thus 2.79g of ^{236}Pu at EOL of the VHTR. ^{237}Pu mass and activity ratios are approximately worth 34. ^{234}U, ^{237}U, ^{239}U, ^{245}Cm, ^{247}Cm are outside the 2% variation range but inside a 5% variation range. Consequently, a substantial modification of the tail of the spectrum only minimally affects the mass and activity of most actinides at EOL. Although some isotopes see their mass and activity being considerably augmented, such as ^{233}U, ^{236}Np or ^{236}Pu, the altered mass and activity are still negligible with respect to the masses of ^{238}Pu (56.17kg), ^{239}Pu (0.3008T), ^{240}Pu (0.3984T), ^{241}Pu (0.1807T) or ^{242}Pu (93.22kg) and the total activity (equals to 0.2758MCi). For instance, even if the modified activity of ^{236}Pu has been multiplied by a factor of 523, it still corresponds to 0.0005% of the total activity. The modified mass of ^{236}Pu represents less than 0.005% of the reference mass of ^{238}Pu and 0.0009% of the reference mass of ^{239}Pu.

When the distribution is increased by 2%, the mass and activity have been modified by less than 1%, with an exception for ^{233}U and ^{237}Pu whose mass and activity have been lowered by 3% and for ^{236}Pu – contained in negligible amount in the reactor –whose ratios are equal to 0.839.

Table 20. Mass and Activity Ratio at EOL for Different Prompt Neutron Fission Spectrum

ZAiD	Original		Full Step Function		Front Step Function		Step Tail Function		2% Increase	
	Mass (g)	Activity (Ci)	Mass Ratio	Activity Ratio	Mass Ratio	Activity Ratio	Mass Ratio	Activity Ratio	Mass Ratio	Activity Ratio
92233	3.04E-02	2.93E-04	0.986	0.986	0.987	0.987	**263.00**	**262.94**	**0.976**	**0.975**
92234	5.75E+0	3.57E+0	0.999	0.999	0.999	0.999	**1.029**	**1.029**	1.000	1.000
92235	2.08E+0	4.49E-01	1.000	1.000	1.000	1.000	1.001	1.001	1.000	1.000
92236	2.28E+04	1.47E+00	1.000	1.000	0.999	0.999	0.999	0.999	1.000	0.999
92237	3.39E+01	2.77E+06	1.012	1.012	0.995	0.9957	**1.055**	**1.055**	1.009	1.008
92238	1.65E+06	5.56E-01	1.000	1.000	1.000	1.000	1.000	1.000	1.000	1.000
92239	2.46E+00	8.24E+07	1.013	1.0136	0.998	0.998	**0.989**	**0.989**	0.993	0.993
93236	1.63E-01	2.15E-03	**0.930**	**0.930**	0.991	0.992	**7.220**	**7.221**	0.986	0.986
93237	3.51E+04	2.47E+01	0.999	0.999	1.000	1.000	1.007	1.007	0.999	0.999
93238	5.69E+01	1.47E+07	1.000	0.999	0.996	0.997	1.003	1.003	0.996	0.996
93239	3.55E+02	8.23E+07	1.013	1.013	0.998	0.998	0.989	0.989	0.994	0.993
94236	5.34E-03	2.79E+00	**0.906**	**0.906**	**0.880**	**0.881**	**522.74**	**522.580**	**0.839**	**0.839**
94237	3.69E-02	4.50E+02	**0.927**	**0.927**	0.991	0.991	**33.929**	**33.933**	**0.988**	**0.988**
94238	5.71E+04	9.78E+05	1.001	1.001	0.999	0.999	0.998	0.998	1.000	1.000
94239	2.93E+05	1.82E+04	1.002	1.002	1.001	1.001	0.998	0.998	1.000	1.000
94240	3.96E+05	8.99E+04	0.998	0.998	1.001	1.001	1.004	1.003	1.000	1.000
94241	1.81E+05	1.87E+07	1.003	1.004	0.997	0.999	0.995	0.995	0.999	0.999
94242	9.41E+04	3.72E+02	0.999	0.999	0.998	0.999	0.999	1.000	1.000	1.000
94243	1.09E+01	2.83E+07	0.996	0.996	0.994	0.994	0.995	0.994	1.010	1.010
94244	4.04E+00	7.40E-05	1.004	1.004	1.000	1.001	0.993	0.993	1.001	1.001
95241	3.90E+04	1.34E+05	1.000	1.000	1.001	1.001	1.001	1.000	0.999	0.999
95242	4.18E+02	4.38E+03	1.005	1.005	1.001	1.002	0.996	0.996	1.002	1.002
95243	2.25E+04	4.50E+03	1.003	1.002	1.002	1.003	0.999	0.999	1.000	1.000
95244	1.08E+01	1.38E+07	1.006	1.006	0.995	0.995	0.994	0.994	0.994	0.993
96242	1.09E+04	3.61E+07	1.002	1.001	0.999	1.000	1.000	1.000	1.000	1.001
96243	4.14E+02	2.14E+04	1.001	1.001	0.998	0.998	0.987	0.986	0.995	0.995
96244	1.34E+04	1.09E+06	1.003	1.004	0.998	0.998	0.992	0.992	1.001	1.001
96245	1.53E+03	2.63E+02	1.014	1.013	0.996	0.996	**0.980**	**0.980**	1.005	1.005
96246	7.39E+01	2.27E+01	1.007	1.007	0.998	0.998	0.982	0.982	1.003	1.003
96247	1.16E+00	1.05E-04	1.012	1.012	0.994	0.995	**0.977**	**0.977**	1.000	1.000

The transmutation efficiency and the TRU destruction capability of the VHTR are thus very unlikely to have been modified following the change in fission spectrum. The results are presented in the next paragraph.

5.4.5 TRANSMUTATION EFFICIENCIES AND TRU DESTRUCTION RATES

For a VHTR fueled with 40% TRU and completed with UO_2, variations are again minimal. None of the change in the fission spectrum produces a variation of the transmutation efficiency. They all equal -0.59% and perfectly match the reference value. The replacement of the fission spectrum by a step function and the change of the front of the spectrum into a step function make the TRU destruction rate lose 0.01% now being -68.18%. The alteration of the tail into a step function or the increase of the distribution by 2% does not change the TRU destruction rate. Indeed the latter equals the reference value (68.19%).

5.5 DISCUSSION OF THE RESULTS

When replacing the entire fission spectrum by a step function from E=0eV to E=2.8MeV, the probability of producing low energy neutrons (below 10eV) is multiplied by at least 193 and equal to the probability of producing any neutron having any energy in the range [0; 2.8MeV]. The probability of producing neutrons with energy above 2.8MeV is on the other hand reduced to 0. The probability of increasing the production of slow neutrons should increase the number fissions and augment the neutron flux in energies lower than 10eV. This is not observed in Figure 58 because of the associated

MCNP uncertainties in the neutron flux computations. If the production of fissions is increased, the effective multiplication factor should be higher. From Figure 53, 9 effective multiplication factor values out of 19 are undoubtedly higher than the reference values. Another 6 values appear higher but the associated MCNP uncertainties are too high to draw any conclusion.

When replacing the front only of the fission spectrum by a step (from 0eV to 730keV), the probability of producing neutrons with energies below 250keV is multiplied by up to 150 times while the probability to produce neutrons with energies between 250keV and 730keV is divided by up to 1.26. More thermal neutrons should be produced, favoring the production of fissions. Therefore the effective multiplication should be increased. However less neutrons should slowdown from an initial energy in the range [250keV; 730keV] to thermal energy. Thus less fissions should be produced by slown-down neutrons. This should offset the raise in the effective multiplication factor. In conclusion, the effective multiplication factor should not be affected by a change in the front of the fission spectrum. From Figure 54, 5 values of the effective multiplication factor out of 19 are surely higher than the reference value. 12 seem higher but no conclusion can be drawn as the related MCNP uncertainties are too important. If less neutrons slow down to thermal energies, the energy spectrum should be lowered in the range [10eV; 0.1MeV]. This feature is not seen in Figure 61 where the energy spectrum seems to be slightly higher in this range. However, in the range [0.4eV; 1.1eV] the spectrum is higher, confirming the increase in the flux of low energy neutrons.

When the tail of the spectrum is replaced by a step function from 2.3MeV, the production of neutrons in the range [2.3MeV; 6.4MeV] is decreased while it is raised above 6.4MeV. A neutron born with an energy above 6.4MeV will require more collisions to slow down to thermal energy and participate in a thermal fission. However if the neutron undergoes more collisions, it is more probable that it will be captured by TRU isotopes or that it will participate in fast fissions instead of a thermal fission. Figure 71 in Appendix M presents various fission and radiative capture cross sections for the main isotopes present in the fuel. The production of thermal fission should be lowered. Thus the flux of neutrons should be decreased in the thermal energy range and k_{eff} should be lowered. Additionally, neutrons born with energies above 6.4MeV are less likely to reach the intermediate energy range than neutron born with energies in the range [2.3MeV; 6.4MeV]. Since the later are less likely to be produced and the former more probable, the flux of neutrons should be lowered in the intermediate energy range. These features are observed in Figures 55 and 63.

Increasing the entire prompt fission neutrons distribution by 2% means that the probability of a neutron being born with any energy has been increased by 2%. Thus the energy spectrum should be increased over the entire energy range. However the MCNP uncertainties associated with each value are too important to draw any conclusions: the uncertainties of 67 values out of 94 are too large. Only 16 values have clearly been increased and 11 values have been reduced. The expected modifications of the energy spectrum are therefore not observed.

In addition, if more neutrons are being born, more fissions should occur and the effective multiplication factor should be increased. From Figure 56, the ratio of the effective multiplication factors appears above 1 but only 4 values out of 19 have uncertainties small enough to conclude that they have been increased by the 2% increase. Additionally, 3 values have been decreased by the increase. As a consequence, because of the uncertainties being too large, no conclusion can be drawn from the 2% increase. Concerning changes in the mass and activity of transuranics, only those of ^{233}U and ^{237}Pu have been decreased by approximately 3%. The mass and activity of ^{236}Pu were the most affected by the 2% modification with a 17% reduction.

CHAPTER VI

CONCLUSIONS

With a world population supposed to grow by one fourth in the next 30 years, meeting a 30% increase in the energy demand appears as a challenge. Increasing the share of nuclear energy in the energy landscape would help meeting the demand by providing clean and reliable baseload electricity at a stable price, reducing a country's energy dependence and securing its energy supplies. Furthermore implementing new advanced nuclear systems such as HTR to produce hydrogen for transportation, process heat or power for energy-intensive industries could shift part of the use of oil, coal or gas use toward advanced nuclear systems. The perceived problem of the accumulation of HLW finds a solution in the reprocessing of TRU arising from LWRs in VHTRs. The use of ThO_2 instead of UO_2 would also limit the production of TRU while reducing Uranium consumption.

This study examines various advanced AP1000-VHTR fuel cycle scenarios by assessing their TRU destruction and their U consumption minimization capabilities, and by computing reactor performance parameters such as the evolution of the effective multiplication factor k_{eff} over time, the reactor energy spectrum or the isotopic composition and activity at EOL. The dependence of the performance metrics to nuclear data uncertainties – and in particular prompt neutron fission spectrum discrepancies – was also quantified to assess the accuracy of the output parameters and consequently guarantee the viability of a fuel cycle scenario.

To begin, the AP1000 and the VHTR were confronted to stress their behavioral differences and similarities when fueled with UO_2 or ThO_2. The performance characteristics of the VHTR fueled with UO_2 and ThO_2 were also of interest so as to later establish variations brought by the use of TRU-based fuels. It was concluded that the VHTR needed a 15wt% ^{235}U-enriched UO_2 to sustain the goal core lifetime of 600 days while the AP1000 only required a 3wt% enriched fuel. When UO_2 fuel is switched to ThO_2 the TRU content at EOL is divided by 100 in the AP1000 and by 10 in the VHTR. However, the AP1000 struggles to become critical when fueled with ThO_2. On the other hand, the VHTR behavior does not seem affected by the use of ThO_2. In both reactors, k_{eff} increases more significantly at EOL when ThO_2 is used. The AP1000 gains 68milli-k in 3 months when the VHTR gains 39milli-k in 346 days. The continuous buildup of ^{233}U, even after shutdown, is the cause of this k_{eff} jump. Reactors fueled with ThO_2 would consequently require extra negative reactivity to prevent these supercriticality excursions. ThO_2 fuels are an asset in minimizing Uranium consumption. They indeed produce ^{233}U the best fissile isotope for thermal spectra. The AP1000 had produced 1068kg of ^{233}U at EOL and produced another 116kg during the 90 days following shutdown. The VHTR produces 37.26kg of ^{233}Uafter 566 days of operation and produces another 7.8kg after shutdown. ThO_2 fuels also produce less Pu isotopes than UO_2 fuels.

The second step of the study consisted in analyzing various advanced AP1000-VHTR fuel cycles strategies. One of these strategies was also used later as a reference

case to allow the quantification of the impact of fission spectrum variation on fuel cycle performance parameters.

The advanced nuclear fuel cycles considered consisted in a 3wt% ^{235}U-enriched UO_2 -fueled AP1000 followed by a partly TRU-fueled VHTR. The proportions of TRU studied in the VHTR were 20%, 40% or 100%. TRU fuels were complemented by either UO_2 or ThO_2. UO_2 + TRU fueled VHTRs performances were compared to ThO_2 +TRU fueled reactors performances. Firstly, adding TRU to the fuel lowers the effective multiplication factor at BOL. The multiplication factor of a fuel containing exclusively TRU is reduced by 14%. The lowest effective multiplication factor at BOL is obtained for a VHTR fueled with 40% of TRU + UO_2 with a value of 1.07146 ± 0.00071, 20% lower than the value obtained in the UO_2-fueled VHTR. Secondly, increasing the fraction of TRU in the fuel increases the core lifetime. Indeed when the core contains only TRU, a lifetime of 2220 days is observed. When the fuel contains 20% of TRU + UO_2, the lifetime of an UO_2-fueled VHTR has been stretched by 36%, from 610 days to 830 days. When the fuel contains 40% of TRU complemented by UO_2, the core lifetime has been extended by 53% to 930 days. Additionally, when UO_2 is replaced by ThO_2 in a VHTR containing 40% of TRU, the core lifetime is stretched from 930 days to 1150 days, i.e. a 24% extension. These results are explained by the competition between the consumption of fissile material in the core and the buildup of isotopes participating in parasitic captures. The more TRU present in the VHTR, the higher the fissile content is. However more parasitic captures also occur. Thirdly, during the VHTRs lifetime, fuels with 40% of TRU containing WgPu have an effective multiplication factor 16.0% higher

than the same fuel containing RgPu. The reduction over time is very similar in both cases. To sum up, when TRUs are added to the fuel, the reactor core lifetime is extended and the effective multiplication factor decreases much more smoothly than in an UO_2-fueled VHTR.

UO_2 fuels produce more Pu isotopes than ThO_2 fuels because shorter core lifetime implies less depletion by fission of ^{239}Pu and ^{241}Pu and because of the presence of ^{238}U instead of ^{232}Th. In the 20% TRU cases, the total mass of Pu is reduced by 26% when ThO_2 is used instead of UO_2. In a VHTR fueled with 40% of TRU, the mass of Pu is reduced by 14%.

The best destruction rates are observed for a VHTR fueled with only 20% of TRU. Completed by ThO_2 88.9% of the amount of TRU initially present in the VHTR is destroyed. When completed with UO_2, 85.7% of the TRU initially present in the VHTR are eliminated. However in 600 days, the first configuration would only have reprocessed 33% of the TRU present at EOL of a single AP1000 while the second configuration (with UO_2) would have reprocessed 80% of the TRU arising from a single AP1000. The worst destruction rate is obtained for a VHTR solely fueled with TRU, only reducing the TRU amount by 35.2%.

The daily ^{235}U consumption is reduced for a VHTR fueled with 40% of TRU containing WgPu and completed by UO_2. The rate of consumption is 0.026% of the initial mass of ^{235}U per day. A VHTR containing 20% of TRU complemented by UO_2 shows the worst ^{235}U daily consumption with a rate of 0.050%. Replacing UO_2 by ThO_2 does not affect significantly the ^{235}U daily consumption.

The activity of TRU+ThO_2 fuels immediately after shutdown is lower than that of TRU+U fuel, easing fuel handling in emergency situations. For a 40% TRU-based fuel, adding ThO_2 reduces the total activity of the fuel by 25%. For a 20% TRU-based fuel, adding ThO_2 reduces the total activity of the fuel by 26%.

The final step of the study consisted in quantifying the impact of nuclear data variations and in particular the prompt neutron fission spectrum discrepancies among evaluated data libraries. Indeed prompt neutron fission spectrum evaluations are intensively used as input parameters in reactor calculation codes. However fission spectrum evaluations are also discrepant. The uncertainties in the prompt neutron fission spectrum are propagated in the calculations and may affect the outputs of the computations. Thus it is of paramount importance to evaluate the dependence of reactors' metrics and fuel cycle parameters to prompt neutron fission spectrum variations in order to assess the accuracy of the results and the viability of the fuel cycle.

First the prompt neutron fission spectrum of ^{235}U, ^{238}U and ^{239}Pu contained in the libraries ENDF/B-VI.8, JEFF-3.1, JENDL-3.3 and CENDL-3.1 were compared to their evaluations in the library ENDF-B/VII.0 chosen as the reference library. Ratios of the value in one library to the value in the reference library were computed using JANIS-3.2.

The discrepancies in the prompt neutron fission spectrum of ^{235}U in the libraries ENDF/B-VI.8, CENDL-3.1 and JEFF-3.1 with respect to ENDF/B-VII.0 are within a 2%-variation range for energies below 3.08MeV. Only above 9.2MeV are these evaluations differing from the reference library by more than 10%. JENDL-3.3

evaluations differ from ENDF/B-VII.0 by more than 10% below 76eV and by more than 15% above 8.5MeV. For energies in the range [61keV; 4.9MeV] the discrepancies are less than 2% of the reference value. The prompt neutron fission spectrum of ^{238}U in the JEFF-3.1 library is in very good agreement with the reference library ENDF/B-VII.0 since the amplitude of the discrepancies are 2% or less from 10eV to 17.8MeV. In CENDL-3.1, from 10eV to 3MeV the amplitude of the discrepancies is 5% or less except between 150keV and 1.5MeV where the discrepancies can attain 7% of variation. Above 4.3MeV, CENDL-3.1 evaluations can differ from ENDF/B-VII.0 by 10% and more. In JENDL-3.3, from 10eV to 6MeV, the evaluation differs by less than 2%. However above 6MeV, the amplitude of the discrepancies can attain up to 20%. In ENDF/B-VI.8 the prompt neutron spectrum has only been evaluated at two points: 0eV and 37eV. The evaluations of the prompt neutron fission spectrum of ^{239}Pu show more discrepancies. Only between 250keV and 5.2MeV is the amplitude of the discrepancies below 5% in CENDL-3.1. The ENDF/B-VI.8 evaluations differ by less than 5% only in the range [350keV; 8.7MeV]. The amplitude of the discrepancies can be lower than 41.3% of the reference value after 99MeV.In JEFF-3.3, the discrepancies are kept in a 5% only in the range [700keV; 6.6MeV]. In JENDL-3.3 only in the ranges [200eV; 64keV] and [1MeV; 2MeV] is the amplitude of the discrepancies 5% or less.

Then the original ENDF/B-VII.0 PNFS was altered in four different ways: first the spectrum was replaced by a step function. Secondly only the front of the spectrum (from 0 to 0.73MeV) was replaced by a step function, ENDF original distribution being up to 20% higher at some energies. Thirdly the tail of the spectrum was replaced by a step

function (from 2.3MeV to the end of the spectrum), the original ENDF probabilities being up to 17 times lower in that case. Finally the whole spectrum was increased by 2%.

The VHTR chosen to quantify fission spectrum uncertainties on the fuel cycle was fueled with 40% of TRU completed by 60% of 3wt% ^{235}U-enriched UO_2. For each alteration of the fission spectrum, the MCNP model of the VHTR was run. To quantify variations in the effective multiplication factor, in the VHTR energy spectrum, in the isotopic composition and activity at EOL, in the buildup of ^{135}Xe and in the transmutation efficiency and the TRU destruction capability, the ratio of each metric to its reference value was computed.

In summary, it has been established that the chosen alterations of the prompt neutron fission of ^{235}U can significantly affect the masses and activities of ^{233}U, ^{236}Np, ^{236}Pu and ^{237}Pu at EOL of the VHTR. The mass and activity of other isotopes are minimally affected (by less than 3%). The mass and activity at EOL of ^{236}Np, ^{236}Pu, ^{237}Pu can be lowered by respectively 7%, 9.45% and 7.3% when the full spectrum is replaced by a step function. When the front of the fission spectrum is replaced by a step function, only ^{236}Pu mass and activity is lowered by 12%. However, all the previously-mentioned nuclides are found in trace amount in the reactor. Therefore these significant modifications in the mass and activity have minimal impact on the VHTR behavior and its capacity to transmute TRUs. When the tail of the spectrum is replaced, the mass and activity of ^{233}U, ^{236}Pu and ^{237}Pu are multiplied by 263, 523 and 34. Nevertheless the final quantities of ^{233}U, ^{236}Pu and ^{237}Pu are still negligible comparatively to those of ^{239}Pu,

^{238}Pu, ^{240}Pu or ^{241}Pu. For example, even if the modified activity of ^{236}Pu has been multiplied by a factor of 523, it still corresponds to 0.0005% of the total activity. When increased by a factor of 523, the modified mass of ^{236}Pu represents less than 0.005% of the reference mass of ^{238}Pu and 0.0009% of the reference mass of ^{239}Pu. As a consequence, the transmutation efficiencies perfectly match the reference value while the TRU destruction rate has lost 0.01% in 2 alterations out of 4. Only the effective multiplication factor and the energy spectrum are marginally lowered when a significantly distorted fission spectrum tail is used. The former is lower by at best 1.3% and at worst 1.7%; the latter is at worst 5% lower than the original value between 50meV and 2MeV.

The feasibility of manufacturing TRU fuels or structural materials able to withstand longer core life time is outside the scope of the study. The reprocessing of TRISO particles, whether the extraction of ^{233}U is sought for further utilization, or simply the immobilization of VHTR spent fuel should equally be investigated in order to complete and ensure the viability of these strategies. Experimental studies would need to be set up and experimental data should be gathered. The costs of implementing new technologies, ThO_2 fuels and TRU-based fuels into the current nuclear landscape will also be key parameters in the possible deployment of such advanced nuclear energy systems.

REFERENCES

[1] ExxonMobil, 2012 The Outlook for Energy: A View to 2040, 2012: Irving, TX.

[2] BP, BP Energy Outlook 2030, 2011: London.

[3] IEA, World Energy Outlook 2011 Executive Summary, 2012.

[4] NEA, Carbon Pricing, Power Markets and the Competitiveness of Nuclear Power - Executive Summary, N. Development, Editor 2011, OECD.

[5] NEA, The Security of the Energy Supply and the Contribution of Nuclear Energy - Executive Summary, N. Development, Editor 2010, OECD.

[6] Piet, S., Which elements should be recycled for a comprehensive fuel cycle? GLOBAL 2007: Advanced Nuclear Fuel Cycles and Systems2007. 1595-1603.

[7] OECD, Projected Costs of Electricity, 2010

[8] IAEA, Fast Reactors Database, 2006.

[9] NEI. Nuclear Engineering International Handbook 2010. 2010 June 2011]; Available from: http://www.world-nuclear.org/info/inf32.html.

[10] Chang, H., et al., Thorium-Based Fuel Cycles in the Modular High Temperature Reactor. Tsinghua Science & Technology, 2006. **11**(6): p. 731-738.

[11] A. E. Finan, A.C.K., Integration of Nuclear Energy Into Oil Sands Projects Journal of Engineering for gas turbines and power 2010. **132**(4).

[12] Hoffelner, W., Materials for the Very High Temperature Reactor (VHTR): A Versatile Nuclear Power Station for Combined Cycle Electricity and Heat Production. CHIMIA International Journal for Chemistry, 2005. **59**(12): p. 977-982.

[13] Rodriguez, C., et al., Deep-Burn: making nuclear waste transmutation practical. Nuclear Engineering and Design, 2003. **222**(2-3): p. 299-317.

[14] IAEA, Thorium fuel cycle - Potential benefits and challenges, 2005, IAEA.

[15] Michel Lung, O.G., Perspectives of the thorium fuel cycle. Nuclear Engineering and Design, 1998. **180**(2): p. 133-146.

[16] Talamo, A. and W. Gudowski, Adapting the deep burn in-core fuel management strategy for the gas turbine – modular helium reactor to a uranium–thorium fuel. Annals of Nuclear Energy, 2005. **32**(16): p. 1750-1781.

[17] Hong, S.G., Y. Kim, and F. Venneri, Characterization of a sodium-cooled fast reactor in an MHR–SFR synergy for TRU transmutation. Annals of Nuclear Energy, 2008. **35**(8): p. 1461-1470.

[18] Lung, M. and O. Gremm, Perspectives of the thorium fuel cycle. Nuclear Engineering and Design, 1998. **180**(2): p. 133-146.

[19] GRUPPELAAR H. and e. al., Thorium as a wate management option, 2000, European Commission.

[20] Chirayath, S.S., et al., Neutronic and nonproliferation characteristics of (PuO_2-UO_2) and (PuO_2–ThO_2) as fast reactor fuels. Nuclear Engineering & Design, 2009. **239**(10): p. 1916-1924.

[21] Heising, C., Safeguards considerations of thorium utilization in nuclear reactor fuel cycles,Proceedings of Risk Management - For Tomorrow's Challenges2011. 245-247.

[22] Thorium Fueled High-Temperature Reactors Analysis: Thorium Utilization in the Modular Helium-Cooled Reactor G.P. 20154, Editor 2008.

[23] Sollychin, R., Exploring Fuel Alternatives, in IAEA Bulletin2009. p. 2.

[24] DOE, U.S., Draft Global Nuclear Energy Partnership Programmatic Environmenta Impact Statement, 2008, U.S. Department Of Energy. p. 79.

[25] Salvatores, M., et al., Needs and Issues of Covariance Data Application. Nuclear Data Sheets, 2008. **109**(12): p. 2725-2732.

[26] Talou, P., et al., Quantification of Uncertainties for Evaluated Neutron-Induced Reactions on Actinides in the Fast Energy Range. Nuclear Data Sheets, 2011. **112**(12): p. 3054-3074.

[27] WPEC, Uncertainty and Target Accuracy Assessment for Innovative Systems Using Recent Covariance Data Evaluations, W.P.o.I.E.C.-o.o.t.N.N.S. Committee, Editor 2008, NEA,OECD.

[28] Salvatores, M., Advanced Fuel Cycles and R&D needs in the nuclear data field, in Nuclear Physics and Related Computational Science R&D for Advanced Fuel Cycle Workshop2006.

[29] Bredeweg, T.A., et al., Recent actinide nuclear data efforts with the DANCE 4 pi BaF2 array, International Conference on Nuclear Data for Science and Technology, Vol.1, Proceedings 2008. 607-610.

[30] OECD, N.E.A. and A.E. Informatique, JANIS (JAva-based Nuclear Information Software), 2011.

[31] Tran, H.N. and Y. Kato, New Np-237 burning strategy in a supercritical CO2-cooled fast reactor core attaining zero burnup reactivity loss. Nuclear science and engineering, 2008. **159**(1): p. 83-93.

[32] U.S.NRC. Combined License Applications for New Reactors. 2011 March, 10 2011 June 2011]; Available from: http://www.nrc.gov/reactors/new-reactors/col.html

[33] Bull, A., The AP1000 Nuclear Power Plant - Global Experience and UK Prospects W. UK, Editor 2010.

[34] IAEA. Latest Data Shows Long-Term Security of Uranium supply. 2010 July 20, 2010 June 2011]; Available from: http://www.iaea.org/newscenter/pressreleases/2010/prn201009.html

[35] Shultis J. K. and R.E. Faw, Fundamentals of Nuclear Science and Engineering. Second Edition ed2008: CC Press.

[36] Ames, D.E.I., High-Fidelity Nuclear Energy System Optimization Towards an Environmentally Benign, Sustainable and Secure Energy Source, in Nuclear EngineeringAugust 2010, Texas A&M University: College Station, TX.

[37] Kim, Y. and F. Venneri, Optimization of one-pass transuranic deep burn in a modular helium reactor. Nuclear science and engineering, 2008. **160**(1): p. 59-74.

[38] Commerce, U.S.D.o., The Commercial Outlook for U.S. Small Modular Nuclear Reactors, February 2011, International Trade Administration

[39] Ashley F. Bershak and A.C. Kadak, Integration of Nuclear Energy with Oil Sands Projects For Reduced Greenhouse Gas Emissions and Natural Gas Consumption, 2007, Massachussetts Institue of Technology.

[40] NRC, Westinghouse AP1000 Design Control Documentation Rev. 16, N.R. Commission, Editor 2007.

[41] IAEA-TECDOC-1382, T.R., Evaluation of high temperature gas-cooled reactor performance:benchmark analysis related to initial testing of the HTTR and HTR-10, 2003, International Atomic Agency: Vienna, Austria.

[42] N. Kodochigov, Y.S., E. Marava, N.Ponomarev-Stepnoy, E. Glushkov, P. Fomichenko, Neutronics features of the GT-MHR reactor. Nuclear Engineering and Design, 2002. **222**: p. 161-171.

[43] Hangbok, C., Advanced fuel cycle scenarios for High Temperature Gas Reactors. Annals of Nuclear Energy, 2011. **38**(11): p. 2338-2349.

[44] Ames, D.E., High-Fidelity Nuclear Energy system Optimization towards an environmentally benign, sustainable, and secure energy source, in Nuclear Engineering, Texas A&M: College Station.

[45] Pandikumar, G., V. Gopalakrishnan, and P. Mohanakrishnan, Impact of spread in minor actinide data from ENDF/B-VII.0, ENDF/B-VI.8, JENDL-3.3 and JEFF-3.0 on an IAEA-CRP FBR benchmark for MA incineration. Annals of Nuclear Energy, 2008. **35**(8): p. 1519-1534.

[46] Noy, R.C., et al., Summary Report Consultants' Meeting on Prompt Fission Neutron Spectra of Major Actinides, 2008, IAEA Headquarters: Vienna.

[47] Enqvist, A., Measurement of Fission Spectrum at LANSCE for the Evaluation of Safeguards Data. 2011.

[48] LANL. An Introduction to the ENDF Formats. T-2 Nuclear Information Service 23 January 1998 [cited 2011; Available from: http://t2.lanl.gov/endf/title.html.

[49] LANL. ENDF, NJOY, and Applications. T-2 Nuclear Information Service 23 January 1998 [cited 2011; Available from: <http://t2.lanl.gov/njoy/njoy01.html>.

[50] Michael L. Fensin, J.S.H., Samim Anghaie, Improved Reaction Rate Tracking and Fission Product Yield Determinations for the Monte Carlo-Linked Depletion Capability in MCNPX. Nuclear Technology, 2008. **164**(1): p. 3-12.

APPENDIX A

MCNP AP1000 REACTOR MATERIAL CARDS

In all cases the fuel temperature is 1200K and structural materials' temperature is 900K. Water temperature has been kept at 900K to allow comparison with the moderator temperature of the VHTR. In the AP1000, water enters the core at 533.15K and leaves it at 594.25K.

Materials 4 to 9 (moderator, burnable poisons, absorbers and core structural materials) have the same compositions whether the fuel is UO_2 or ThO_2 and thus are presented in section 3 of the Appendix.

1. AP1000 fueled with UO_2 3% ^{235}U enriched

Table 21. Weight Fraction for Material 1: UO_2 1.95% enriched

Nuclide	ZAID and cross sections library extension	Weight Fraction
Uranium	92235.73c	0.0171888918
	92238.73c	0.86429274
Oxygen	8016.73c	0.11851837
Americium	95241.72c	10^{-35}
	95242.72c	10^{-35}
	95243.72c	10^{-35}
	95244.72c	10^{-35}
Curium	96241.72c	10^{-35}
	96242.72c	10^{-35}
	96243.72c	10^{-35}
	96244.72c	10^{-35}
	96245.72c	10^{-35}

Table 22. Weight Fraction for Material 2:UO_2 3% enriched

Nuclide	ZAID and cross section library extension	Weight Fraction
Uranium	92235.73c	0.026444028
	92238.73c	0.85502357
Oxygen	8016.73c	0.118532399
Americium	95241.72c	10^{-35}
	95242.72c	10^{-35}
	95243.72c	10^{-35}
	95244.72c	10^{-35}
Curium	96241.72c	10^{-35}
	96242.72c	10^{-35}
	96243.72c	10^{-35}
	96244.72c	10^{-35}
	96245.72c	10^{-35}

Table 23. Weight Fraction for Material 3: UO_2 4.05% enriched

Nuclide	ZAID and cross section library extension	Weight Fraction
Uranium	92235.73c	0.0356988697
	92238.73c	0.8457547
Oxygen	8016.73c	0.118546428
Americium	95241.72c	10^{-35}
	95242.72c	10^{-35}
	95243.72c	10^{-35}
	95244.72c	10^{-35}
Curium	96241.72c	10^{-35}
	96242.72c	10^{-35}
	96243.72c	10^{-35}
	96244.72c	10^{-35}
	96245.72c	10^{-35}

2. AP1000 with ThO_2 (3% ^{235}U enriched U + 97% ^{232}Th).

Table 24. Weight Fraction for Material 1: ThO_2 1.95% enriched

Nuclide	ZAID and cross section library extension	Weight Fraction
Uranium	92235.73c	0.0171888918
Thorium	90232.73c	0.86429274
Oxygen	8016.73c	0.11851837
Americium	95241.72c	10^{-35}
	95242.72c	10^{-35}
	95243.72c	10^{-35}
	95244.72c	10^{-35}
Curium	96241.72c	10^{-35}
	96242.72c	10^{-35}
	96243.72c	10^{-35}
	96244.72c	10^{-35}
	96245.72c	10^{-35}

Table 25. Weight Fraction for Material 2:ThO_2 3% enriched

Nuclide	ZAID and cross section library extension	Weight Fraction
Uranium	92235.73c	0.026444028
Thorium	90232.73c	0.85502357
Oxygen	8016.73c	0.118532399
Americium	95241.72c	10^{-35}
	95242.72c	10^{-35}
	95243.72c	10^{-35}
	95244.72c	10^{-35}
Curium	96241.72c	10^{-35}
	96242.72c	10^{-35}
	96243.72c	10^{-35}
	96244.72c	10^{-35}
	96245.72c	10^{-35}

Table 26. Weight Fraction for Material 3: ThO_2 4.05% enriched

Nuclide	ZAID and cross section library extension	Weight Fraction
Uranium	92235.73c	0.0356988697
Thorium	90232.73c	0.8457547
Oxygen	8016.73c	0.118546428
Americium	95241.72c	10^{-35}
	95242.72c	10^{-35}
	95243.72c	10^{-35}
	95244.72c	10^{-35}
Curium	96241.72c	10^{-35}
	96242.72c	10^{-35}
	96243.72c	10^{-35}
	96244.72c	10^{-35}
	96245.72c	10^{-35}

3. AP1000 Materials Cards for Moderator and Structural Materials

Table 27. Weight Fraction for Material 4: Helium

Isotope	ZAiD and cross sections library extension	Weight Fraction
He-3	2003.72c	0.00000137
He-4	2004.72c	0.99999863

Table 28. Weight Fraction for Material 5: Zirconium Cladding

Nuclide	ZAiD and cross sections library extensions	Weight Fraction
Zirconium	40090.72c	0.505393
	40091.72c	0.110214
	40092.72c	0.168464
	40094.72c	0.170724
	40096.72c	0.027504
Tin	50112.72c	0.000141
	50114.72c	0.000096
	50115.72c	0.000049
	50116.72c	0.002108
	50117.72c	0.001114
	50118.72c	0.003512
	50119.72c	0.001246
	50120.72c	0.004724
	50122.72c	0.000671
	50124.72c	0.00084
Iron	26054.72c	0.000187
	26056.72c	0.002936
	26057.72c	0.000068
	26058.72c	0.000009

Table 29. Mass Fractions for material 6: Integral Fuel Burnable Absorber

Nuclide	ZAiD and cross sections library extensions	Weight Fraction
Boron	5010.72c	0.0187
	5011.72c	0.1713
Zirconium	40090.72c	0.416745
	40091.72c	0.090882
	40092.72c	0.138915
	40094.72c	0.140778
	40096.72c	0.02268

Table 30. Mass Fractions for Material 7: SS304 for Discrete Burnable Poison Rods

Nuclide	ZAiD and cross section library extensions	Weight Fraction
Iron	26054.72c	0.039965
	26056.72c	0.627368
	26057.72c	0.014489
	26058.72c	0.001928
Chromium	24050.72c	0.008256
	24052.72c	0.159199
	24053.72c	0.018052
	24054.72c	0.004494
Nickel	28058.72c	0.064673
	28060.72c	0.024912
	28061.72c	0.001083
	28062.72c	0.003453
	28064.72c	0.000879
Magnesium	12024.72c	0.015798
	12025.72c	0.002
	12026.72c	0.002202
Silicon	14028.72c	0.009223
	14029.72c	0.000468
	14030.72c	0.000309
Carbon	6000.72c	0.0008
Phosphorus	15031.72c	0.00045

Table 31. Mass Fractions for Material 8: Absorber for Discrete Burnable Poison Rods

Nuclide	ZAiD and cross sections library extensions	Weight Fraction
Boron	5010.72c	0.007
	5011.72c	0.0319
Oxygen	8016.72c	0.5522
Silicon	14028.72c	0.3772
	14029.72c	0.0191
	14030.72c	0.0126

Table 32. Mass Fractions for Material 9: Water (moderator)

Nuclide	ZAiD and cross sections library extensions	Weight Fraction
Hydrogen	1001.72c	0.111
Oxygen	8016.72c	0.889
	Lwtr.18t	

APPENDIX B

MCNP VHTR MATERIAL CARDS

In all cases the fuel temperature is 1200K and moderator temperature is 900K.

Similarly to the AP1000 case, Americium and Curium isotopes were specified in the material card with a weight fraction of 10^{-35}. Indeed these isotopes can have important cross sections and may alter the MCNP calculated fission spectrum if their buildup is not taken into account in MCNP transport calculations [50].

Materials 2 to 9 (helium, different types of graphite, burnable poison, TRISO coatings) have the same compositions whether the fuel is UO_2 or ThO_2 and thus are presented in section 3 of the Appendix.

4. UO_2 15% ^{235}U enriched

Table 33. Material 1: UO_2

Nuclide	ZAiD and cross section library extension	Weight fraction
Uranium	92235.73c	0.13222905
	92238.73c	0.74929795
Oxygen	8016.73c	0.118473
Americium	95241.72c	10^{-35}
	95242.72c	10^{-35}
	95243.72c	10^{-35}
	95244.72c	10^{-35}
Curium	96241.72c	10^{-35}
	96242.72c	10^{-35}
	96243.72c	10^{-35}
	96244.72c	10^{-35}
	96245.72c	10^{-35}

5. ThO_2 15% ^{235}U enriched

Table 34. Material 1: ThO_2

Nuclide	ZAiD and cross section library extension	Weight fraction
Uranium	92235.72c	0.13222905
Thorium	90232.72c	0.74929795
Oxygen	8016.72c	0.118473
Americium	95241.72c	10^{-35}
	95242.72c	10^{-35}
	95243.72c	10^{-35}
	95244.72c	10^{-35}
Curium	96241.72c	10^{-35}
	96242.72c	10^{-35}
	96243.72c	10^{-35}
	96244.72c	10^{-35}
	96245.72c	10^{-35}

6. Moderator, absorbers and structural materials

Table 35. Material 2: TRISO Particles Carbon Coating

Nuclide	ZAiD and cross section library extension	Weight fraction
Carbon	6000.72c	1

Table 36. Material 3: TRISO Particles SiC Coating

Nuclide	ZAiD and cross section library extension	Weight fraction
Silicon	14028.72c	0.64561
	14029.72c	0.03278
	14030.72c	0.02161
Carbon	6000.72c	0.3
	grph.10t	

Table 37. Material 4: Helium (coolant)

Isotope	ZAiD and cross section library extension	Weight fraction
Helium-3	2003.72c	0.00000137

Table 38. Material 5: Burnable Poison B_4C

Nuclide	ZAiD and cross section library extension	Weight fraction
Carbon	6000.72c	0.978556
Boron	5010.72c	0.004267
	5011.72c	0.017177
	grph.10t	

Table 39. Material 6: Graphite Inside Fuel Compact (Graphite Matrix)

Nuclide	ZAiD and cross section library extension	Weight fraction
Carbon	6000.72c	0.9999992
Boron	5010.72c	0.0000001631
	5011.72c	0.0000006569
	grph.10t	

Table 40. Material 7: Graphite for Prismatic Block

Nuclide	ZAiD and cross section library extension	Weight fraction
Carbon	6000.72c	0.9999996
Boron	5010.72c	0.0000000796
	5011.72c	0.0000003204
	grph.10t	

Table 41. Material 8: Rod Graphite Sleeve

Nuclide	ZAiD and cross section library extension	Weight fraction
Carbon	6000.72c	0.99999963
Boron	5010.72c	0.0000000736
	5011.72c	0.0000002964
	grph.10t	

Table 42. Material 9: Graphite for Outer Cylinder

Nuclide	ZAiD and cross section library extension	Weight fraction
Carbon	6000.72c	0.999998
Boron	5010.72c	0.000000398
	5011.72c	0.000001602
	grph.10t	

APPENDIX C

COMPOSITION OF TRU FUELS AT EOL OF THE AP1000 AND THE VHTR

These tables represent the composition of the fuel after 600 days in the AP1000 and the VHTR. The composition was extracted from MCNP outputs.

Table 43. Fuel Composition for Reactors Fueled with UO_2

Nuclide	Isotope	ZAiD	Mass (g) in AP1000	Mass (g) in VHTR	Relative Difference (VHTR vs. PWR, %)	Half-Life
Thorium	Th-232	90232	none	6.28E-17	n/a	1.40E+10 yr
Uranium	U-234	92234	7.15E-09	1.04E-08	1.455E+02	2.455E+5 yr
	U-235	92235	2.11E-08	6.32E-08	2.995E+02	7.04E+8 yr
	U-236	92236	2.18E-07	1.28E-06	5.872E+02	2.342E+7 yr
	U-237	92237	5.98E-01	3.19E+00	5.334E+02	6.75 d
	U-238	92238	3.20E-07	2.76E-07	8.625E+01	4.468E+9 yr
	U-239	92239	2.13E+01	5.03E+01	2.362E+02	23.45 m
Neptunium	Np-236	93236	7.81E-12	none	0.000E+00	153E+3 y
	Np-237	93237	1.65E-07	5.65E-07	3.424E+02	2.144E+6 yr
	Np-238	93238	2.08E-01	1.70E+00	8.173E+02	2.117 d
	Np-239	93239	2.13E+01	5.00E+01	2.347E+02	2.356 d
Plutonium	Pu-237	94237	9.81E-04	none	0.000E+00	45.64 d
	Pu-238	94238	2.17E-04	4.94E-03	2.276E+03	87.7 yr
	Pu-239	94239	4.61E-04	1.55E-04	3.362E+01	24,110 yr
	Pu-240	94240	8.93E-02	6.83E-04	7.648E-01	6,561 yr
	Pu-241	94241	1.39E-06	1.38E-01	9.928E+06	14.325 yr
	Pu-242	94242	2.42E-01	5.63E-06	2.326E-03	3.75E+5 yr
	Pu-243	94243	1.43E-13	1.06E+00	7.413E+14	4.956 hr
	Pu-244	94244	5.45E-05	7.04E-13	1.292E-06	8.00E+7 yr
Americium	Am-241	95241	8.58E-07	4.44E-05	5.175E+03	432.6 yr
	Am-242	95242	8.68E-06	7.07E-07	8.145E+00	16.02 h
	Am-243	95243	5.14E-02	3.09E-05	6.012E-02	7,370 yr

Table 43. Fuel Composition for Reactors Fueled with UO_2 (continued)

Nuclide	Isotope	ZAiD	Mass (g) in AP1000	Mass (g) in VHTR	Relative Difference (VHTR vs. PWR, %)	Half-Life
	Am-244	95244	2.37E-02	2.40E-01	1.013E+03	10.1 h
Curium	Cm-242	96242	5.26E-06	7.29E-02	1.386E+06	162.8 d
	Cm-243	96243	9.01E-04	1.81E-05	2.009E+00	29.1 yr
	Cm-244	96244	6.88E-08	3.37E-03	4.898E+06	18.1 yr
	Cm-245	96245	8.80E-09	1.96E-07	2.227E+03	8,423 yr
	Cm-246	96246	none	3.86E-08	n/a	4,706 yr

Table 44. Fuel Composition for Power Reactors fueled with ThO_2

Nuclide	Isotope	ZAiD	Mass (g) in AP1000	Mass (g) in VHTR	Relative Difference (VHTR vs. PWR, %)	Half-life
Thorium	Th-231	90231	1.18E-01	2.12E-02	1.797E+01	25.52 h
	Th-232	90232	1.04E-07	9.02E-08	8.673E+01	1.40E+10 yr
	Th-233	90233	3.00E+01	5.79E+01	1.930E+02	21.83 m
Proactinium	Pa-233	91233	2.88E+01	5.09E+01	1.767E+02	26.975 d
Uranium	U-233	92233	9.93E-05	1.07E-04	1.078E+02	1.592E+5 yr
	U-234	92234	8.58E-06	1.13E-05	1.317E+02	2.455E+5 yr
	U-235	92235	1.96E-08	6.56E-08	3.347E+02	7.04E+8 yr
	U-236	92236	2.29E-07	1.27E-06	5.546E+02	2.342E+7 yr
	U-237	92237	5.26E-01	3.14E+00	5.970E+02	6.75 d
Neptunium	Np-236	93236	4.05E-12	none	0.000E+00	153E+3 y
	Np-237	93237	1.34E-07	5.18E-07	3.866E+02	2.144E+6 yr
	Np-238	93238	1.77E-01	1.61E+00	9.096E+02	2.117 d
	Np-239	93239	1.28E-03	2.09E-02	1.633E+03	2.356 d
Plutonium	Pu-238	94238	7.03E-04	4.26E-03	6.060E+02	87.7 yr
	Pu-239	94239	2.60E-07	1.34E-06	5.154E+02	24,110 yr
	Pu-240	94240	2.42E-07	2.82E-06	1.165E+03	6,561 yr
	Pu-241	94241	5.51E-05	4.49E-04	8.149E+02	14.325 yr
	Pu-242	94242	4.25E-10	6.77E-09	1.593E+03	3.75E+5 yr
	Pu-243	94243	none	1.34E-03	n/a	4.956 hr

Table 44. Fuel Composition for Reactors Fueled with ThO_2 (continued)

Nuclide	Isotope	ZAiD	Mass (g) in AP1000	Mass (g) in VHTR	Relative Difference (VHTR vs. PWR, %)	Half-life
Americium	Am-241	95241	1.72E-08	7.68E-08	4.465E+02	432.6 yr
	Am-243	95243	1.50E-09	1.81E-08	1.207E+03	7,370 yr
Curium	Cm-242	96242	4.67E-06	5.72E-05	1.225E+03	162.8 d
	Cm-244	96244	8.33E-08	9.99E-07	1.199E+03	29.1 yr
	Cm-245	96245	none	1.96E-07	n/a	18.1 yr
	Cm-246	96246	none	3.86E-08	n/a	8,423 yr

APPENDIX D

COMPOSITION OF THE U-CYCLE TRU-BASED VHTR FUELS

A. 20% TRU

Table 45. Fuel Composition for 20% TRU + UO_2 fuel

Nuclide	ZAiD	Mass Fraction
Neptunium	93236	1.5660E-08
	93237	6.6311E-03
Plutonium	94238	1.5235E-03
	94239	1.0218E-01
	94240	5.5494E-02
	94241	1.3212E-02
	94242	9.0090E-03
	94244	1.9468E-07
Americium	95241	1.0673E-02
	95242	2.0416E-06
	95243	1.0908E-03
Curium	96243	1.8932E-06
	96244	1.7234E-04
	96245	9.4845E-06
	96246	6.5240E-07
Uranium	92235	0.104619518
	92238	*0.600428044*
Oxygen	8016	0.094952438

Table 46. Fuel Composition for 20% TRU + ThO_2 fuel

Nuclide	ZAiD	Mass Fraction
Neptunium	93236	1.56602E-08
	93237	0.00663113
Plutonium	94238	0.001523485
	94239	0.102179692
	94240	0.055493854
	94241	0.013212025
	94242	0.00900896
	94244	1.94681E-07
Americium	95241	0.010673441
	95242	2.04158E-06
	95243	0.001090787
Curium	96243	1.89322E-06
	96244	0.000172342
	96245	9.48453E-06
	96246	6.52396E-07
Thorium	*90232*	*5.59953E-01*
Uranium	92235	1.04446E-01
Oxygen	8016	9.6023E-02

B. 40% TRU

Table 47. Fuel Composition for 40% TRU + UO_2 fuel

Nuclide	ZAiD	Mass Fraction
Neptunium	93236	3.1320E-08
	93237	1.3262E-02
Plutonium	94238	3.0470E-03
	94239	2.0436E-01
	94240	1.1099E-01
	94241	2.6424E-02
	94242	1.8018E-02
	94244	3.8936E-07
Americium	95241	2.1347E-02
	95242	4.0832E-06
	95243	2.1816E-03
Curium	96243	3.7864E-06
	96244	3.4468E-04
	96245	1.8969E-05
	96246	1.3048E-06
Uranium	92235	0.078464639
	92238	*0.450321033*
Oxygen	8016	0.071214329

Table 48. Fuel Composition for 40% TRU + ThO_2

Nuclide	ZAiD	Mass Fraction
Neptunium	93236	3.1320E-08
	93237	1.3262E-02
Plutonium	94238	3.0470E-03
	94239	2.0436E-01
	94240	1.1099E-01
	94241	2.6424E-02
	94242	1.8018E-02
	94244	3.8936E-07
Americium	95241	2.1347E-02
	95242	4.0832E-06
	95243	2.1816E-03
Curium	96243	3.7864E-06
	96244	3.4468E-04
	96245	1.8969E-05
	96246	1.3048E-06
Thorium	*90232*	*0.44964767*
Uranium	92235	0.078334822
Oxygen	8016	0.072017508

C. 100% TRU

Table 49. Fuel Composition for 100% TRU Fuel

Nuclide	ZAiD	Mass fraction
Neptunium	93236	7.83E-08
	93237	3.32E-02
	94238	7.62E-03
Plutonium	94239	5.11E-01
	94240	2.77E-01
	94241	6.61E-02
	94242	4.50E-02
	94244	9.73E-07
Americium	95241	5.34E-02
	95242	1.02E-05
	95243	5.45E-03
Curium	96243	9.47E-06
	96244	8.62E-04
	96245	4.74E-05
	96246	3.26E-06

APPENDIX E

EFFECTIVE MULTIPLICATION FACTOR IN VHTR FOR TRU-BASED FUELS ARISING FROM A THORIUM CYCLE

Table 50. k_{eff} at BOL

Fuel in the AP1000	Complement	BOL k_{eff}
ThO_2	20 % UO_2	0.68204 ± 0.00058
	40 % UO_2	0.43319 ± 0.00036
	40% ThO_2	0.98979 ± 0.00065
	100% TRU	0.12884 ± 0.00014

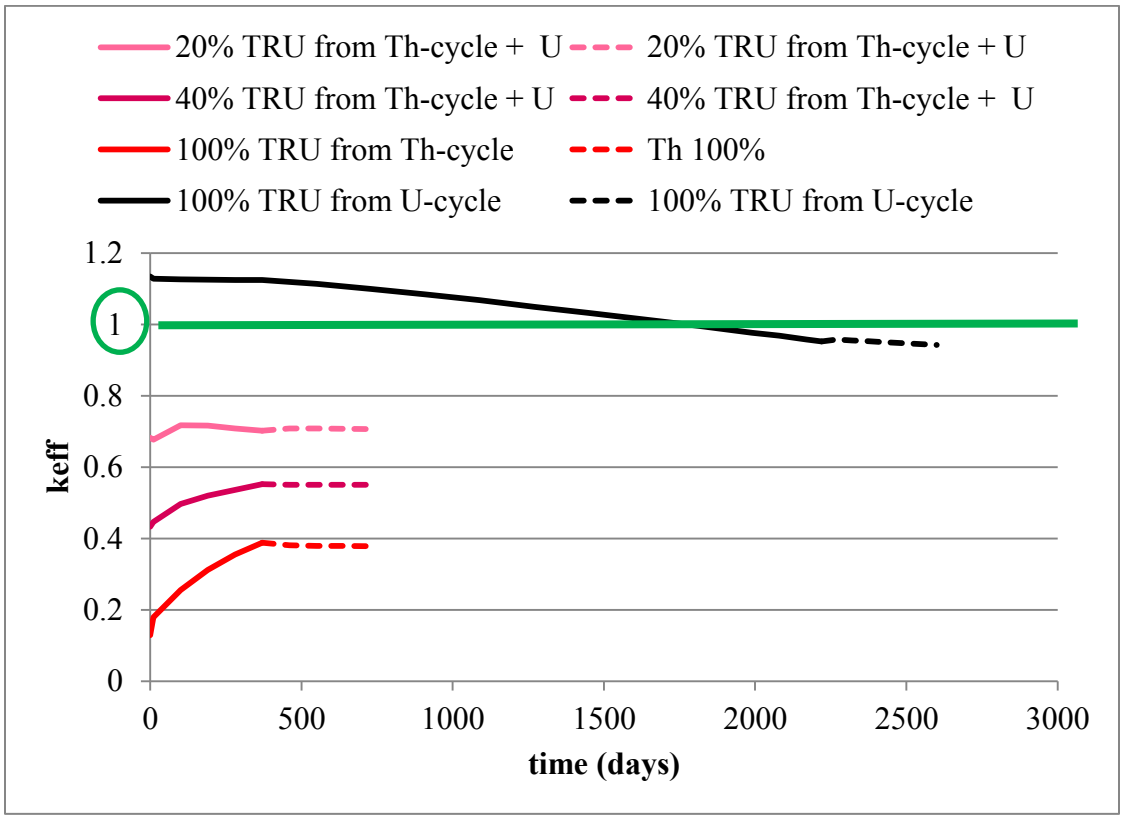

Figure 68. Evolution of the Effective Multiplication Factor Over Time

APPENDIX F

TOTAL FISSION CROSS SECTIONS OF THE FISSILE ISOTOPES ^{233}U, ^{235}U, ^{237}U, ^{239}U, ^{239}Pu, ^{241}Pu, ^{243}Pu, ^{243}Cm AND ^{245}Cm

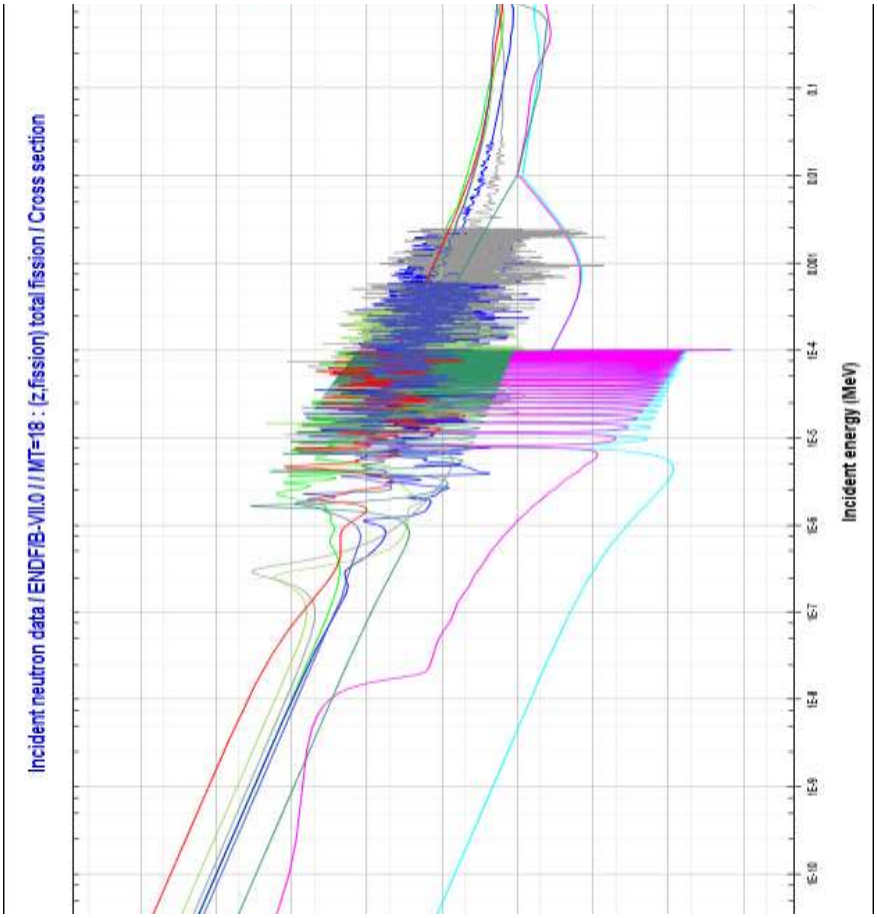

Figure 69. Total Fission Cross Sections of Fissile Isotopes

APPENDIX G

COMPOSITION OF TRU-BASED FUELS CONTAINING WEAPON-GRADE PLUTONIUM OR REACTOR-GRADE PLUTONIUM

Table 51. Composition of 40% TRU + UO_2 where the Plutonium is WgPu or RgPu

Nuclides	ZAiD	Atomic fraction with WgPu	Weight fraction with RgPu
Neptunium	93236.73c	3.3209E-08	3.1320E-08
	93237.73c	1.4119E-02	1.3262E-02
Plutonium	94238.73c	3.9059E-05	3.0470E-03
	94239.73c	3.6646E-01	2.0436E-01
	94240.73c	2.2654E-02	1.1099E-01
	94241.73c	1.3671E-03	2.6424E-02
	94242.73c	7.8119E-05	1.8018E-02
	94244.73c	4.2676E-07	3.8936E-07
Americium	95241.73c	2.3110E-02	2.1347E-02
	95242.73c	4.4387E-06	4.0832E-06
	95243.73c	23814E-03	2.1816E-03
Curium	96243.73c	4.1331E-06	3.7864E-06
	96244.73c	3.7779E-04	3.4468E-04
	96245.73c	2.0876E-05	1.8969E-05
	96246.73c	1.4419E-06	1.3048E-06
Uranium	92238.73c	4.8144E-01	0.450321033
	92235.73c	8.2829E-02	0.078464639
Oxygen	8016.73c	5.1183E-03	0.071214329

APPENDIX H

RADIATIVE CAPTURE CROSS SECTIONS OF ^{237}NP, ^{240}PU, ^{242}PU AND ^{241}AM

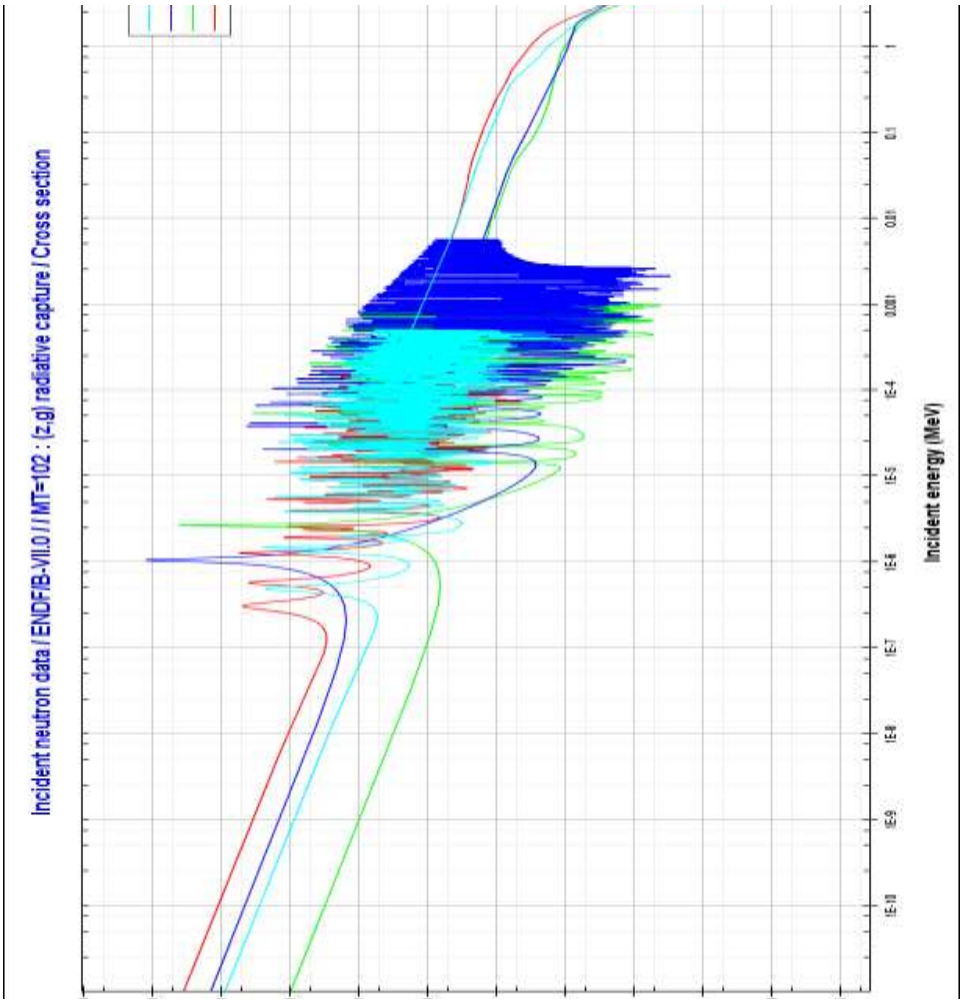

Figure 70. Radiative Capture Cross Section

APPENDIX I

EXCERPT OF AN ENDF/B-VII.0 FILE

The following excerpt corresponds to the beginning and the end of the evaluation of the prompt neutron fission spectrum of ^{235}U in the ENDF6 Format. The file has been retrieved from http://www.nndc.bnl.gov.

```
 9.223500+4 2.330248+2          0           0           1           09228 5 18    1
 0.000000+0 0.000000+0          0           1           1           29228 5 18    2
          2          2                                                9228 5 18    3
 1.000000-5 1.000000+0 2.000000+7 1.000000+0                          9228 5 18    4
 0.000000+0 0.000000+0           0           0          1          209228 5 18    5
         20          2                                                9228 5 18    6
 0.000000+0 1.000000-5           0           0          1         5639228 5 18    7
        563          2                                                9228 5 18    8
 0.000000+0 0.000000+0 1.000000+1 1.850569-9 1.100000+1 1.940894-99228 5 18    9
 1.200000+1 2.027196-9 1.300000+1 2.109973-9 1.400000+1 2.189621-99228 5 18   10
 1.500000+1 2.266473-9 1.600000+1 2.340803-9 1.700000+1 2.412844-99228 5 18   11
```

[…]

```
 9.900000+6 1.487460-9 1.000000+7 1.391632-9 1.100000+7 7.14958-109228 5 18 799
 1.200000+7 3.67010-10 1.300000+7 1.87935-10 1.400000+7 9.60558-119228 5 18 800
 1.500000+7 4.89662-11 1.600000+7 2.49034-11 1.700000+7 1.26421-119228 5 18 801
 1.800000+7 6.40644-12 1.900000+7 3.24072-12 2.000000+7 1.63662-129228 5 18 802
 2.100000+7 8.25406-13 2.200000+7 4.15880-13 2.300000+7 2.09418-139228 5 18 803
 2.400000+7 1.05413-13 2.500000+7 5.30392-14 2.600000+7 2.66722-149228 5 18 804
 2.700000+7 1.34023-14 2.800000+7 6.72738-15 2.900000+7 3.37277-159228 5 18 805
 3.000000+7 1.68887-15 3.100000+7 0.000000+0                          9228 5 18 806
 0.000000+0 0.000000+0          0           0          0           09228 5  99999
```

APPENDIX J

DESIGNATION OF ENDF MT AND MF IDENTIFIERS

The descriptions and definition found in this Appendix were acquired from the ENDF Manual, *ENDF-6 Formats Manual Data Formats and Procedures for the Evaluated Nuclear Data File ENDF/B-VI and ENDF/B-VII*, by M. Herman and A. Trkov.

The general form of ENDF files is one-dimensional tabulations. On the ASCII versions of ENDF files, data are stored in columns, using numbers only. Data have to be read from left to right, line after line. A function f of x would be represented as a succession of (x,f(x)) pairs ordered by increasing values of x. For instance, simple cross sections are stored as (energy, cross sections) pairs, the energy being in eV and the cross sections in barn. Special values of MT, MF and MAT numbers indicate respectively the end of a section, file or material and the beginning of a new section, file or material.

1. **MF** labels an ENDF **F**ile. "Files" are usually used to store different types of data, thus:
    - MF=1 contains descriptive and miscellaneous data,
    - MF=2 contains resonance parameter data,
    - MF=3 contains reaction cross sections vs. energy,
    - MF=4 contains angular distributions,
    - MF=5 contains energy distributions,

- MF=6 contains energy-angle distributions,
- MF=7 contains thermal scattering data,
- MF=8 contains radioactivity data
- MF=9-10 contain nuclide production data,
- MF=12-15 contain photon production data, and
- MF=30-36 contain covariance data.

2. The ENDF format uses **MT numbers** to define reaction types, and some additional MT numbers are used for special sections, such as the descriptive data, or the resonance parameters. In the following tables, "z" stands for any of the particles, *i.e.*, n, p, d, t, ^{3}He, α, or photonuclear gamma.

Table 52. Definition of the Main MT Numbers

MT	Reaction	Description	Comments
1	(n,total)	Neutron total cross section. Sum of MT=2, 4, 5, 11, 16-18, 22-26, 28-37, 41-42, 44-45, and 102-117.	Redundant. Undefined for incident charged particles.
2	(z,z_0)	Elastic scattering cross section for incident particles.	
3	(z,nonelastic)	Nonelastic cross section. Sum of MT=4, 5, 11, 16-18, 22-26, 28-37, 41-42, 44-45, 102-117.	Redundant. For photon production only.
4	(z,n)	Production of one neutron in the exit channel. Sum of MT=50-91.	Redundant. For incident neutrons, this is total inelastic scattering (MT=50 is undefined for neutrons).
5	(z,anything)	Sum of all reactions not given explicitly in another MT number. This is a partial reaction to be added to obtain MT=1.	Each particles can be identified and its multiplicity given in File 6. Not allowed in Files 4, 5.
6-9		Not allowed in version 6.	^{9}Be(n,2n) in version 5.
10	(z,continuum)	Total continuum reaction; excludes all discrete reactions.	Redundant; to be used for derived files only.
27	(z,abs)	Absorption. Sum of MT=18 and MT=102-117.	Redundant. Rarely used.
101	(z,disap)	Disappearance. Sum of MT=102-117.	Redundant. Rarely used.

Table 53. Definition of the MT Numbers for Neutron-Producing Continuum Reactions

MT	Reaction	Description	Comments
11	(z,2nd)	Production of two neutrons and a deuteron, plus a residual.	
16	(z,2n)	Production of two neutrons, plus a residual.	
17	(z,2n)	Production of three neutrons, plus a residual.	
18	(z,fission)	Total fission. Equal to the sum of MT=19, 20, 21, and 38, if present.	Redundant if MT=19 is present. Basic otherwise.
19	(z,f)	First-chance fission.	
20	(z,nf)	Second-chance fission.	
21	(z,2nf)	Third-chance fission.	
22	(z,na)	Production of a neutron and alpha particle, plus a residual.	
23	(z,n3a)	Production of a neutron and three alpha particles, plus a residual.	
24	(z,2na)	Production of two neutrons and an alpha particle, plus a residual.	
25	(z,3na)	Production of three neutrons and an alpha particle, plus a residual.	
28	(z,np)	Production of a neutron and a proton, plus a residual.	
29	(z,n2a)	Production of a neutron and two alpha particles, plus a residual.	
30	(z,2n2a)	Production of two neutrons and two alpha particles, plus a residual.	
32	(z,nd)	Production of a neutron and a deuteron, plus a residual.	
33	(z,nt)	Production of a neutron and a triton, plus a residual.	

Table 54. Definition of the MT Numbers for Neutron-Producing Continuum Reactions (continued)

MT	Reaction	Description	Comments
34	(z,n^{3}He)	Production of a neutron and a ^{3}He particle, plus a residual.	
35	(z,nd2a)	Production of a neutron, a deuteron, and two alpha particles, plus a residual.	
36	(z,nt2a)	Production of a neutron, a triton, and two alpha particles, plus a residual.	
37	(z,4n)	Production of four neutrons, plus a residual.	
38	(z,3nf)	Fourth-change fission.	
41	(z,2np)	Production of two neutrons and a proton, plus a residual.	
42	(z,3np)	Production of three neutrons and a proton, plus a residual.	
44	(z,n2p)	Production of a neutron and two protons, plus a residual.	
45	(z,npa)	Production of a neutron, a proton, and an alpha particle, plus a residual.	

Table 54. Definition of the MT Numbers for Neutron-Producing Discrete Reactions

MT	Reaction	Description	Comments
50	(z,n_0)	Production of a neutron, leaving the residual nucleus in the ground state.	Not allowed for incident neutrons. Use MT=2.
51	(z,n_1)	Production of a neutron, leaving the residual nucleus in the first excited state.	
52	(z,n_2)	Production of a neutron, leaving the residual nucleus in the second excited state.	

Table 55. Definition of the MT Numbers for Neutron-Producing Discrete Reactions (continued)

MT	Reaction	Description	Comments
	...		
90	(z,n_{40})	Production of a neutron, leaving the residual nucleus in the 40th excited state.	
91	(z,n_c)	Production of a neutron in the continuum not included in the above discrete representation.	

Table 55. Definition of the MT Numbers for Reactions That Do Not Produce Neutrons

MT	Reaction	Description	Comments
102	(z,gamma)	Radiative capture.	
103	(z,p)	Production of a proton, plus a residual. Sum of MT=600-649, if they are present.	For incident protons, this is inelastic scattering, and MT=600 is undefined (use MT=2).
104	(z,d)	Production of a deuteron, plus a residual. Sum of MT=650-699, if they are present.	For incident deuterons, this is inelastic scattering, and MT=650 is undefined (use MT=2).
105	(z,t)	Production of a triton, plus a residual. Sum of MT=700-749, if they are present.	For incident tritons, this is inelastic scattering, and MT=700 is undefined (use MT=2).
106	(z,^{3}He)	Production of a <sup3< sup="">He particles, plus a residual. Sum of MT=750-799, if they are present.</sup3<>	For incident ^{3}He particles, this is inelastic scattering, and MT=750 is undefined (use MT=2).
107	(z,a)	Production of an alpha particle, plus a residual. Sum of MT=800-849, if they are present.	For incident alphas, this is inelastic scattering, and MT=800 is undefined (use MT=2).
108	(z,2a)	Production of two alphas, plus a residual.	

Table 56. . Definition of the MT Numbers for Reactions That Do Not Produce Neutrons **(continued)**

MT	Reaction	Description	Comments
109	(z,3a)	Production of three alphas, plus a residual.	
111	(z,2p)	Production of two protons, plus a residual.	
112	(z,pa)	Production of a proton and an alpha particle, plus a residual.	
113	(z,t2a)	Production of a triton and two alphas, plus a residual.	
114	(z,d2a)	Production of a deuteron and two alphas, plus a residual.	
115	(z,pd)	Production of a proton and a deuteron, plus a residual.	
116	(z,pt)	Production of a proton and a triton, plus a residual.	
117	(z,da)	Production of a deuteron and an alpha particle, plus a residual.	

Table 56. Definition of the MT Numbers for Charged-Particle-Producing Discrete Reactions

MT	Reaction	Description	Comments
600	(z,p_0)	Production of a proton, leaving the residual nucleus in the ground state.	Not allowed for incident protons. Use MT=2.
601	(z,p_1)	Production of a proton, leaving the residual nucleus in the first excited state.	
602	(z,p_2)	Production of a proton, leaving the residual nucleus in the second excited state.	
	...		
648	(z,p_{48})	Production of a proton, leaving the residual nucleus in the 48th excited state.	
649	(z,p_c)	Production of a proton in the continuum not included in the above discrete representation.	
650	(z,d_0)	Production of a deuteron, leaving the residual nucleus in the ground state.	Not allowed for incident deuterons. Use MT=2.
651	(z,d_1)	Production of a deuteron, leaving the residual nucleus in the first excited state.	
	...		
698	(z,d_{48})	Production of a deuteron, leaving the residual nucleus in the 48th excited state.	
699	(z,d_c)	Production of a deuteron in the continuum not included in the above discrete representation.	
700	(z,t_0)	Production of a triton, leaving the residual nucleus in the ground state.	Not allowed for incident tritons. Use MT=2.

Table 56. . Definition of the MT Numbers for Reactions That Do Not Produce Neutrons (continued)

MT	Reaction	Description	Comments
701	(z,t_1)	Production of a triton, leaving the residual nucleus in the first excited state.	
	...		
748	(z,t_{48})	Production of a triton, leaving the residual nucleus in the 48th excited state.	
749	(z,t_c)	Production of a triton in the continuum not included in the above discrete representation.	
750	$(z,{}^3He_0)$	Production of a ^{3}He particle, leaving the residual nucleus in the ground state.	Not allowed for incident ^{3}He particles. Use MT=2.
751	$(z,{}^3He_1)$	Production of a ^{3}He particle, leaving the residual nucleus in the first excited state.	
	...		
798	$(z,{}^3He_{48})$	Production of a ^{3}He particle, leaving the residual nucleus in the 48th excited state.	
799	$(z,{}^3He_c)$	Production of a ^{3}He particle in the continuum not included in the above discrete representation.	
800	(z,a_0)	Production of an alpha particle, leaving the residual nucleus in the ground state.	Not allowed for incident alphas. Use MT=2.
801	(z,a_1)	Production of an alpha particle, leaving the residual nucleus in the first excited state.	
	...		
848	(z,a_{48})	Production of an alpha particle, leaving the residual nucleus in the 48th excited state.	
849	(z,a_c)	Production of an alpha particle in the continuum not included in the above discrete representation.	

APPENDIX K

NJOY MODULES

NJOY was first developed to read evaluated data stored in ENDF format, transform the data and create new libraries to be used in various research or nuclear industry related applications. The code is based on modules, each module performing a specific task. For the purpose of the present research, the only modules used were those allowing the creation of a new ACE formatted library containing the modified fission spectrum. Consequently only MODER, RECONR, BROADR and ACER were employed.

The complete list of NJOY modules is available from the 'T-2 Nuclear Information Service' of Los Alamos National Laboratory. *ENDF, NJOY, and Applications* can be found online at http://t2.lanl.gov/njoy/njoy01.html. The following full list of NJOY modules was retrieved in December 2011 from the website.

- **NJOY** directs the flow of data through the other modules and contains a library of common functions and subroutines used by the other modules.
- **RECONR** reconstructs pointwise (energy-dependent) cross sections from ENDF resonance parameters and interpolation schemes.
- **BROADR** Doppler broadens and thins pointwise cross sections.
- **UNRESR** computes effective self-shielded pointwise cross sections in the unresolved energy range.
- **HEATR** generates pointwise heat production cross sections (KERMA coefficients) and radiation-damage cross sections.

- **THERMR** produces cross sections and energy-to-energy matrices for free or bound scatterers in the thermal energy range.
- **GROUPR** generates self-shielded multigroup cross sections, group-to-group scattering matrices, photon-production matrices, and charged-particle cross sections from pointwise input.
- **GAMINR** calculates multigroup photoatomic cross sections, KERMA coefficients, and group-to-group photon scattering matrices.
- **ERRORR** computes multigroup covariance matrices from ENDF uncertainties.
- **COVR** reads the output of ERRORR and performs covariance plotting and output formatting operations.
- **MODER** converts ENDF "tapes" back and forth between ASCII format and the special NJOY blocked-binary format.
- **DTFR** formats multigroup data for transport codes that accept formats based in the DTF-IV code.
- **CCCCR** formats multigroup data for the CCCC standard interface files ISOTXS, BRKOXS, and DLAYXS.
- **MATXSR** formats multigroup data for the newer MATXS material cross-section interface file, which works with the TRANSX code to make libraries for many particle transport codes.
- **RESXSR** prepares pointwise cross sections in a CCCC-like form for thermal flux calculators.

- **ACER** prepares libraries in ACE format for the Los Alamos continuous-energy Monte Carlo code MCNP.
- **POWR** prepares libraries for the EPRI-CELL and EPRI-CPM codes.
- **WIMSR** prepares libraries for the thermal reactor assembly codes WIMS-D and WIMS-E.
- **PLOTR** reads ENDF-format files and prepares plots of cross sections or perspective views of distributions for output using VIEWR.
- **VIEWR** takes the output of PLOTR, or special graphics from HEATR, COVR, DTFR, or ACER, and converts the plots into Postscript format for printing or screen display.
- **MIXR** is used to combine cross sections into elements or other mixtures, mainly for plotting.
- **PURR** generates unresolved-resonance probability tables for use in representing resonance self-shielding effects in the MCNP Monte Carlo code.
- **LEAPR** generates ENDF scattering-law files (File 7) for moderator materials in the thermal range. These scattering-law files can be used by THERMR to produce the corresponding cross sections.
- **GASPR** generates gas-production cross sections in pointwise format from basic reaction data in an ENDF evaluation. These results can be converted to multigroup form using GROUPR, passed to ACER, or displayed using PLOTR.

APPENDIX L

Table 57. k_{eff} Values and Respective Standard Deviation for Different Sets of Prompt Neutron Fission Spectra

Time (days)	Original		Full Step Function		Front Step Function		Step Tail function	
	k_{eff}	standard deviation	k_{eff}	standard deviation	k_{eff}	standard deviation	k_{eff}	standard deviation
0	1.07112	0.00068	1.07275	0.00064	1.0722	0.00069	1.05487	0.00067
10	1.05873	0.00072	1.05833	0.00069	1.05838	0.00069	1.04372	0.00068
100	1.05937	0.00068	1.0599	0.00062	1.05807	0.00064	1.04394	0.00066
190	1.06307	0.00066	1.06373	0.00061	1.06339	0.00068	1.04723	0.00071
280	1.06328	0.00066	1.06364	0.00067	1.06427	0.00063	1.04737	0.00067
370	1.06012	0.00069	1.05934	0.00067	1.06105	0.0007	1.04567	0.00064
550	1.04411	0.00071	1.04563	0.00071	1.04495	0.00067	1.02817	0.00059
730	1.0238	0.0007	1.02592	0.00064	1.02516	0.00066	1.01055	0.00063
910	1.00168	0.00068	1.00326	0.00067	1.00234	0.00067	0.98666	0.00068
930	1.00052	0.00059	1.00025	0.00062	0.99932	0.00068	0.98409	0.00066
950	1.01189	0.00065	1.01373	0.00069	1.01314	0.00072	0.99615	0.00064
970	1.01172	0.00069	1.01248	0.00065	1.01198	0.00064	0.9947	0.00069
990	1.01039	0.00063	1.01162	0.00063	1.01082	0.0006	0.99416	0.00065
1010	1.00825	0.00062	1.00963	0.00064	1.00948	0.00073	0.99439	0.00069
1100	1.00558	0.00063	1.00537	0.00065	1.00653	0.00064	0.99001	0.00068
1190	1.00237	0.00066	1.00279	0.00063	1.00144	0.00073	0.98677	0.00066
1280	0.99853	0.00065	0.99971	0.00058	0.99833	0.0006	0.9838	0.00064
1370	0.99489	0.00064	0.99561	0.00066	0.99512	0.00059	0.98014	0.00063
1.460	0.9914	0.0006	0.99349	0.00068	0.99124	0.00063	0.97594	0.00067

APPENDIX M

^{235}U, ^{239}Pu, ^{241}Pu TOTAL FISSION AND ^{238}U, ^{238}Pu, ^{240}Pu, ^{242}Pu, ^{242m}Am, ^{245}Cm RADIATIVE CAPTURE CROSS SECTIONS

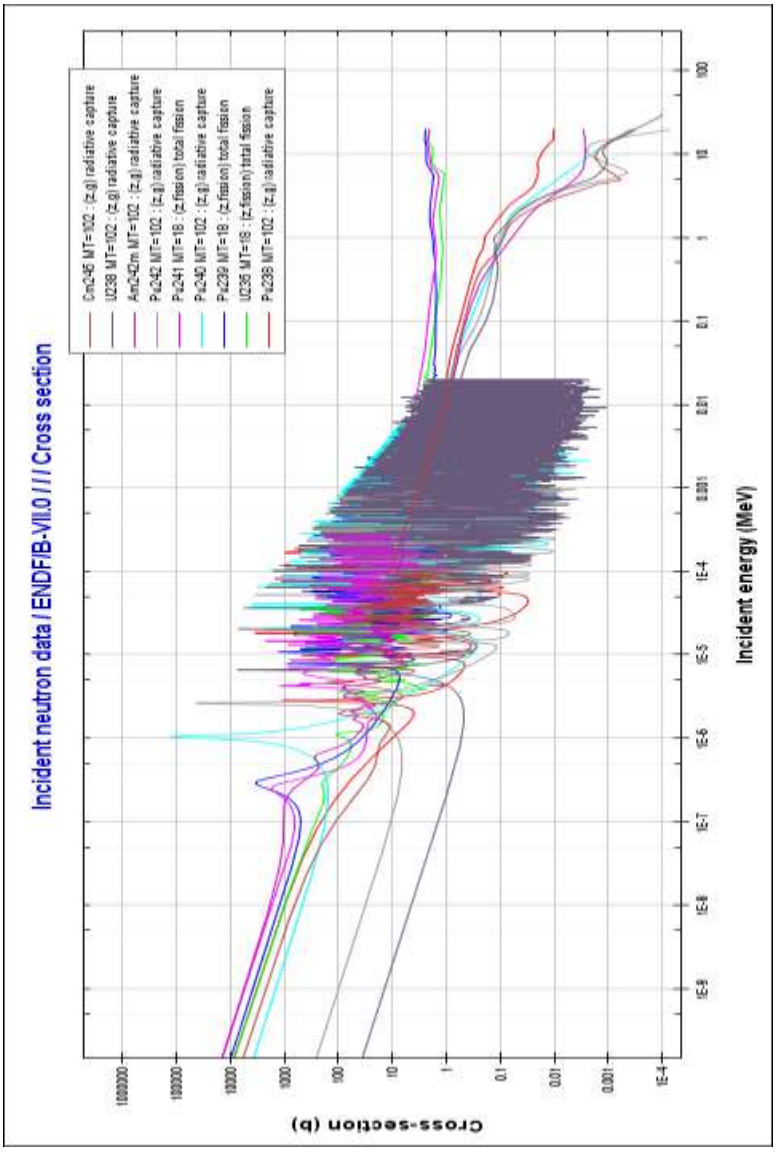

Figure 71. Radiative Capture and Fission Cross Section of TRU-fuels main isotopes

VITA

Name: Marie-Hermine Mathilde Solange Cuvelier

Address: Department of Nuclear Engineering, 337 Zachry Engineering Center, 3133 TAMU, College Station, TX-77843-3133

Email Address: marie_cuvelier@tamu.com

Education: B.S., General Engineering, EPF-Ecole d'Ingenieurs, 2009

M.S., General Engineering, EPF-Ecole D'Ingenieurs, 2012

M.S., Nuclear Engineering, Texas A&M University, 2012